Low-Bandgap Near-IR Conjugated Polymers/Molecules for Organic Electronics

ARTICLE *in* CHEMICAL REVIEWS · AUGUST 2015

Impact Factor: 46.57 · DOI: 10.1021/acs.chemrev.5b00165

CHEMICAL REVIEWS

Review

pubs.acs.org/CR

Low-Bandgap Near-IR Conjugated Polymers/Molecules for Organic Electronics

Letian Dou,[†,‡,§] Yongsheng Liu,[†,‡,§] Ziruo Hong,[†] Gang Li,[*,†] and Yang Yang[*,†,‡]

[†]Department of Materials Science and Engineering, and [‡]California NanoSystems Institute, University of California, Los Angeles, California 90095, United States

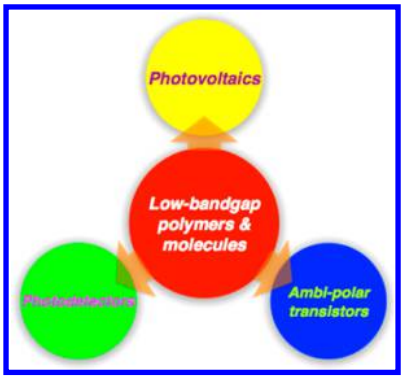

CONTENTS

1. INTRODUCTION

An important topic in materials science in the past few decades has been the development of organic semiconductors and their broad applications in electronics and photonics.[1,2] These materials are promising in terms of their electronic properties, low cost, versatility of functionalization, thin film flexibility, ease of processing, etc. What is particularly exciting is the chemistry that has allowed the synthesis of conjugated polymers/small molecules with narrow optical bandgaps, tunable energy levels, and desired electronic properties.[1,2] Such low-bandgap polymers/molecules (absorbing in the near-IR range and typically having a bandgap smaller than 1.6 eV) are particularly attractive in organic photovoltaics (OPV), photodetectors (PDs), and ambipolar field-effect transistors (FETs).[3,4] Intense efforts have been devoted to creating new polymers for such applications, and tremendous progress has been achieved. For example, organic solar cells[5] with >10% power conversion efficiency, organic photodetectors[6] with up to 1450 nm response and $>10^{12}$ cm $Hz^{1/2}/W$ detectivity, and organic

Special Issue: Solar Energy Conversion

Received: March 20, 2015

DOI: 10.1021/acs.chemrev.5b00165
Chem. Rev. XXXX, XXX, XXX−XXX

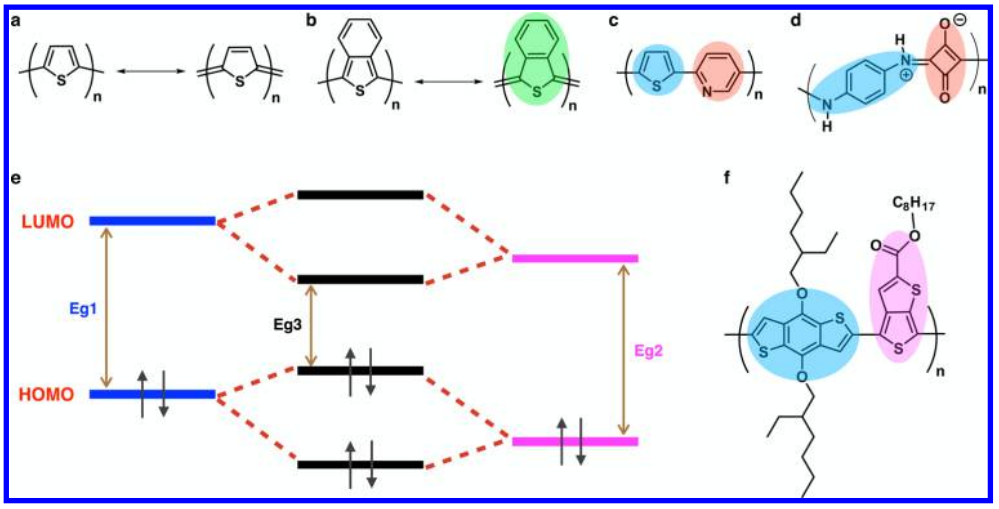

Figure 1. Strategies to make low-bandgap polymers. (a) Aromatic (left) and quinoid (right) resonance structures of polythiophene. (b) Stabilization of the quinoid resonance structure (green color). (c) Donor–acceptor copolymer made by Yamamoto (blue part is donor and red part is acceptor). (d) Donor–acceptor copolymer made by Havinga. (e) Simplified mechanism of bandgap lowering by donor–acceptor interaction. (f) Modern synthetic approach that combines both methods (purple part is electron-accepting and can stabilize the quinoid resonance structure).

transistors with ambipolar mobilities of ~10 $cm^2\ V^{-1}\ s^{-1}$ have been achieved.[7] In addition to its smaller energy gap, some of the physical properties of this class of materials are very interesting. For example, in photovoltaic devices, many of the state-of-the-art near-IR polymers/molecules have open circuit voltages (V_{OC}) closer to the bandgap (or smaller bandgap–V_{OC} offset) than wider bandgap materials, perhaps because these low bandgap polymers/molecules' electronic orbitals are much more closely overlapping and the π electrons are easier to delocalize.[8] Furthermore, charge separation in such materials is more efficient, which may be linked to the properties such as larger dielectric constant, stronger dipole moment, and lower exciton binding energy.[9] As a result, the photophysics and charge transport of such materials are rather unique in organic semiconductors. Therefore, the low-bandgap polymers/molecules are an interesting family of semiconductor materials, and have enabled many recent exciting breakthroughs in the field of organic electronics.[3−9]

In this Review, we discuss the scientific origins, practical approaches of designing the low-bandgap polymers/molecules, and their associated physical properties. We then provide a synopsis of major advances in the above-mentioned applications that particularly require small bandgap materials (with an emphasis on solar cells). Future developments in materials design and potential applications will also be addressed to stimulate innovation and creativity in the future. In this Review, we focus on the solution-processable organic materials with optical bandgap smaller than 1.6 eV (near-IR absorbing), and only limited numbers of representative molecules are chosen for discussion. This Review emphasizes the correlation between chemical structures, physical properties, and resulting device performance of the solution-processed polymers/small molecules, and tries to provide a comprehensive understanding from materials design to a variety of device applications. For a more complete description of the chemical structures and synthetic routes of different organic semiconductors for solar cells and FETs, please see recent review articles.[10−16]

2. LOW-BANDGAP POLYMER/MOLECULE DESIGN

2.1. Intrinsic Properties of Organic Semiconductors

Different from inorganic semiconductors, the π-conjugated organic macromolecules, or polymers, are comprised of a linear series of overlapping p_z orbitals with sp^2 or sp hybridization, thereby creating a conjugated chain of delocalized electrons.[17] The charge carriers (polarons) move freely in the conjugated backbone, but intermolecular charge transport is much more difficult and normally limited by charge hopping from one molecule to the adjacent molecule. As a result, the charge carrier mobility of organic materials is significantly lower than the mobility of inorganic materials, such as crystalline Si.[18] Another difference is that, upon photoexcitation, tightly bound Frenkel excitons (electron–hole pairs) with short lifetime are observed in organic materials (usually Wannier excitons observed in inorganic materials), resulting from their low dielectric constant ($\varepsilon_r \approx 2-4$).[17] The binding energy is in the range of 0.3–1 eV (much higher than the kinetic energy of electrons and holes at room temperature [~26 meV]), requiring a heterojunction to dissociate the excitons into electrons and holes.[8]

There are many intrinsic advantages for organic semiconductors that make them competitive alternatives to inorganic materials for optoelectronic applications. First, the absorption coefficient of organic semiconductors is very high.[19] As a result, a very thin layer of the material is enough to fully absorb the incident photons, making them useful for photovoltaics and photodetectors. Second, a relatively high photoluminescence quantum efficiency can be achieved, which makes them promising candidates for light emitting diodes.[20] Such high quantum yield also indicates a low rate of nonradiative decay, and is thus beneficial for semiconductor applications. Third, the small bandgap allows easy charge injection of electrons into LUMO and/or holes into HOMO, and the strong molecular polarity enables effective charge transport of both negative and positive charges. As a result, the materials exhibit p-type and n-type charge transport property and show great promise for ambipolar field effect transistors.[21] Fourth, deposition of large area organic thin films on low-cost

DOI: 10.1021/acs.chemrev.5b00165
Chem. Rev. XXXX, XXX, XXX−XXX

substrates such as glass, plastic, or metal foils is feasibile through the easy and high-throughput solution process.[1−3]

2.2. Synthetic Approaches toward Bandgap/Energy Level Tuning−A Concise Review

2.2.1. Conjugated Polymers. The story of polymer electronics starts from the invention of polyphenylenevinylenes (PPV) derivatives in the early 1990s. Friend, Holmes, and their co-workers demonstrated an organic light-emitting device using PPV from a solution-processed precursor.[22] Wudl, Heeger, and their co-workers synthesized a soluble polyphenylenevinylene, MEH-PPV, and applied it to OPV devices.[23] These groundbreaking works have a great impact on the development of new conjugated polymers for organic electronics. Later, polythiophenes was developed and became the most popular conjugated polymers for a broad spectrum of applications such as conducting polymers, light-emitting diodes, field-effect transistors, and plastic solar cells due to its excellent optical and electrical properties as well as good thermal and chemical stability.[10−20]

However, both polyphenylenevinylenes and polythiophenes have relatively large optical bandgaps and are not able to utilize the near-IR photons, which limit the performance of the corresponding devices. Narrowing the bandgap and fine-tuning the energy levels of the conjugated polymers have been major tasks for polymer chemists and material scientists for a long time. Basic quantum mechanics (one-dimensional quantum well model) shows that larger π-conjugation will lead to smaller energy bandgap. Increasing chain length and fusing more aromatic rings in the polymer backbone indeed help, but the bandgap shrinking becomes negligible when the molecule is longer than a certain point, typically 7−10 repeating units.[1,2,10−20] Conceptually novel strategies must be developed to have a better control over the bandgap and energy levels. Two major chemistry design approaches were developed to effectively lower the bandgap of the conjugated polymers: (1) stabilizing the quinoid resonance structure and (2) utilizing donor−acceptor interactions.[24−27]

The strategies to synthesize low-bandgap polymers are illustrated in Figure 1. The first approach is to stabilize the quinoid resonance structure. In general, any conjugated polymer has two resonance structures: aromatic and quinoid (Figure 1a). As compared to the aromatic form, the quinoid form has a smaller bandgap but is energetically less stable, because adopting the quinoid structure requires destruction of the aromaticity and a loss in the stabilization energy. It was demonstrated that the quinoid form can be stabilized by fusing another aromatic ring to the polymer backbone.[24] As shown in Figure 1b, when a thiophene ring shifts from aromatic to quinoid form in a poly(isathianapthene) molecule, an aromatic benzene ring that is fused to the thiophene ring forms simultaneously, providing a large aromatic resonance stabilization energy. As such, poly(isathianapthene) became the first well-known conjugated polymer with a narrow bandgap as low as 1 eV. This achievement spurred the initial concept, suggesting that the modulation of the bandgap can be achieved when the conjugated backbone consists of an alternating sequence of aromatic and quinoid units.[10]

Alternatively, the bandgap of conjugated polymers can also be modulated via the donor−acceptor (D−A) approach. The idea was to use alternating electron-donating (D) and electron-withdrawing (A) units to modulate the bandgap of the polymer, also known as a "D−A" conjugated polymer. An initial observation was made by Yamamoto et al. when studying a thiophene (D)−pyridine (A) copolymer (Figure 1c).[25] Havinga et al. started the effective implementation of this concept via the synthesis of polysquaraines through condensation reactions, resulting in polymers with bandgap below 0.5 eV (Figure 1d).[26] The simplified mechanism is shown in Figure 1e. After polymerization, the highest occupied molecular orbital (HOMO) of the donor segment will interact with the HOMO of the acceptor segment to create two new HOMOs. Similarly, the lowest unoccupied molecular orbital (LUMO) of the donor will interact with that of the acceptor to produce two new LUMOs of the D−A polymer. After the electrons redistribute from their original noninteracting orbitals to the new hybridized orbitals of the polymer, higher HOMO and lower LUMO energy levels are generated, leading to a narrowing of the optical bandgap.[10,25,26]

Although the initial designs of these two methods are different, recent research suggests that the two concepts are closely related and beneficial to each other, and the design of modern donor−acceptor polymers requires a hybridization of both.[27,28] The quinoid-stabilized polymers typically have too small bandgap and poor stability toward oxidation.[24] To overcome these issues, for example (Figure 1f), an aromatic benzodithiophene unit can be inserted into the backbone to "dilute" the quinoid building block, and thus the bandgap was widened in a controllable way.[29] A strong electron-withdrawing ester group can also be attached to the thienothiophene unit to lower the HOMO/LUMO level of the monomer and the polymer to improve the stability against oxidization. As a result, the polymer shows both D−A and quinoid characteristics.

2.2.2. Conjugated Small Molecules. As a counterpart to the polymers, semiconducting organic small molecules have also attracted intense research attention and showed great promise in photoelectric/electric applications. Initially, the vacuum processed small molecules were first used in the organic photovoltaic and light emitting diodes devices.[16] However, the solution-processed small molecules for organic electronic devices have not been massively investigated until the past decade. The advantages of small molecules include well-defined molecular structures, high purity without batch-to-batch variations, and the absence of end group contaminants.[30−34] Moreover, crystalline small molecules exhibit high charge mobility due to their long-range order.[30−34]

The bandgap engineering of solution-processed small molecules is similar to that of polymers. To achieve near-IR absorbing/emitting abilities, strong donor−acceptor interaction and stabilization of the quinoid resonant structure are required. However, due to the smaller one-dimensional quantum well length, bandgap lowering is more difficult and normally requires very strong donor or acceptor units in the case of small molecules. For more detailed discussion on the bandgap engineering of the organic small molecules, see recent review articles.[30−32]

2.3. Rational Design for Different Applications

Generally, thiophene, bithiophene, thieno[3,2-*b*]thiophene, benzodithiophene (BDT), cyclopentadithiophene (CPDT), dithienosilole (DTS), and dithienopyrrole are commonly used as strong electron-donating units; benzothiadiazole (BT), isoindigo (II), diketopyrrolopyrrole (DPP), naphthalene diimide, and benzobisthiadiazole (BBT) are used as strong electron-withdrawing units with weak quinoid characteristics; and ester/carbonyl-substituted thieno[3,4-*b*]thiophene (TT),

DOI: 10.1021/acs.chemrev.5b00165
Chem. Rev. XXXX, XXX, XXX−XXX

Scheme 1. Palladium-Catalyzed Stille (Top) or Suzuki (Bottom) Cross-Coupling Reactions

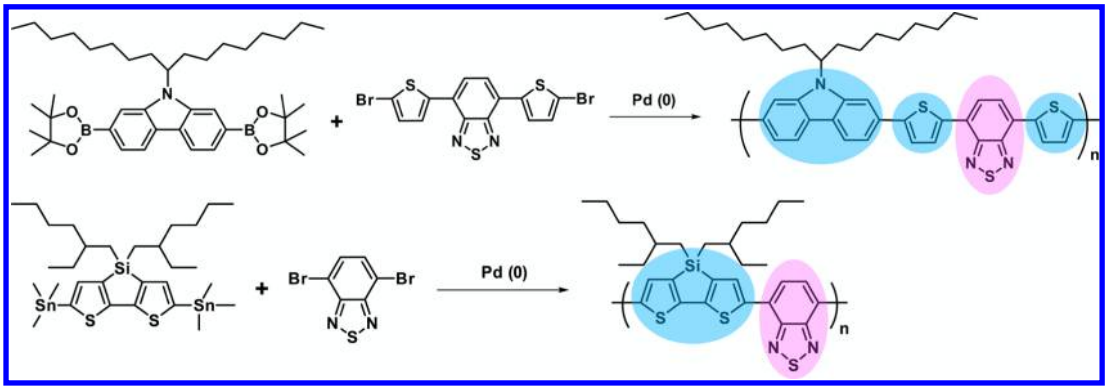

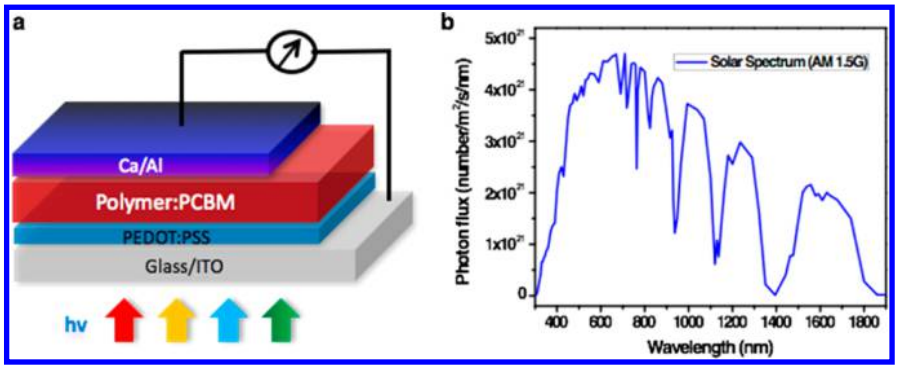

Figure 2. Polymer solar cells and solar spectrum. (a) Device structure of a regular polymer solar cell. (b) Solar spectrum under standard condition (AM 1.5 G).

thieno[3,4-*b*]pyrazine (TP), and quinoxaline (QX) are weak electron-withdrawing units with strong quinoid characteristics. Normally the polymers are made using palladium-catalyzed Stille or Suzuki cross-coupling reactions (Scheme 1).[10,28] Through modification and combination of different building blocks, many new polymers have been designed and synthesized toward different applications.

In the various applications of low-bandgap polymers, there are similarities as well as differences. For solar cells, polymers with a bandgap of 1.2−1.6 eV (to achieve high photocurrent), a deep HOMO of ∼−5.2 eV (to increase the V_{OC} of the device),[33] and a LUMO shallower than −3.7 eV (to make sure efficient exciton dissociation occurs at the donor−acceptor interfaces) are required; moreover, ideal thin film morphology (nanoscale continuous interpenetrating network) and high charge carrier mobility are also needed to achieve optimized performance.[10,19] To fulfill these requirements, moderate electron-donating and electron-withdrawing units with good planarity and $\pi-\pi$ stacking are used, such as BDT, BT, and ester/carbonyl substituted TT units.[10] For photodetectors, a broad photoresponse from UV into near-IR region, small noise, high sensitivity, and fast response are important merits. Polymers with very small bandgap (<1 eV), high charge carrier mobility, high absorption coefficient, and low leakage current under dark are desired.[6] For ambipolar field effect transistors, good electron and hole mobility are essential, which require relatively shallow HOMO and deep LUMO levels (basically the opposite of organic solar cells). Typically, very strong electron-withdrawing groups such as BBT are used to downshift the LUMO levels to increase the electron affinity and improve electron transport.[28] In addition to the bandgap and energy level control, many other factors such as thin film morphology, molecular packing, and device interface design need to be considered to achieve high performance. Several representative materials systems, their intrinsic/extrinsic properties, and specific device architecture design will be discussed in detail.

3. PHOTOVOLTAICS HARVESTING THE NEAR-IR LIGHT

Photovoltaic technology is a promising solution for solar energy harvesting. A basic OPV device structure is shown in Figure 2a. The active layer is simply sandwiched by two electrodes with different work functions. Because of the large binding energy and short diffusion length of the excitons, a bulk heterojunction (BHJ) is preferred for the organic materials to maximize the interfacial area for efficient charge separation.[3] Conjugated polymers are normally used as the donor material, and fullerene derivatives (phenyl-C_{61}-butyric acid methyl ester, or PCBM) are often used as the acceptor material.[3] The most important figure-of-merit for a solar cell is the power conversion efficiency (PCE), which equals the product of short circuit current (J_{SC}), V_{OC}, and fill factor (FF) divided by the radiant flux density. To cover a broader spectrum of solar irradiation (Figure 2b), semiconducting polymers with bandgap from 1.2 (absorption onsite ∼1000 nm) to 1.6 eV (absorption onsite ∼800 nm) are desired. Some unique applications of such low-bandgap polymers/molecules include tandem/multijunction, semitransparent (or visibly transparent), and ternary blend solar cells.[34]

Photoactive polymers for solar cell application have undergone continuous progress since the observation of photoinduced electron transfer in 1992.[35] The large bandgap of PPV derivatives (∼2.2 eV) limits the light absorption. Along with a low carrier mobility, OPV efficiency has been limited at the 2−3% range. Poly(3-hexylthiophene) (P3HT), with a bandgap of

DOI: 10.1021/acs.chemrev.5b00165
Chem. Rev. XXXX, XXX, XXX−XXX

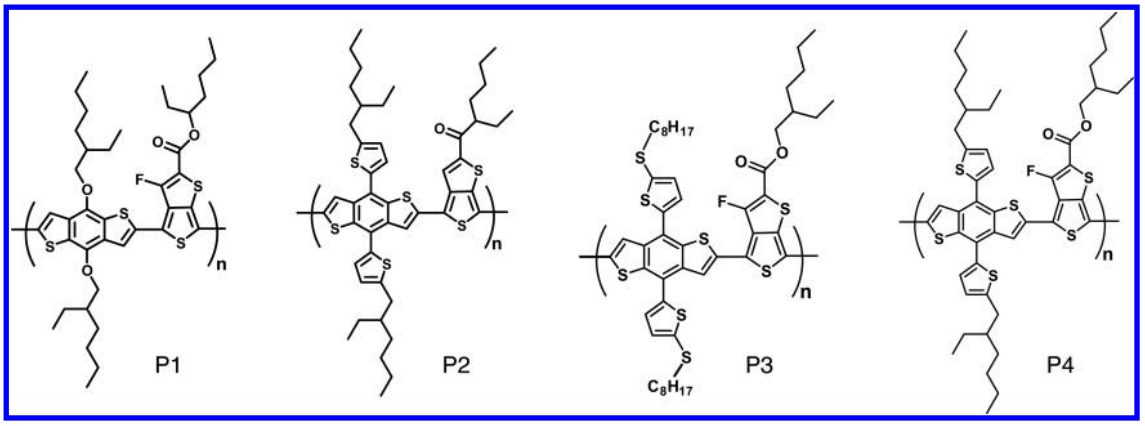

Figure 3. Chemical structures of **P1**−**P4**.

1.9 eV, high hole mobility, and broader spectral coverage, has become the most studied electron donor polymer material in polymer solar cell devices in the past decade. The regioregularity of the material and the morphology manipulation of P3HT:PCBM blend were found to be critical in achieving high efficiency.[36−38] While the P3HT:PCM system was limited to 4−5% PCE, it is worth mentioning that the progress in the acceptor material has enabled significant efficiency improvement through V_{OC} enhancement, and 6−7% PCE has been reported.[39,40] There have also been reports on polymers with bandgaps similar to P3HT, but with deeper HOMO levels allowing higher V_{OC} and thus PCE to be realized.[8−16]

3.1. Low-Bandgap Polymers for Solar Cells

3.1.1. Low-Bandgap Polymers Based on Thieno[3,4-*b*]thiophene. Polymers with bandgap of less than ∼1.6 eV with near-IR absorption played an important role in OPV progress. The thieno[3,4-*b*]thiophene building block, which stabilizes the quinoid structure to reduce the bandgap, was introduced by Yu et al. into the OPV field. When the TT unit was combined with planar BDT unit to form the PTB series polymers, ∼50% enhancement in J_{SC} and PCE (from 4% to ∼6%) was obtained.[29] The lower bandgap (E_g of 1.6 eV) and the large planar BDT structure, which enhanced molecular packing (and thus high carrier mobility), are believed to be critical for this breakthrough. Adding a fluorine atom on the TT unit to lower the HOMO level, and the following side chain engineering from Yu, Li, and Hou et al., enabled several high performance polymers, such as PTB-7 (**P1**) and PBDT-TT-CF (both have bandgaps of around 1.6 eV and HOMO level of around −5.2 eV).[41−43] These developments enable over 8% certified PCE using a conventional device structure (ITO/PEDOT:PSS/polymer:$PC_{71}BM$/Ca/Al).[44] Wu and Cao's efforts on interface improvement using conjugated polyelectrolytes successfully increased the PTB-7-based cell performance from 7.4% to 9.2% PCE using an inverted device structure (ITO/ZnO/PFN/polymer:$PC_{71}BM$/MoO_3/Ag).[45] The chemical structure of PTB-7 (**P1**) and related structures can be found in Figure 3. The fluorinated PTB related polymer can harvest most of the visible light and partially the near-IR light (up to 770 nm), and, more importantly, the charge separation at the donor−acceptor interface is highly efficient (internal quantum efficiency ∼100%). As shown in Figure 4, the external quantum efficiency (EQE) of the device approaches 80%.

This family of material has excited numerous studies for understanding the fundamentals. By studying the material in

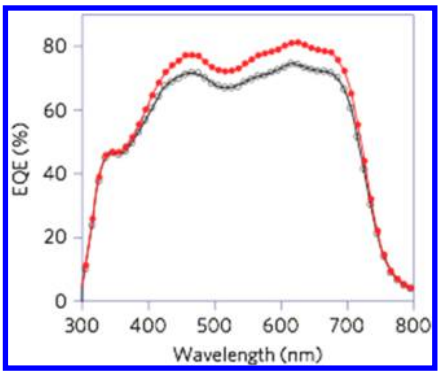

Figure 4. External quantum efficiency of PTB-7 (**P1**)-based single junction solar cell with power conversion efficiency of 9.2%. The red curve indicates the EQE of an inverted device configuration of ITO/ZnO/PFN/PTB-7:$PC_{70}BM$/MoO_3/Ag, and the gray curve indicates the EQE of a regular device. With the help of device engineering, very high EQE can be achieved for the PTB-7-based solar cells. Reprinted with permission from ref 45. Copyright 2012 Nature Publishing Group.

magnetic fields, it was found that the D−A polymers, particularly the fluorinated one, show higher dielectric constants and reduced exciton binding energy.[46] In their study, light-assisted dielectric response was measured to show that the PTB:PCBM solar cells exhibit larger capacitances relative to P3HT:PCBM device under photoexcitation (Figure 5), indicating a larger effective dielectric constant. Magnetic field effects of photocurrent at high-field (>150 mT) were also examined to reveal that the charge-transfer complexes formed at PTB:PCBM interfaces have much lower binding energies due to stronger electron-withdrawing abilities, as compared to the P3HT:PCBM device. Yu also proposed that the fluorine

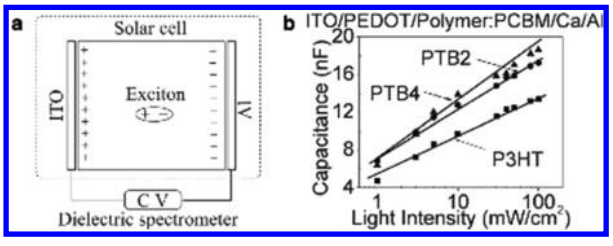

Figure 5. Light-assisted dielectric response setup (a) and results (b) based on PTB series polymers. Reprinted with permission from ref 46. Copyright 2011 Wiley-VCH.

DOI: 10.1021/acs.chemrev.5b00165
Chem. Rev. XXXX, XXX, XXX−XXX

atom induces large changes in dipole moment between the ground state and the excited state, due to the strong electron-withdrawing effect.[47] Comprehensive theoretical and experimental studies were carried out to prove the concept. Figure 6

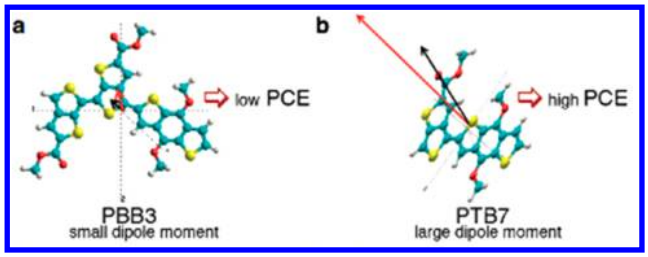

Figure 6. Dipole moments of PBB3 and PTB-7 (**P1**) calculated by density function theory. PBB3 is a polymer with one BDT and two TT units in one repeating unit. The dipole moment is canceled by the two polar TT units, and this polymer shows low charge separation efficiency and power conversioin efficiency in a solar cell device. Reprinted with permission from ref 47. Copyright 2011 American Chemical Society.

shows the calculated dipole moment of PTB-7 (large dipole moment) and PBB3 (small dipole moment).[47] More recently, Ade and You observed a very interesting phenomenon. By using the soft X-ray technique, they found that the fluorinated polymers had a tendency to form "face-on" configuration on the surface of the PCBM domain, which is more favorable for efficient charge transfer from polymer to PCBM molecules as compared to the "edge-on" configuration that is typically observed in nonflourinated polymers.[48] Figure 7 shows an

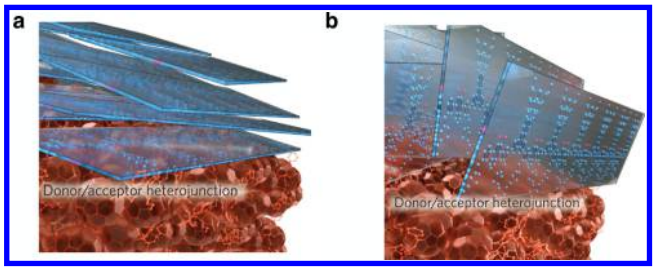

Figure 7. An illustration of the "face-on" (a) and "edge-on" (b) configuration at the donor−acceptor interface. Reprinted with permission from ref 48. Copyright 2014 Nature Publishing Group.

illustration of the "face-on" and "edge-on" configuration at the donor−acceptor interface. All of the results indicate that fluorination is beneficial for D−A polymers and should be considered as a general design rule when making new materials.

Recently, inspired by this molecular design, several similar polymers have been reported with efficiencies of ∼9%.[49−54] Some representative polymers are shown in Figure 3. For example, the BDT unit was modified by replacing the 2-ethylhexoyl group with the 2-(2-ethylhexyl)-thienyl group, which has better planarity and lower electron-donating properties. A new polymer **P2** was reported by Huo et al. by polymerizing the new unit with a thieno[3,4-*b*]thiophene unit. Devices based on **P2**:PCBM resulted in efficiencies of 7.6%,[51] and recently were pushed up to 8.3% by Adhikary et al., when the cell was exposure to UV-ozone.[52] Ye et al. introduced linear alkyl-thio thienyl side chains on the BDT unit to produce another PBDTTT-based copolymer known as **P3**. Under similar device fabrication conditions, it shows high efficiency up to 9.48%.[53] PTB7 was modified by incorporating the 2-(2-ethylhexyl)-thienyl group into the BDT unit of PTB7 to produce **P4**. By using a deterministic aperiodic nanostructure based on nanoimprint technology, a highly efficient single junction device with PCE > 10% was achieved.[54]

3.1.2. Low-Bandgap Polymers Based on Benzothiadiazole. Further lowering the bandgap below 1.5 eV is meaningful. It is well-known from inorganic solar cell development that the multijunction or tandem solar cell concept is a very attractive approach to go beyond the Shockley−Quiesser limitation of a single-junction cell (∼33% efficiency at bandgap ∼1.4 eV) by significantly reducing the thernalization loss.[55] Inorganic multijunction solar cells with efficiencies over 40% (GaInP 1.8 eV/GaInAs 1.4 eV/Ge 0.67 eV, 2-terminal connection) have been achieved (current record is 43.5%).[56,57] To mimic the inorganic tandem design, we already have good polymers with bandgap of 1.8−1.9 eV, and then pursuing polymers at bandgap of ∼1.4 eV becomes critical. Indeed, great efforts and significant progress have been made to achieve such polymers, which lead to a certified efficiency of over 10%.[5,58,59]

The chemical structures of some representative low-bandgap IR polymers are shown in Figure 8. One of the first reported high performance polymers with a bandgap of ∼1.4 eV is probably **P5** based on alternating strongly electron-rich CPDT and electron-deficient BT units by Brabec et al. with an initial PCE of ∼3%.[60] This system was then pushed to ∼5% by Bazan et al. via a novel solvent additive approach.[61] Yang et al.[62,63] and Brabec[64] et al. later found that replacing the carbon atom with a silicon atom as the bridging atom between the two thiophenes gave DTS units, which has significant benefit on the hole mobility of **P6** over **P5**. Calculations showed that the C−Si bond is longer than the C−C bond, indicating less steric hindrance in the DTS core by the side chains, which lead to a better $\pi-\pi$ stacking and enhanced crystallinity.[63] Silicon is not the only heteroatom that gives enhanced performance in BT-based polymers. Replacing Si with Ge atom produces a new polymer **P7** with a reduced bandgap.[65] The polymer changes to "face-on" orientation in the thin film (the Si-based polymer was "edge-on"). Such favorable orientation leads to an improved charge transport and higher J_{SC} in the solar cell devices. Because of the relatively lower V_{OC}, comparable efficiency was obtained with the Si-based polymer. Recently, an oxygen atom as heteroatom at the bridging site to form an asymmetric electron-rich dithieno[3,2-*b*:2′,3′-*d*]pyran (DTP) unit was reported.[5,66] The electron-donating property of the DTP unit is stronger than CPDT. Strongly electron-deficient difluorobenzothiadiazole unit was used to replace the BT unit, and a regiorandom polymer (**P8**, bandgap = 1.38 eV) was obtained. The polymer shows superb photovoltaic performance. Preliminary results on conventional OPV structure give 8.0% PCE, over 60% EQE, and a good V_{OC} of ∼0.7 V.[66] The EQE is high in the near-IR region, which is particularly attractive for tandem solar cell structures.

3.1.3. Low-Bandgap Polymers Based on Diketopyrrolopyrrole. Besides benzothiadizole, diketopyrrolopyrrole is another important electron-withdrawing building block particularly attractive for low-bandgap materials for OPV applications. Janssen et al. first used DPP unit in OPV polymers in 2008. They copolymerized thiophene-flanked DPP with electron-rich bithiophene, and successfully reduced the optical bandgap of the polymer to 1.4 eV.[67] Shortly after, the same group showed polymerization of DPP with a thiophene unit via

DOI: 10.1021/acs.chemrev.5b00165
Chem. Rev. XXXX, XXX, XXX−XXX

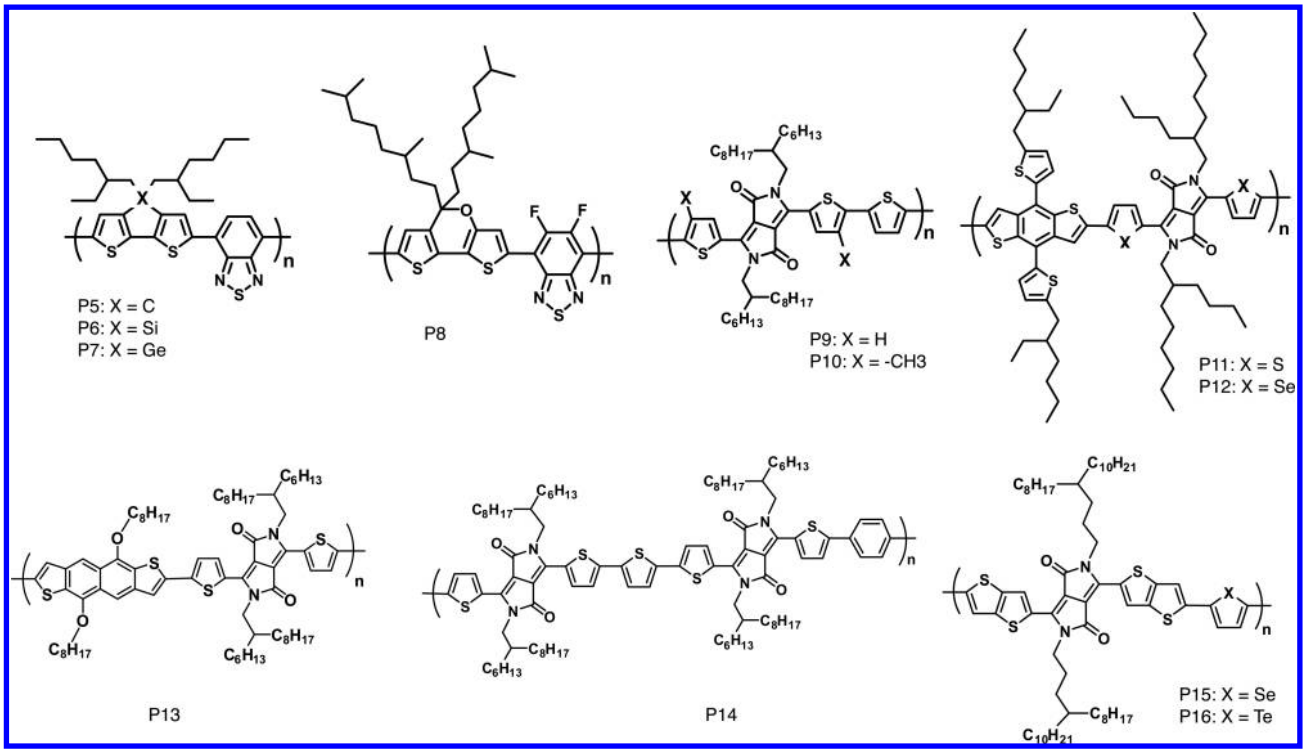

Figure 8. Chemical structures of **P5**−**P16**.

Suzuki cross-coupling, and a low-bandgap polymer **P9** was achieved with 1.31 eV bandgap.[68] When combined with $PC_{71}BM$, the EQE in the near-IR (700−850 nm) reached 35%. Initial PCE of 4.7% with V_{OC} = 0.65 V, J_{SC} = 11.7 mA/cm^2, and FF = 60% was reported in 2009. The polymer actually has more potential, envisioned by the fact that by increasing the molecular weight and improving the thin film morphology, PCEs over 7% have been achieved recently.[69] Fine-tuning the energy level and bandgap by adding two additional methyl groups on the thiophene units led to a new polymer **P10**, which gave a reduced bandgap of 1.29 eV and enhanced efficiency of 7.0%.[70] In another work, encouraged by the success of the BDT unit in PBT series of polymer, Yang's group carried out a systematic investigation on the BDT and DPP-based low-bandgap polymers. A first encouraging polymer, **P11**, has a bandgap of 1.44 eV, and a deep HOMO level that favors high V_{OC}. The enhanced planarity from thienyl-substituted BDT unit enables high charge carrier mobility.[71,72] The HOMO level of PBDTT-DPP is −5.30 eV, which enabled a high V_{OC} of 0.74 V. An efficiency of 6.5% was achieved in single junction devices with EQE approaching 50% in the near-IR region. By substituting the sulfur atoms on the DPP unit with selenium atoms, a new polymer **P12** was reported, which has a lower bandgap of 1.38 eV and improved hole mobility.[73] High efficiency of 7.2% was demonstrated in single junction devices with largely enhanced photocurrent.

More DPP-based polymers with high performance were reported, and the chemical structures are shown in Figure 8. When dithieno[3,2-*b*:2′,3′-*d*]thiophene was polymerized with a DPP unit, the new polymer shows a small bandgap of 1.2 eV and good performance up to 6.0% with a V_{OC} of 0.66 V, a J_{SC} of 13.7 mA/cm^2, and a FF of 66.1%.[74,75] Another polymer **P13** contains a large planar naphthodithiophene unit in the main chain. The rigid polymer chain provides an improved charge mobility and high performance of 7%.[76,77] Higher efficiencies of 8% were achieved in a ternary polymer **P14** with alternating benzene or thiophene as the donor unit.[78] Very recently, more selenium- and tellurium-based polymers were reported with very small bandgap and promising performance. Grubbs et al. reported a tellurium containing polymer with 4.4% PCE.[79] McCulloch et al. reported **P15** and **P16**.[80] Interestingly, **P15** shows a very high charge carrier mobility and photocurrent. The single junction device shows a PCE up to 8.8% with a V_{OC} of 0.57 V, a J_{SC} of 23.5 mA/cm^2, and a FF of 66%, which is the highest efficiency for the DPP-based polymer so far. At the same time, the tellurium-based **P16** gave a fairly good efficiency of 7.1%, demonstrating the great promise of tellurium-based low bandgap polymers for organic electronics.

3.1.4. Low-Bandgap Polymers Based on Isoindigo. Isoindigo is another important building block for low-bandgap polymers. Since Reynolds et al. first introduced this unit into organic solar cells, many new polymers have been synthesized. For a complete list of these polymer, see a recent review article by Stalder et al. and Wang et al.[81,82] The first isoindigo-based polymers reported were copolymers with thiophene, thienothiophene, and benzodithiophene, but either a low fill factor or low J_{SC} limited the overall efficiency to below 2%. Andersson et al. copolymerized the isoindigo with terthiophene to form P3TI.[83] By introducing a long and branched side chain, the solubility and film quality were dramatically improved. It has an optical bandgap of 1.5 eV and a good performance of 6.3%, which was the first isoindigo-based polymer with over 5% efficiency. Recently, Bao et al. systematically studied the side chains on the isoindigo-bithiophene-based polymers. By introducing 10% bulky polystyrene side chain into the polymer, an improved efficiency over 7% was achieved.[84] The benzene-based isoindigo normally led to polymers with bandgap around 1.5 eV, which is not small enough for some specific applications. To further lower the bandgap, thiophene-based isoindigo was recently reported by a number of groups.[85−88] By

DOI: 10.1021/acs.chemrev.5b00165
Chem. Rev. XXXX, XXX, XXX−XXX

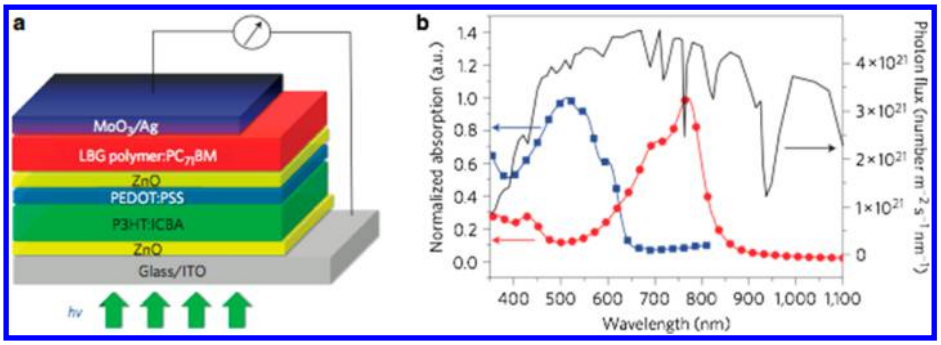

Figure 9. (a) A typical device structure of tandem solar cells and (b) the absorption spectra of a wide-bandgap (blue curve), a low-bandgap (red curve) polymer, and solar spectrum. Reprinted with permission from ref 71. Copyright 2012 Nature Publishing Group.

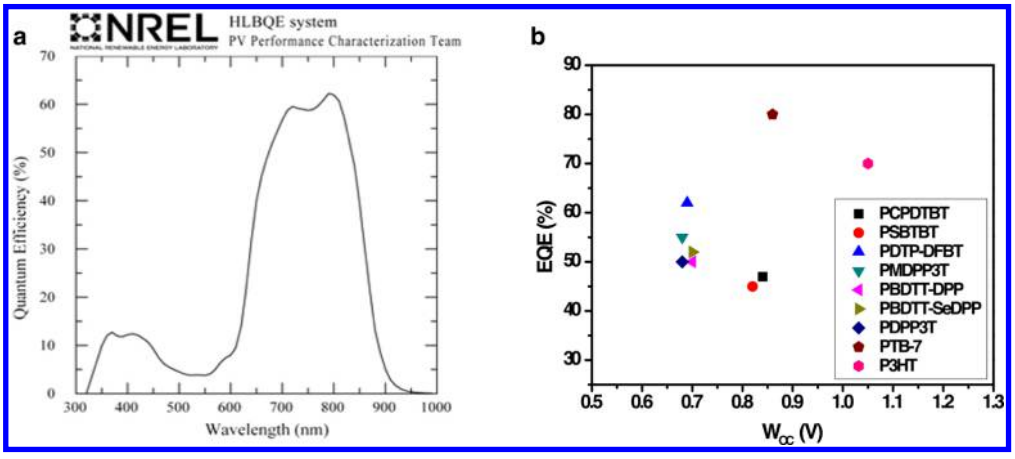

Figure 10. (a) External quantum efficiency of the rear cell of the tandem device using PDTP-DFBT that was measured by the National Renewable Energy Laboratory. Reprinted with permission from ref 5. Copyright 2013 Nature Publishing Group. (b) Bandgap−open circuit voltage offset (W_{OC}) vs external quantum efficiency (EQE) of representative polymers.

copolymerizing with different donor units, the bandgap can be reduced to below 1 eV. However, the photovoltaic performance was very much limited by the small V_{OC} and J_{SC}.

3.2. Low-Bandgap Polymers in Tandem Solar Cells

The low-bandgap polymers are particularly important for tandem solar cells, in which two materials with complementary absorption are required. Figure 9 shows a typical device structure of a tandem solar cell and the absorption spectra of a wide and a small bandgap polymer. At early stage, **P5** and **P6** showed relatively lower V_{OC}, J_{SC}, and FF in single junction devices. Therefore, the performance of tandem cells was limited to less than 7%.[89,90] The recent progress in low-bandgap polymers enabled smaller bandgap-V_{OC} offset in OPV, which significantly improved the V_{OC} of tandem devices. On the other hand, matching the photocurrent between two junctions in the tandem device requires the low-bandgap polymer to deliver high EQE in the near-IR region. Higher efficiency tandem devices were demonstrated using high molecular weight **P8**−**P13** (PCE = 8−10%).[5,70−73,77] For tandem solar cell current matching, the high EQE at long wavelength is particularly important. These mentioned polymers have a broad absorption range, up to 950 nm, and provide a high EQE of over 50% from 600 to 900 nm. Among them, **P8** gives the highest EQE of 60% and leads to tandem devices that achieved 10.6% PCE. The EQE spectrum of the tandem device using PDTP-DFBT measured at the National Renewable Energy Laboratory (NREL) is shown in Figure 10a. However, the EQE response is still far below the state-of-art single junction devices based on PTB-7 and P3HT (EQE 70−80%) using similar device structures. A fundamental question remains: What are the factors that limit the quantum efficiency of the low-bandgap polymers? Janssen et al. pointed out that the LUMO level of such polymers is too close to the LUMO level of PCBM, probably smaller than the minimum LUMO−LUMO offset required for efficient electron transfer.[91] **P10** was actually designed with a slightly higher LUMO level over **P9** to prove the argument, which seems to be successful, at least to certain degree (EQE improved from 50% to 55%).[70] Another possible reason is that the triplet states of the low-bandgap polymers are lower than the charge transfer states in the blend film, providing additional recombination pathways for the excitons.[92] So far, the hypnosis still lacks experimental support, and more photophysical studies on the low-bandgap polymers are required.

Because of the relatively deeper HOMO and LUMO energy levels, the above-mentioned low-bandgap polymers show smaller bandgap-V_{OC} offset (W_{OC}) as compared to other polymers. W_{OC} is defined as the bandgap divided by elementary charge minus the V_{OC} of the device ($W_{OC} = E_g/e - V_{OC}$). For **P8**−**P13**, the W_{OC}'s are around 0.7 V, approaching the limit predicted by Nelson.[93] Figure 10b shows the W_{OC} versus EQE of representative polymers. In general, the polymers with smaller W_{OC}'s also give lower EQE values (as compared to PTB-7 or P3HT-based devices). The question now becomes how to downshift the energy levels of the polymers to reduce the W_{OC}. Also, can we design new molecules with a larger dielectric constant to lower the exciton binding energy and thus

DOI: 10.1021/acs.chemrev.5b00165
Chem. Rev. XXXX, XXX, XXX−XXX

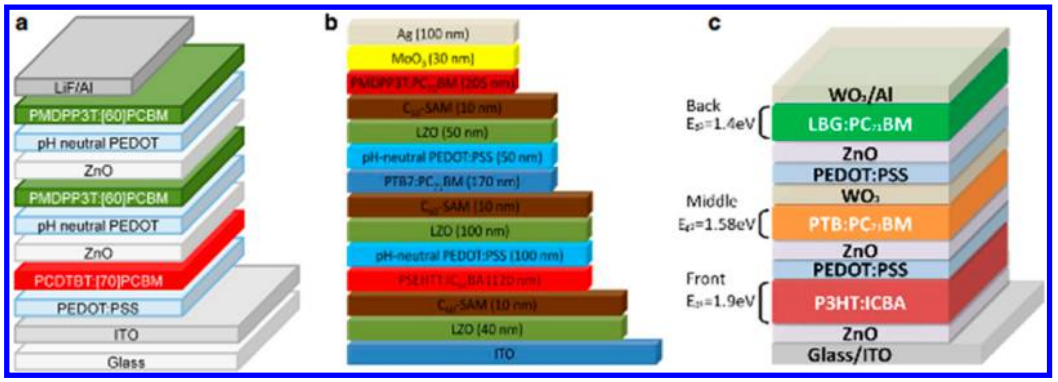

Figure 11. Device structures of the triple junction solar cells. Reprinted with permission as follows: (a) Reference 70. Copyright 2013 American Chemical Society. (b) Reference 95. Copyright 2015 Royal Society of Chemistry. (c) Reference 96. Copyright 2014 Wiley-VCH.

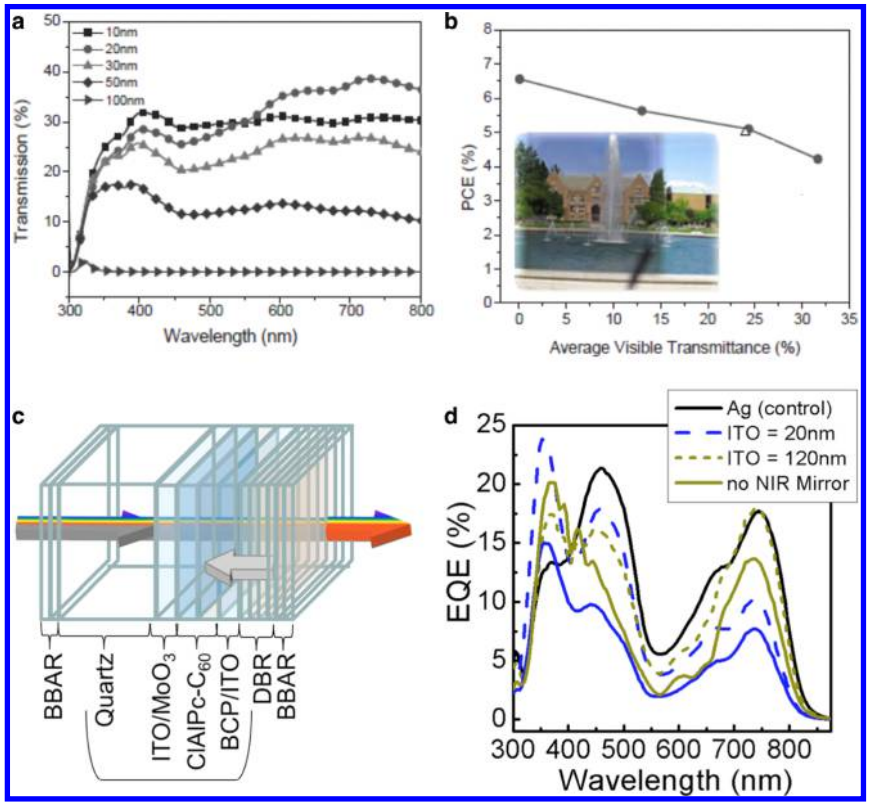

Figure 12. (a) Transmission spectra of opaque and transparent polymer solar cells with different Ag thickness. The cell is based on PIDQ-PhanQ:$PC_{71}BM$. (b) PCE vs AVT for semitransparent OPV. Reprinted with permission from ref 103. Copyright 2013 Wiley-VCH. (c) Device structure of tranparent OPV devices using ClAlPc and C_{60} as donor and acceptor. Broad-band antireflection coating (BBAR) and distributed Bragg reflector (DBR) were used to enhance TOPV performance. (d) EQE for the opaque control cell and for the TOPV with the near-IR reflector as a function of ITO cathode thickness. Reprinted with permission from ref 104. Copyright 2011 American Institute of Physics.

reduce the W_{OC}? At the same time, the next challenge will be 80% external quantum efficiency in the near-IR region. Under these conditions, 20% PCE is achievable in double junction tandem configuration with polymers with bandgaps of 1.4 and 1.9 eV.[3] Note that an alternative way to broaden the absorption is to use the ternary systems by blending a wide and a narrow bandgap polymer together. In this way, the V_{OC} of device will not add up, and the upper limit of PCE is not higher than conventional single junction devices. The compatibility and morphology control becomes critical for such device configuration. Impressive progress has been achieved and reviewed recently.[34]

Another advantage of the low-bandgap polymers is that they can be applied to highly efficient triple junction solar cells.[94] Recent work indicates that by stacking a wide and two small bandgap polymer is a feasible way, and PCE up to 9.6% has been obtained.[70] Higher efficiencies were achieved by staking a wide, a medium bandgap, and a small bandgap polymer together. By fine-tuning the thickness of each layer to match the photocurrents, efficiencies of over 11% have been reported.[95,96] Figure 11 summaries the device structures of the above-mentioned triple junction solar cells. Currently, the efficiency is still limited by the overlapping of the absorption of each layers; further lowering the bandgap should lead to even higher performance for the triple junction solar cells. It is worth mentioning that the vacuum-processed small molecule multi-junction solar cells have also achieved over 11% PCE, but the

DOI: 10.1021/acs.chemrev.5b00165
Chem. Rev. XXXX, XXX, XXX−XXX

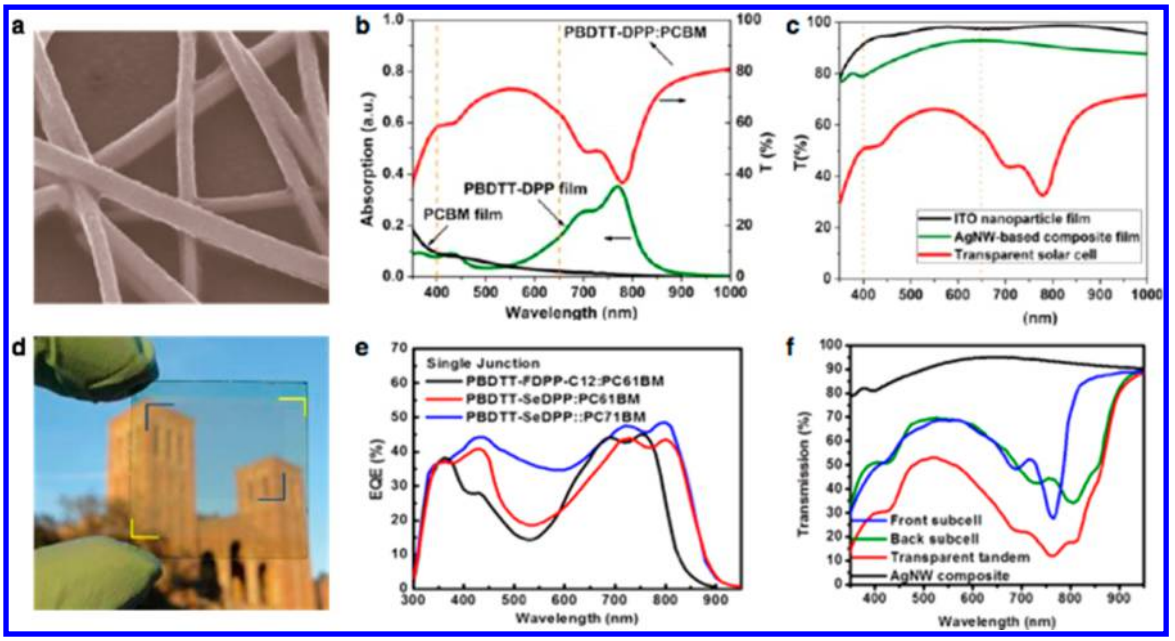

Figure 13. (a) Scanning electron microscope (SEM) image of an Ag-NW:TiO_2 sol−gel composite film; (b) absorption spectra of low-bandgap polymer donor PBDTT-DPP (**P11**), and acceptor PCBM, and transmission spectrum of polymer blend film; (c) transmission spectra of ITO nanoparticle film, AgNW:TiO_2 film, and complete TOPV device; and (d) picture of a large area TOPV device. Reprinted with permission from ref 105. Copyright 2012 American Chemical Society. (e) EQE curves of single junction TOPV devices with different polymer−acceptor combinations. (f) Comparison of the transmission spectra of single junction and tandem TOPV devices based on low-bandgap polymers. Reprinted with permission from ref 107. Copyright 2013 Royal Society of Chemistry.

details will not be discussed because it is beyond the scope of this Review.[97]

3.3. Low-Bandgap Polymers in Semitransparent Organic Solar Cells

Aside from traditional solar farm applications, transparent solar cells may find use for a variety of applications including powered windows for building-integrated photovoltaics (BIPV), automobiles, green houses, and, more recently, portable electronics. The absorption (and transmission) of both active materials and the transparent conductors are important contributors to the performance of semitransparent solar cells. Significant efforts have been made in developing transparent conductors over the past few decades, including both vacuum-based (e.g., ITO, FTO, AZO, thin metal films) and solution-based (e.g., conductive polymers, carbon nanotubes, graphene, metal nanowires, etc.) approaches.[98−100] However, the absorption and photoresponses of the active layers set the intrinsic limit of the solar conversion efficiency. Here, we will focus on addressing this topic.

Traditional solar cells are not designed for transparent applications. To obtain higher efficiencies, a strong absorption across the solar spectrum is necessary. Si, CIGS, and GaAs absorb nearly all of the visible light, and a certain portion of the near-infrared, depending on the bandgap. Thin film amorphous silicon technology is advantageous in its transparency, and can typically achieve semitransparency through sputtering of a transparent conducting oxide (e.g., ITO) as a top electrode or removal of part of the metal electrode (typically by laser ablation) to achieve the intrinsic reddish-brown color of a-Si.

Semiconducting organic molecules/polymers provide an unprecedented possibility for tuning semiconductor bandgap and color that enables a rich opportunity in transparent solar cell research. In the early days of OPV research, the polymers or small molecules that yielded high efficiencies typically possessed a strong absorption in the visible region. For example, there have been multiple reports of semitransparent OPVs using the traditional P3HT as a donor absorber material in both conventional and inverted cell configurations.[101] With absorption up to 650 nm, the "transparent" device has color tunability similar to that of the a-Si semitransparent solar cell. Shrotriya et al. used a thin metal layer as a transparent electrode to a construct a MEH-PPV (bandgap of 2.2 eV, absorb up to 550 nm)-based semitransparent cell with ∼1.1% PCE, and also realized a four-terminal tandem OPV device through stacking two cells together.[102] Another excellent example is Jen's group's semitransparent OPV work using a high performance polymer, poly(indacenodithiophene-*co*-phenanthro[9,10-*b*]quinoxaline), with a bandgap of 1.67 eV.[103] A surfactant/thin Ag electrode allowed the building of color-neutral semitransparent OPVs (Figure 12a). The power conversion efficiency is strongly correlated to the average visible-light transmittance (AVT) of the devices (Figure 12b). The PCE ranges from 2.6% (@30.2 AVT) to 5.63% (@13% AVT).

Pushing the active layer donor material into even lower bandgap (∼1.4 eV or lower), and thus longer wavelength absorption, effectively enabled so-called visibly transparent solar cells (TOPV). The new generation of donor polymers with lower bandgap is dominated by using donor moiety and acceptor moieties to lower the bandgap and tune the energy level position. These copolymers showed two distinct absorption bands. When one of them is deep in the near-IR range, the other one is typically in the UV range. This leaves the visible range with much weaker absorption. As a result, when incorporating good transparent conductor electrodes, it is possible to use thick enough active layer materials to pursue high efficiency using near-IR and UV photons, and at the same time maintain high transparency in the visible range. In applications requiring high visible transparency, for example,

DOI: 10.1021/acs.chemrev.5b00165
Chem. Rev. XXXX, XXX, XXX−XXX

power window (building and/or automobile), or screen of portable electronics such as smart phone or pad, the new type of solar cell is unique and very attractive. The progress in achieving high efficient TOPV is, however, limited by the low bandgap active material, which can give not high external quantum efficiency (EQE) in the near-IR and UV region, but also minimal photovoltage loss. In 2011, Lunt et al. reported a visibly transparent OPV device using an evaporated small molecule, chloroaluminum phthalocyanine (bandgap ∼1.5 eV, absorption up to ∼820 nm), as a donor material, and C_{60} as an acceptor.[104] The device structure is shown in Figure 12c. ITO was used as both transparent electrodes, and MoO_3 and BCP were used as hole and electron transport buffer layers. Figure 12d shows the EQE curves of several devices. A dip in the visible region (450−650 nm) is clearly seen, which is due to the weak material absorption in the spectrum range. The weakness of the system is also clear, as even the nontransparent cell only had the highest EQE value of ∼20%, much lower than the state-of-the-art OPVs. The best TOPV device has a near-IR EQE of ∼17.5%. Two smart optical components were used to enhance the performance. By putting broad-band antireflection (BBAR) coatings on both sides of the TOPV device, the total transparency was increased by 4−6%. The second component is a distributed Bragg reflector (DBR) formed by alternating TiO_2 and SiO_2 layers, which functions as near-IR mirrors that are transparent in the visible region. Therefore, without much sacrifice in visible transparency, the near-IR photons can be used as effectively as in nontransparent cell to improve efficiency, verified by the similar near-IR EQE peak at ∼740 nm. The effect of DBR is clearly visible, which enhances the near-IR EQE peak value from ∼13% to ∼17.5%. Overall, a TOPV with 1.7% PCE was achieved with an impressive 56% AVT.

The low EQE issue was greatly relieved via the progress in low bandgap polymer research. As we have reviewed in the former sections, there have been several reports on polymer solar cells with a near-IR EQE over 50%. It is particularly interesting that many of these low bandgap polymers also have a low bandgap−V_{OC} offset, another important parameter for achieving high efficiency.

To realize the full potential of TOPV, Yang et al. explored an all-solution-processed TOPV concept using **P11**, as it had proven success by achieving 6.5% in a single junction device, 50% near-IR EQE.[105] The solution-processed transparent electrode is based on the work of an Ag-NW:metal oxide composite electrode concept. Figure 13a shows the SEM image of an Ag-NW:TiO_2 sol−gel composite film, in which the TiO_2 NPs were fused at the junction between Ag-NWs during solvent removing and significantly enhanced the conductivity of the thin film.[106] The absorption spectra of PBDTT-DPP and PCBM films are shown in Figure 13b, together with the transmission spectrum of the blend film. Using the C_{60}-based PCBM, high visible transmission is clear to see. The transparent electrode consists of the Ag-NW:TiO_2 sol−gel and another ITO nanoparticle layer coated on top to fill the empty space between nanowires. Figure 13c shows the transmission spectra of the Ag-NW:TiO_2 film, ITO NP film, as well as the complete TOPV device. Fully solution-processed visibly transparent TOPV with an AVT of almost 70% was achieved over the 400−650 nm range. Figure 13d shows a photograph of a large area TOPV device. When illuminated from the ITO substrate side, a high PCE of 4.02% was achieved with V_{OC} = 0.77 V, J_{SC} = 9.3 mA/cm^2, and FF = 56.2%. The EQE peak in the near-IR region (∼780 nm) is over 35%, more than double that of the small molecule-based device.

The same strategy is easily transferrable to other polymers. A good example is **P12**, which is comparable to **P11**, has red-shifted absorption up to 900 nm, and enhanced EQE and PCE (6.5% to 7.2%) in preliminary material testing. As shown in Figure 13e, the TOPV device based on **P12** now has a peak near-IR EQE of ∼45% when use PCBM as the acceptor. The PCE cannot achieve 4.5% with an AVT of 63% from 400−650 nm. In replacing the acceptor with $PC_{71}BM$, the visibly transparent solar cell yields 5.6% efficiency, and the AVT remains at 48%. The semitransparent version of the cell has a neutral tune similar to Jen's case, and the color neutral high visible transmittance is expected to be attractive in certain applications. To further test the potential of TOPV, a tandem structure was utilized. In addition to **P12** polymer with 1.38 eV bandgap, they combined it with another 1.49 eV bandgap polymer to form tandem transparent cell.[107] The two materials were selected on the basis of parameters of transparency in visible region, and current balancing (particularly photo-response in near-IR region). Figure 13f shows the transmission spectra of single junction TOPV cells (front cell PBDTT-FDPP-C12, a polymer similar to **P11** but two thiophene units are substituted by furan, back cell **P12**) and the tandem TOPV. In all cases, the acceptor is PCBM for high visible transparency. With two absorption layers, the tandem TOPV still shows impressive peak visible transmission of over 50% (AVT 43%), and PCE of 6.4%. A 7.3% semitransparent solar cell was achieved when a $PC_{71}BM$ acceptor was used in a **P12** subcell, for which the AVT remained at 30%. It is worth mentioning that this is achieved without DBR and BBAR components, which will further enhance the TOPV performance.[108]

3.4. Low-Bandgap Small Molecules-Based Solar Cells

At present, one of the key limiting factors for organic solar cells is the mismatch of the absorption spectrum of the active layer and the solar spectrum. In parallel with low-bandgap polymer donor materials, recently, bulk heterojunction (BHJ) OSCs based on solution-processed near-IR small molecules photovoltaic materials have attracted increasing attention, and several reviews have been published.[109−113] To fully utilize the solar emission spectrum and increase the power conversion efficiency (PCE) of OSCs, it is necessary to design and synthesize low bandgap conjugated organic molecules with a strong absorption from the visible region to the near-IR. Such low-bandgap small molecules should have the same applications as the polymeric counterparts in tandem solar cells, semi-transparent solar cells, near-IR photodetectors, ambipolar field-effect transistors, etc. To date, the efficiency of solution-processed low-bandgap small molecule OSCs has reached 7%, making these materials ideal candidates for solution-processed OSCs.[114] One of the main approaches toward near-IR small molecules is the implementation of a strong donor−acceptor push−pull system with single or multiple electron-withdrawing units.[115] Various low bandgap small molecules involving median acceptor units such as DPP, BT, isoindigo, and squaraine have been reported, and the presence of these planar, proquinoid building blocks in the π-conjugated systems dramatically reduced the HOMO−LUMO gap of the materials.

3.4.1. Low-Bandgap Small Molecules Based on DPP. Organic dyes based on diketopyrrolopyrrole (DPP) have been widely used to construct low-bandgap materials due to its planar conjugated structure, high extinction coefficient, photo-

DOI: 10.1021/acs.chemrev.5b00165
Chem. Rev. XXXX, XXX, XXX−XXX

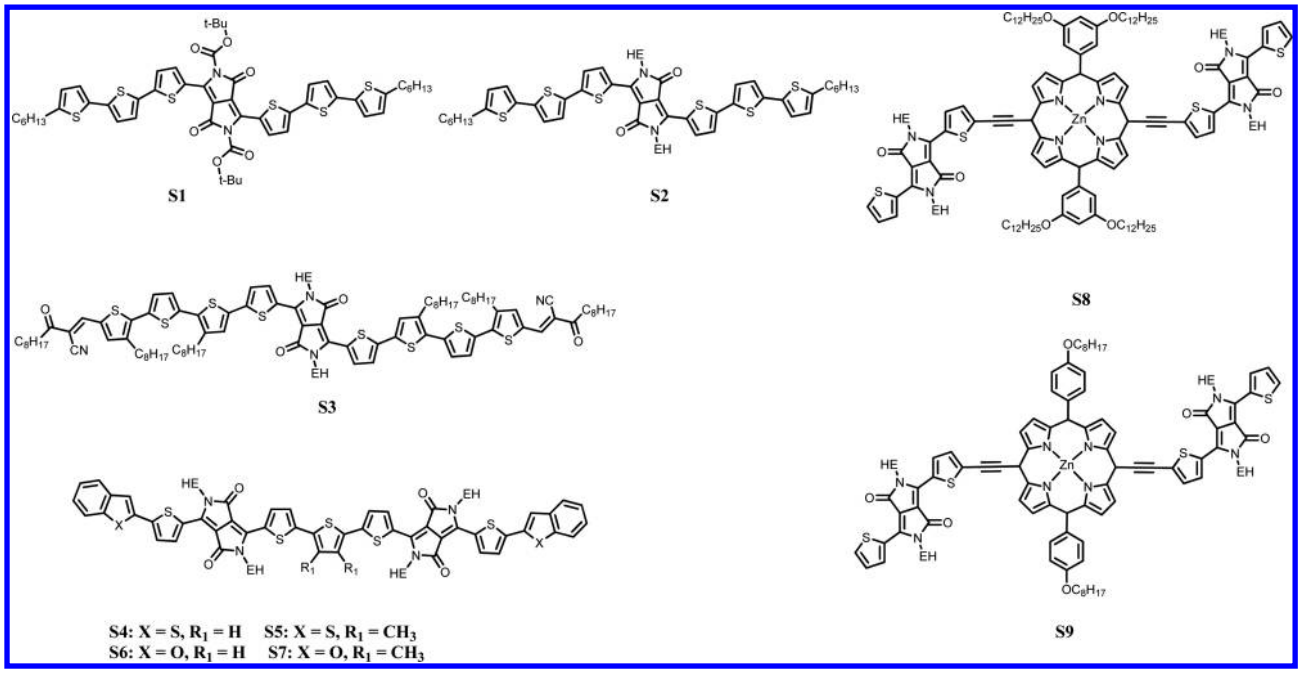

Figure 14. Chemical structure of near-IR small molecules **S1**−**S9**.

chemical stability, as well as its strong electron-accepting ability.[116,117] The energy levels and the optical bandgaps can be tuned finely by introducing the DPP unit into a conjugated backbone of small molecules. The DPP-based low bandgap small molecules have been widely used for BHJ OSCs, and some representative molecules are shown in Figure 14.

Nguyen et al. reported two near-IR D−A−D small molecules **S1** and **S2** (Figure 14) containing DPP as the core unit in the backbone and with oligothiophene as end-capping groups.[118,119] The films of the two molecules all showed strong absorption in the visible and near-infrared regions. As shown in Figure 15, the absorption band edge of compound **S1**, which using *t*-Boc as protecting group, is shifted from 1.72 eV in solution to 1.51 eV in film due to the molecular ordering in the solid state.[118] Solar cells using blend solutions of **S1** with PCBM exhibit a best PCE of 2.33%, with a V_{OC} of 0.67 V, a J_{SC} of 8.42 mA cm^{-2}, and a FF of 0.45, when the donor/acceptor ratio is 70:30. This small molecule **S1**, however, might not be thermally stable in the long term as the *t*-Boc protecting groups can be cleaved off at high temperatures. Nguyen et al. further synthesized a new DPP-based small molecule **S2**, which contains ethylhexyl substitute in the DPP unit, with onset absorption extent to 800 nm and HOMO and LUMO levels of −5.2 and −3.7 eV, respectively.[119] The high degree of ordering in the pure donor film is maintained in blended films, resulting in good hole mobilities. The HOMO and LUMO levels of this small molecule are −5.2 and −3.7 eV, respectively. A PCE of 3.0% is obtained with a J_{SC} of 9.2 mA/cm^2, a V_{OC} of 0.75 V, and a FF of 44%. This is the highest PCE reported at that time for solution-processed small molecule solar cells. Attachment of ethylhexyl groups on the oligothiophene-DPP donor (**S2**) system increases the thermal stability and solubility, lowers the HOMO level, and further enhances film-forming properties as compared to the *t*-Boc derivative (**S1**).

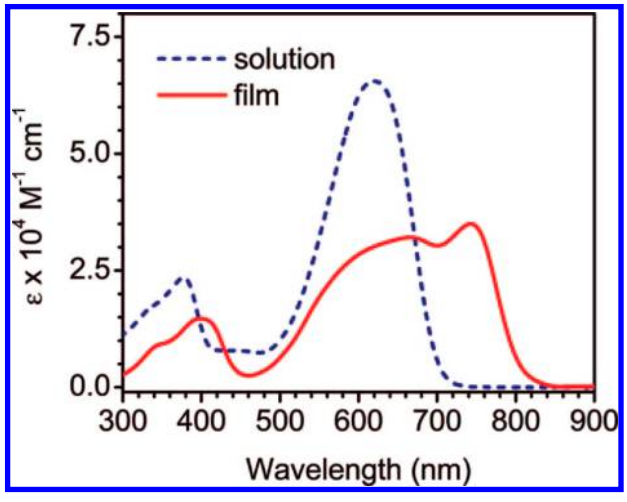

Figure 15. UV−vis of **S1** in solution and film. Reprinted with permission from ref 118. Copyright 2008 American Chemical Society.

Russell et al. developed a near-IR photon-active small molecule **S3**, a multi electron-withdrawing group-based molecule, by using octyl cyanoacetate units end-capping the DPP-based D−A−D molecule to further narrow the optical bandgap.[120] The optical bandgap is approximately 1.41 eV, as determined from the absorption onset of the thin film (880 nm). The photovoltaic device based on as-cast S3/PC$_{71}$BM film showed a poor PCE of 1.18%, with a J_{SC} of 2.8 mA/cm^2, a V_{OC} of 0.74 V, and a FF of 58%. The PCE was significantly improved to 4.73% with an optimized DIO concentration of 3%, combined with a V_{OC} of 0.72 V, a high J_{SC} of 13.6 mA/cm^2, and a FF of 47.6%. This increased J_{SC} is a direct indication of the formation of a better interpenetrating morphology with larger interfacial area.

One useful method to further narrow the optical bandgap of small molecules is to introducing more electron-withdrawing DPP units into their conjugation backbone. Near-IR small molecules based on bis-DPP and tri-DPP have been designed and synthesized for application in organic solar cells by different research groups.[121] Janssen and co-workers developed four structurally similar bis-DPP-based low bandgap small molecules

DOI: 10.1021/acs.chemrev.5b00165
Chem. Rev. XXXX, XXX, XXX−XXX

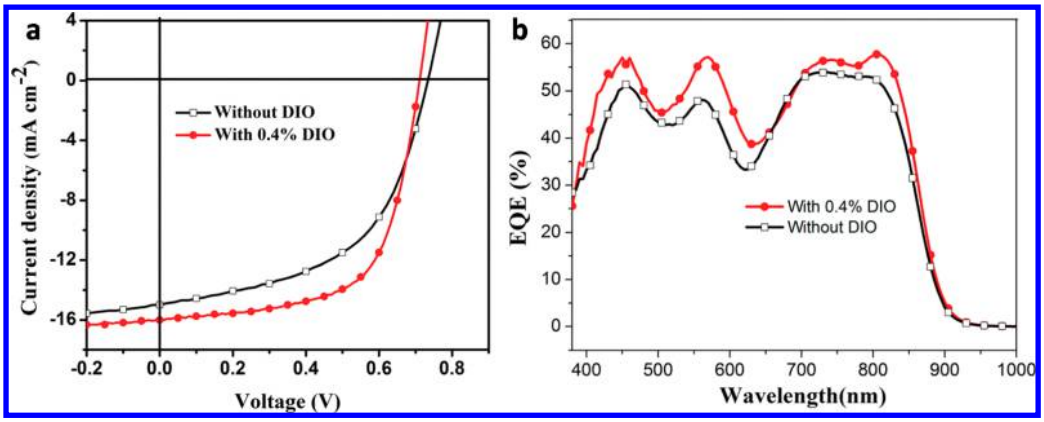

Figure 16. (a) $J-V$ characteristics of the OSCs based on **S12**/PCBM blends (1:1.2, w/w) processed with 0.4% DIO additive. (b) The EQE curves of the devices based on **S12**/PCBM blends (1:1.2, w/w) processed with and without 0.4% DIO. Reprinted with permission from ref 114. Copyright 2014 Royal Society of Chemistry.

end-capped with benzothiophene or benzofuran.[122] All absorption bands of these small molecules extend to the near-IR region, shown as the onset absorptions of 821, 838, 837, and 838 nm for **S4**, **S5**, **S6**, and **S7**, respectively. The four bis-DPP molecules (**S6**–**S9**) possess nearly identical bandgaps (from 1.48 to 1.51 eV) and energy levels, but their solubility is very different. **S4** and **S5** with a central thiophene ring are poorly soluble in chloroform at room temperature (<1 mg/mL), but can be dissolved (>10 mg/mL) in 1,1,2,2-tetrachloroethane (TCE) at 90 °C. In contrast, **S6** and **S7** with a central 3,4-dimethylthiophene ring are easily soluble in chloroform (>10 mg/mL). The bis-DPP molecules were blended with $PC_{71}BM$ and used as photoactive layers in photovoltaic devices. With carefully adjusted processing conditions, the PCEs obtained for the four bis-DPP derivatives can be optimized to a fairly limited range between 3.6% and 4.6%, but the highest PCE is obtained for the derivative with the lowest solubility (**S4**). The optimized BHJ devices based on **S4** with a concentration of 16 mg/mL in TCE reach PCE of 4.6%, with a V_{OC} of 0.69 V, a J_{SC} of 11.9 mA/cm^2, and a FF of 57%. The photovoltaic devices from 3,4-dimethylthiophene-based molecules **S6** and **S7** processed from TCE solution gave a dramatically reduced performance as a result of a significant drop in J_{SC} and FF. The results illustrate that fairly small structural changes in the molecular structure can strongly affect solubility and that the solubility is an important parameter in making efficient blend layers and improving the photovoltaic performance.

Porphyrin-based π-conjugated systems have been extensive studied due to their fast electron transportation, high molar absorption coefficients, and easily tunable properties via synthetic modifications.[123] These physical and chemical properties make porphyrins suitable for photovoltaic properties studies, and significant efforts have been devoted to porphyrin-based OSCs with a bandgap as low as 1.3 eV reported.[124,125] Peng and co-workers successfully designed and synthesized a class of interesting bis-DPP-based near-IR small molecules using porphyrin as the core unit (Figure 14). The typical DPP electron-withdrawing units was linked by an ethynylene bridge to a porphyrin core. Because of the π-conjugation of the whole molecule and the push–pull property of the porphyrin core and DPP, the small molecule, **S8**, showed significant red-shifts of the absorption spectrum. Notably, the absorption of **S8** film shows a shoulder peak at 790 nm, which is attributed to the formation of a vibronic crystalline structure and could be beneficial to a higher hole mobility and photovoltaic performance for OSCs. The optical bandgap of **S8** is estimated to be 1.41 eV from the onset of the absorption spectrum in the film. The HOMO and LUMO energy levels of **S8** are estimated to be −5.18 and −3.39 eV, respectively. The near-IR small molecule **S11** shows a PCE of 3.71%, combined with a J_{SC} of 9.75 mA/cm^2, a V_{OC} of 0.76 V, and a FF of 50.0%. The PCEs of the BHJ OSCs are increased to 4.78% from 3.71% by incorporating 3.0% pyridine into the host solvent of S8:PCBM, combined with a V_{OC} of 0.80 V, a J_{SC} of 11.88 mA/cm^2, and a FF of 50.2%. The enhanced PCEs are attributed to the fact that a small quantity of pyridine additive could lead to a better interpenetrating network by preventing the active layers from undergoing large-scale phase separation, a more balanced charge transport, and a slightly enhanced crystallinity.

Most recently, as an analogue of molecule **S8**, **S9** was synthesized by replacing the 3,5-di(dodecyloxy)-phenyl groups with 4-octyloxy-phenyl groups (Figure 14), which simultaneously facilitate intramolecular charge transport and increase the intermolecular $\pi-\pi$ stacking in film due to the less bulky substituents at the porphyrin periphery.[114] This small molecule **S9** shows a very low optical bandgap of 1.36 eV obtained from the onset absorption of the film. The HOMO and LUMO energy levels were estimated to be −5.07 and −3.60 eV according to the CV measurement. As shown in Figure 16, when processed without any additive, the best BHJ device provided a PCE of 5.83% with a V_{OC}, a J_{SC}, and a FF of 0.74 V, 14.97 mA/cm^2, and 52.64%, respectively. When the widely used additive 1,8-diiodooctane (DIO) was employed, the performance of the OSCs based on **S9** was enhanced significantly. The best device, which was processed with 0.4% DIO, provided a PCE of up to 7.23% (with V_{OC} = 0.71 V, J_{SC} = 16.0 mA/cm^2, and FF = 63.67%), which is the highest PCE of solution-processed BHJ solar cells based on porphyrins and their derivatives to date. All of the devices processed with and without a DIO additive show a very wide range of photocurrent generation in the region of 380–900 nm, and the EQEs (Figure 16) in the whole region increased when DIO was used due to more even film and continuous interpenetrating networks.

3.4.2. Low-Bandgap Small Molecules Based on Isoindigo. Isoindigo, which has been used in the dye industry for a long time, has some advantages similar to DPP such as strong electron-withdrawing ability, low HOMO levels, and

DOI: 10.1021/acs.chemrev.5b00165
Chem. Rev. XXXX, XXX, XXX–XXX

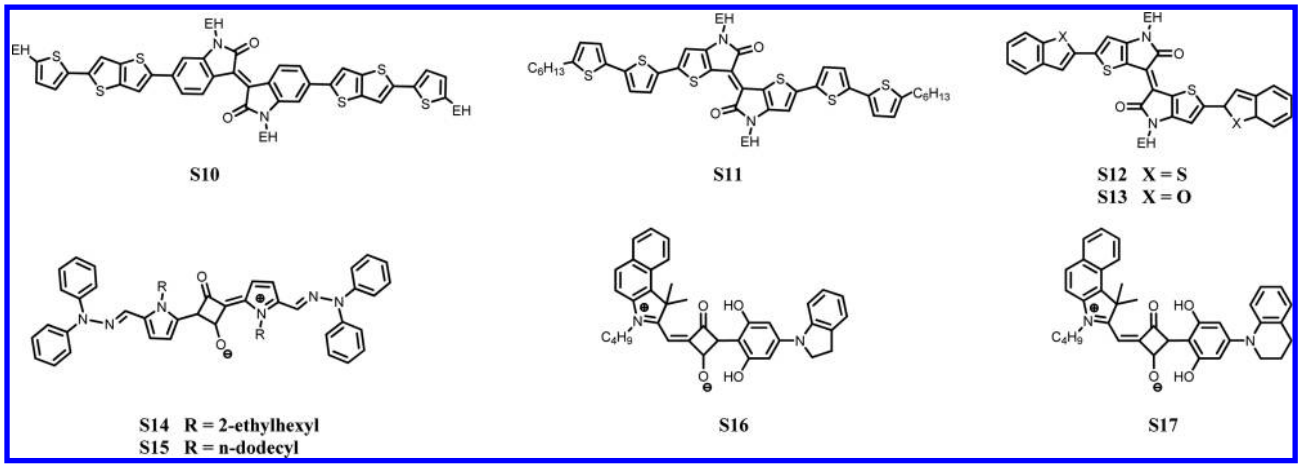

Figure 17. Chemical structures of near-IR small molecules **S10**−**S17**.

large planar architecture.[126−132] Roncali et al. reported an isoindigo-based D−A−D near-IR small molecule, which exhibits a low bandgap of 1.48 eV.[127] However, the photovoltaic device based on this molecule gave very poor performances (PCE = 0.01%), suggesting that the hydrogen bonding locks the molecular packing into an organization unfavorable for efficient exciton diffusion and/or charge transport. Yang et al. design an isoindigo-based low bandgap small molecule (**S10**) by introducing the rigid and coplanar thieno[3,2-*b*]thiophene (TT) unit.[128] This small molecule shows a low bandgap of ∼1.5 eV and a low-lying HOMO energy level of ∼5.39 eV. The photovoltaic device based on **S10** as the donor and PCBM as the acceptor exhibited a preliminary PCE of 1.41%, with a V_{OC} of 0.72 V, a J_{SC} of 6.03 mA/cm^2, and a FF of 32.5%. The low PCE may be ascribed to the serious phase separation of the active layer because of the low miscibility with PCBM.

The thienoisoindigo was thienopyrrolone units but replacing the outer phenyl rings of isoindigo with thiophenes, in which the short oxygen−sulfur interaction of thienoisoindigo enhances the planarity. The thiophene ring shows stronger electron-donating properties than the benzene ring, and the optical absorption of the thienoisoindigo-based conjugated materials can extend into the near-IR region. Yang et al. reported a thienoisoindigo-based near-IR small molecule **S11**, which showed a low bandgap of 1.42 eV calculated from the UV−vis absorption onset.[129] The devices show a power conversion efficiency of 1.14% with a V_{OC} of 0.44 V, a J_{SC} of 7.76 mA/cm^2, and a FF 33%. The EQE curve extends to the near-infrared region (around 900−1000 nm).

Near-IR small molecules **S12** and **S13**, where a thienoisoindigo unit is capped with benzothiophene or benzofuran, were synthesized by Mori et al. (Figure 17).[130] From the film absorption spectra, both absorption bands of **S12** and **S13** extend to ∼850 nm. From the single-crystal structure analyses of **S12** and **S13**, these two π-frameworks of thienoisoindigo-based molecules show high planarity as predicted by the DFT calculation, and form slipped one-dimensional stacks. The OFETs of **S12** and **S13** show typical p-channel properties. Notably, the OFETs of **S12** and **S13** on tetratetracontane-modified substrates exhibit well-balanced ambipolar performance resulting from the delocalization of the frontier molecular orbitals. The photovoltaic devices of **S12** and **S13** show PCE of 0.4% and 1.1%, respectively. After being annealed at 110 °C for 15 min, the PCEs were improved to 1.5% for **S16** and 2.4% for **S17**. The planar structure of the thienoisoindigo unit changes the molecular packing and the thin-film morphology, and consequently improves the OFET and OPV properties.

Cabanetos et al. reported a low bandgap π-conjugated small molecule based on a central thienoisoindigo end-capped with triphenylamine moietiy attached by acetylenic linkers.[131] Using chloroform as solvent, the best BHJ device exhibits a maximum PCE of 2.23%, with a V_{OC} of 0.82, a J_{SC} of 5.48 mA/cm^2, and a FF of 39.8%. Karakawa et al. developed an unsymmetrical A−D−A′ type near-IR conjugated small molecule.[132] In this small molecule, both thienoisoindigo and isoindigo thiophene analogue, in which one of the benzopyrrolidone parts of isoindigo is replaced with thienopyrrolidone to form an unsymmetrical structure, were used as electron-withdrawing end group, and benzodithiophene was used as electron-rich core unit. The optical bandgap of 1.49 eV was estimated from the film absorbance onset, and a best PCE of 1.51% was achieved.

3.4.3. Low-Bandgap Small Molecules Based on Squaraine. Another class of dyes with high extinction coefficients in the red and near-IR spectral regions are squaraines and have been explored for use in OPV.[133] Squaraine dyes are notable for their advantages such as facile synthetic access, a wide variety of possible structural motifs, excellent photochemical and photophysical stability, and exceptionally high absorption coefficients that can extend absorption spectra to near-IR.[134] In 2008, Marks et al. reported the use of appropriately designed squaraines (**S14**, **S15**) as effective, long-wavelength donor components in BHJ OSCs and the effects of core modification on active layer film morphology and OPV response.[135] As shown in Figure 18, the absorption of the films is broad and covers the 550−900 nm region, where the solar photon flux is maximum. The HOMO and LUMO energies of **S14** and **S15**, estimated by cyclic voltammetry, are −3.3 and −5.0 eV, respectively, for both molecules, demonstrating that the alkyl chains negligibly affect the redox properties. Spin-casting of a 1:3 squaraine:PCBM blend film from $CHCl_3$ solutions yields PCEs of 1.24% and 0.89%, with V_{OC} of 0.62 and 0.59 V, J_{SC} of 5.70 and 4.72 mA/cm^2, and FF of 35% and 32%, for **S14** and **S15**-based devices, respectively. The PCE of 1.24% is among the highest efficiencies reported for small-molecule OSCs at that time.

By introducing the pyrylium salts into the squaraine dyes, Rao et al. reported two low bandgap small molecules, which show optical bandgaps of 1.48−1.52 eV.[136] The best device

DOI: 10.1021/acs.chemrev.5b00165
Chem. Rev. XXXX, XXX, XXX−XXX

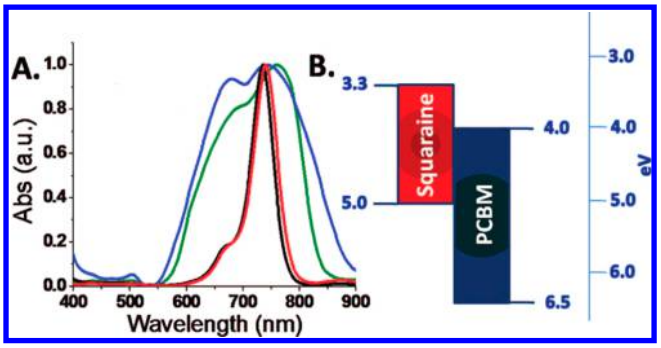

Figure 18. (A) Normalized optical absorption spectra: **S14** (red line) and **S15** (black line) as solutions in $CHCl_3$; **S14** (green line) and **S15** (blue line) as films from $CHCl_3$. (B) HOMO/LUMO levels for **S14** and **S15** vs PCBM. Reprinted with permission from ref 135. Copyright 2008 American Chemical Society.

processed from BHJ blend cast from additive DIO−THF and then thermally annealed showed a PCE of 3.14%. The increased performance has been attributed to the improvement of the crystalline nature of the blend, leading to the balanced charge transport due to the increased hole mobility. Zhao et al. designed and synthesized two near-IR asymmetrical squaraine dyes **S16** bearing indoline as an end-capper and **S17** bearing 1,2,3,4-tetrahydroquinoline as an end-capper.[137] Determined by the absorption spectra onset of the films, the optical bandgap of **S16** is lower than that of **S17** (1.43 vs 1.49 eV), which was among the lowest bandgap of photovoltaic materials based on asymmetrical squaraine dyes. As compared to **S17**, **S16** exhibits a lower bandgap, broader absorption band, much shorter intermolecular distance, and higher carrier mobility, which are attributed to its more planar conformation. Solution-processed BHJ device based on **S16** shows an impressive J_{SC} of 11.03 mA cm^{-2}, a FF of 0.48, and an excellent PCE of 4.29%, while that based on **S17** exhibits a J_{SC} of 9.50 mA/cm^2, an FF of 47%, and a PCE of 3.66%. The results indicate that **S16** is a perspective electron donor candidate, and the indoline-modification strategy may pave a new way for achieving photovoltaic devices with greatly improved J_{SC} and PCE.

3.4.4. Low-Bandgap Small Molecules Based on BODIPY. Boron dipyrromethane (BODIPY) dye has excellent photophysical properties such as good chemical and photochemical stabilities, a high extinction coefficient, and optical features that can easily be tailored by chemical transformation, allowing them to be used in BHJ solar cells.[138−141]

Yao et al. reported three BODIPY-based near-IR small molecules, **S18**, **S19**, and **S20** (Figure 19).[142] All of these small molecules show broad absorption bands with onset absorption extending to 880−900 nm. They found that **S19** tends to pack in a more ordered way than **S18** in the pristine film, which might benefit from the intermolecular interaction from the halogen bond. However, when $PC_{71}BM$ is blended, the packing ordering from the two monomers (**S18** and **S19**) is devastated. In contrast, the dimer **S20** forms an even more ordered packing than monomer **S19** in pure film, and, more interestingly, the packing ordering can be held well in blend films with $PC_{71}BM$. The enlarged conjugation and twisted structure of **S20** contributes to the enhancement of the intermolecular interaction, which is conductive to the well-ordered packing even in blend films. The enhancement of the packing is in agreement with the values of hole and electron mobility: **S20**-based device gives the highest and the most balanced hole and electron mobility. *J*−*V* and EQE curves of **S18**, **S19**, and **S20**-based devices are shown in Figure 20. The J_{SC} values of the three molecule-based devices share the same sequence with the charge carrier mobility: **S18** (6.80 mA/cm^2) < **S19** (7.62 mA/cm^2) < **S20** (11.28 mA/cm^2). With the great enhancement of the J_{SC}, the **S20**-based system possesses the highest PCE of 3.13%. The results demonstrate that dimerization via the meso-position is an effective way to improve the J_{SC} of BODIPY-based small molecule solar cells without bringing on a negative effect on the thermal stability with respect to introduction of the halogen atom. Note that all of these molecule-based devices show the low FF (<40%). The low FF is always seen from the BODIPY-based solar cells, suggesting that the performance of BODIPY-based devices could be further improved by material design and device optimization.[143] The crystalline behavior of the three donors in the solid state with and without $PC_{71}BM$ was also investigated by grazing-incidence X-ray diffraction (2D GIXRD) (Figure 21). As clearly seen from Figure 21b and c, higher order up to fourth and even fifth diffractions can be clearly seen from the **S19** and **S20** pure films, while only the second-order reflection is detected from the **S18** neat one. Clearly, **S19** tends to pack more orderly and tightly than **S18** in

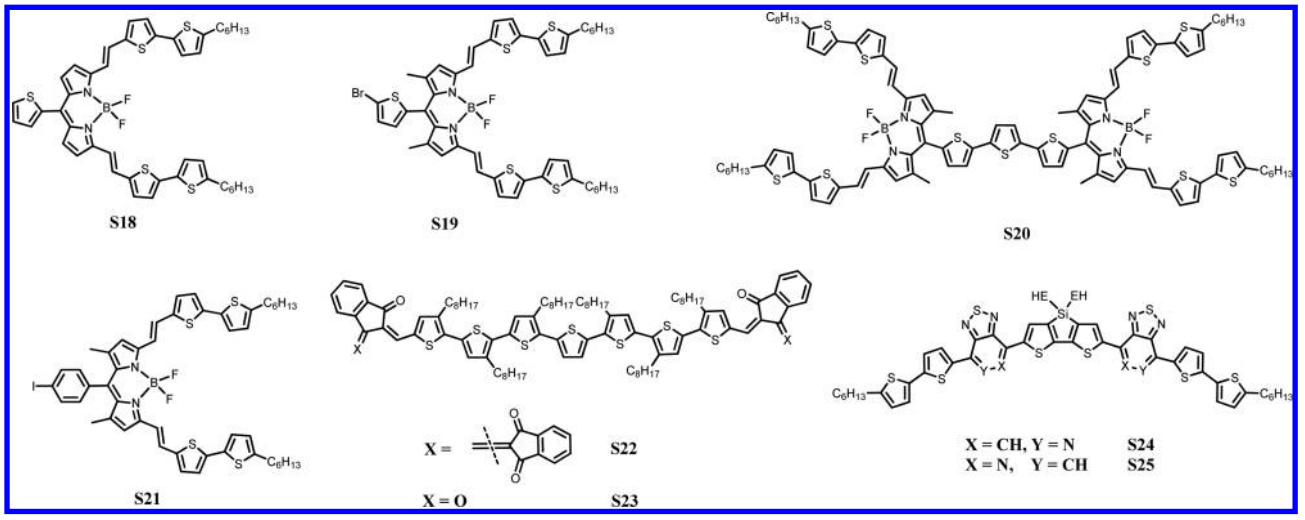

Figure 19. Chemical structure of near-IR small molecules **S18**−**S25**.

DOI: 10.1021/acs.chemrev.5b00165
Chem. Rev. XXXX, XXX, XXX−XXX

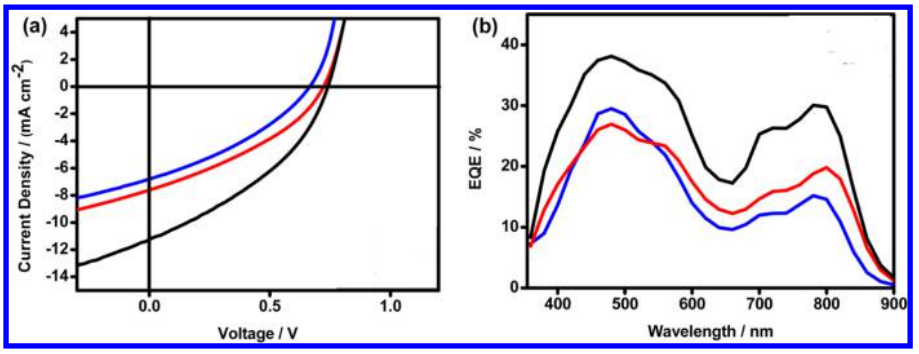

Figure 20. (a) *J*–*V* characteristics and (b) EQE curves of **S18** (blue line), **S19** (red line), and **S20** (black line)-based cells under the optimal D:A weight ratio. Reprinted with permission from ref 142. Copyright 2014 American Chemical Society.

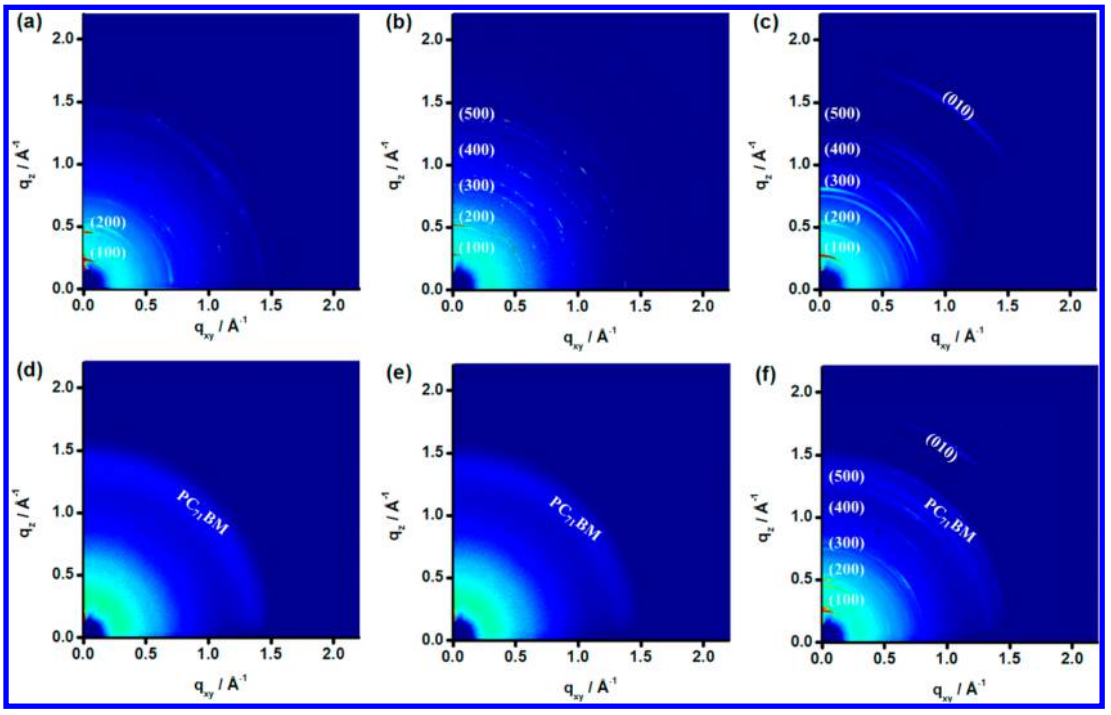

Figure 21. 2D GIXRD images of the three donors in neat (a–c) and blend films with $PC_{71}BM$ (d–f): (a) **S18**, (b) **S19**, (c) **S20**, (d) **S18**:$PC_{71}BM$, (e) **S19**:$PC_{71}BM$, and (f) **S20**:$PC_{71}BM$. Reprinted with permission from ref 142. Copyright 2014 American Chemical Society.

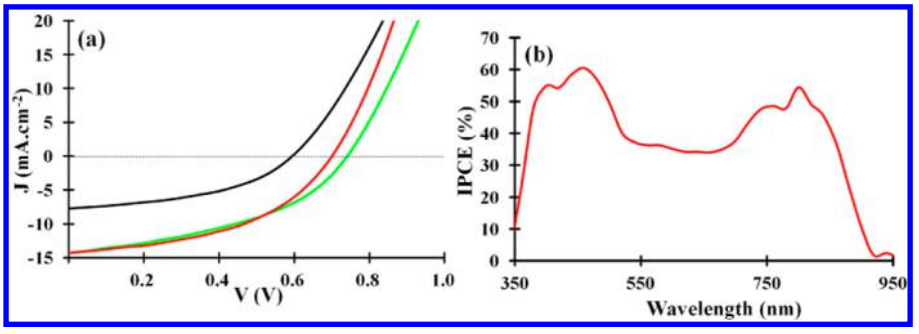

Figure 22. (a) *J*–*V* characteristics for the best **S21** photovoltaic cells with an active layer obtained from chloroform solution with a **S21** concentration of 5 mg/mL (black) and from chlorobenzene solutions with a **S21** concentration of 40 mg/mL and an Al cathode (green) or a Ca/Al cathode (red). (b) IPCE spectrum corresponding to the best **S21**-based device. Reprinted with permission from ref 144. Copyright 2012 American Chemical Society.

the neat films, and **S20** forms even more ordered packing because **S20** gives stronger higher order diffractions and, particularly, shows a clear arch shape of the (010) diffraction in the 2D GIXRD image (Figure 21c).

Ziessel et al. have designed and synthesized a BODIPY-based near-IR green-absorbing dye, **S21**, which shows a low bandgap of 1.45 eV.[144] These planar bis-thienyl-BODIPY derivatives favor short contact distances between neighboring molecules in the solid state and exhibit high charge mobility (in the 1×10^{-3}

DOI: 10.1021/acs.chemrev.5b00165
Chem. Rev. XXXX, XXX, XXX–XXX

$cm^2\ V^{-1}\ s^{-1}$ range) and an ambipolar behavior as measured by using **S21** as a semiconductor layer in standard bottom-contact OFET. The HOMO and LUMO levels calculated from cyclic voltammetry are −5.32 and −3.86 eV, respectively. These data indicate that **S21** dye is a suitable candidate to be used as electron donor when blended with PCBM in BHJ solar cells. As shown in Figure 22, solution-processed BHJ device based on **S21**/PCBM provides a maximum PCE of 4.7%, with a V_{OC} of 0.7 V, a high J_{SC} of 14.2 mA/cm^2, a FF of 47%, and a broad EQE ranging from 350 to 920 nm with a maximum value of 60%. The relatively high V_{OC} is attributed to the low-lying HOMO level (−5.32 eV) of **S21**.

BODIPY-based low bandgap small molecules can also be used as acceptor in BHJ OSCs. Two low bandgap (∼1.5 eV) A−D−A molecules containing terminal BODIPY moieties conjugated through the meso- position were synthesized by Thayumanavan and coauthors.[145] Inverted photovoltaic device with P3HT:acceptor weight ratio of 1:1.5 using 3% CN additive shows the best PCE of 1.51%, which indicates the potential application of BODIPY-based acceptor materials in OSCs.

3.4.5. Low-Bandgap Small Molecules Based on Oligothiophene. Oligothiophenes possess extensive π-electron delocalization along the molecular backbone and are well-known as good electron-donating building blocks for high performance solar cells. Conjugated small molecules with highly polarizable π-electron systems involving oligothiophene electron-donating units and electron-withdrawing units have been widely investigated for narrowing the bandgaps of small molecules.[146] Chen et al. designed and synthesized two near-IR small molecules based on oligothiophene end-capped with electron-withdrawing dye moieties (1,3-indanedione and its derivative), forming A−D−A type molecules **S22** and **S23** in 2014.[146d] The optical bandgaps of **S22** and **S23** thin film were estimated from the onset of the film absorption spectra to be 1.33 and 1.49 eV, respectively. The authors found that the electron-withdrawing end groups not only have a huge effect on the bandgap and energy level of these small molecules, but also have a great impact on the solubility of the molecules and the packing mode in the film. The poor packing at solid state and too low LUMO level (ca. −3.72 eV) of **S22** lead to a relatively low PCE of 0.66%. Molecule **S22** lacked sufficient solubility to be processed into a SM BHJ device. In contrast, **S23**-based devices have a high PCE of 4.71%, with a V_{OC} of 0.80 V, a J_{SC} of 8.21 mA/cm^2, and a notable FF of 0.72. With the addition of 0.3 mg/mL PDMS, the performance of the optimized devices was slightly improved to a PCE of 4.93%, with a V_{OC} of 0.80 V, a J_{SC} of 8.56 mA/cm^2, and a FF of 0.72. The improved efficiency is due to the slightly reduced domain size (probably closer to the ideal domain size for charge separation and transportation) in the active layer.

In 2011, Bazan and co-workers reported a class of low bandgap small molecules with a modular molecular framework, which contained PT, dithieno[3,2-*b*;2′,3′-*d*]silole, and oligothiophene chromophores.[147] Photophysical properties of these compounds can be tuned by controlling the electron-withdrawing PT unit. The small molecule **S24**, in which the pyridyl N atoms of the PT unit are in a distal regiochemistry, exhibit absorption throughout the region of greatest photon flux in the solar spectrum, with a maximum absorption peak of 720 nm and an onset absorption of 820 nm. The effects of thermal annealing on thin films of **S24** were also examined. The authors found that the optical density of the lowest energy absorption peak is progressively increased upon thermal annealing at temperatures at or below 110 °C, which were attributed to better $\pi-\pi$ packing. Further heating above 110 °C results in no significant changes. The HOMO and LUMO energy levels of **S24** were estimated to be −5.16 and −3.60 eV, respectively, from the onset of oxidation and reduction. The optimized device made from **S24** and $PC_{71}BM$ gave a PCE of 3.2%, a J_{SC} of 10.9 mA/cm^2, a V_{OC} of 0.70 V, and a FF of 42%. As an analogue of molecule **S24**, the small molecule **S25**, in which the two pyridyl nitrogen atoms of the PT unit are in a proximal orientation, exhibits a bandgap of ∼1.5 eV, as determined from the onset of the thin film (815 nm).[148] The HOMO and LUMO levels were estimated to be −5.2 and −3.6 eV, respectively, which is similar to **S34**. A record PCE of 6.7%, with a J_{SC} of 14.4 mA/cm^2, a V_{OC} of 0.78 V, and a FF of 59%, was achieved for the optimized photovoltaic devices. As compared to the pristine active layer, the BHJ film cast with a small amount of DIO (0.25% v/v) as solvent additive shows reduced domain size and improved crystallinity, which allows for a higher donor−acceptor interfacial area and hence more efficient charge carriers generation. It should be noted that MoO_x was used as the hole transport layer to eliminate possible chemical interactions between pyridyl of PT units and weakly acidic PEDOT:PSS film.

4. PHOTODETECTORS SENSING THE NEAR-IR LIGHT

4.1. Basic Concepts of Photodetectors

Sensing the near-IR light is critical for many industrial and scientific applications. Near-IR light carries important information for various application purposes, including optical communications, remote control, nighttime surveillance, and chemical/biological sensing.[149] For inorganic-based photodetectors, tuning the spectral response range is a challenging topic, and fabrication cost is another issue that limits the application.[149] Conjugated low-bandgap polymers with easily tunable chemical structures and electronic properties are promising candidates for high performance, low cost near-IR photodetectors. In combination with printing technology as illustrated in Figure 23a and b, the near-IR polymer

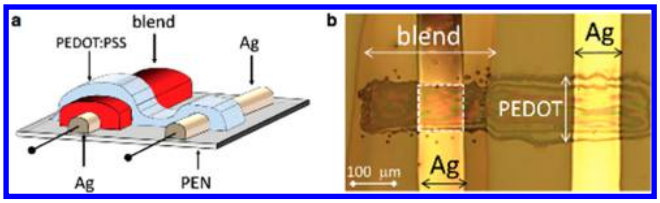

Figure 23. (a) Device structure of a fully inkjet printed polymer photodetector. (b) Optical micrograph of a printed device. Reprinted with permission from ref 151. Copyright 2013 Wiley-VCH.

photodetector array should have the potential for imaging.[150,151] Polymers with bandgap as low as 1 eV have been used in high performance devices, showing detectivities greater than 10^{12} cm $Hz^{1/2}/W$ (or jones).[6] As previously described with solar cells, further accurate tuning of the bandgap and material properties will be the focus for improving the detection sensitivity, selectivity, etc. Such high performance is very competitive for capturing very weak near-IR signals, and thus we can imagine that polymer-based photodetectors may find their future applications in the biocompatible field.[152]

Essentially all photodetectors are operated under the principle that the incident photons cause respective electrical

DOI: 10.1021/acs.chemrev.5b00165
Chem. Rev. XXXX, XXX, XXX−XXX

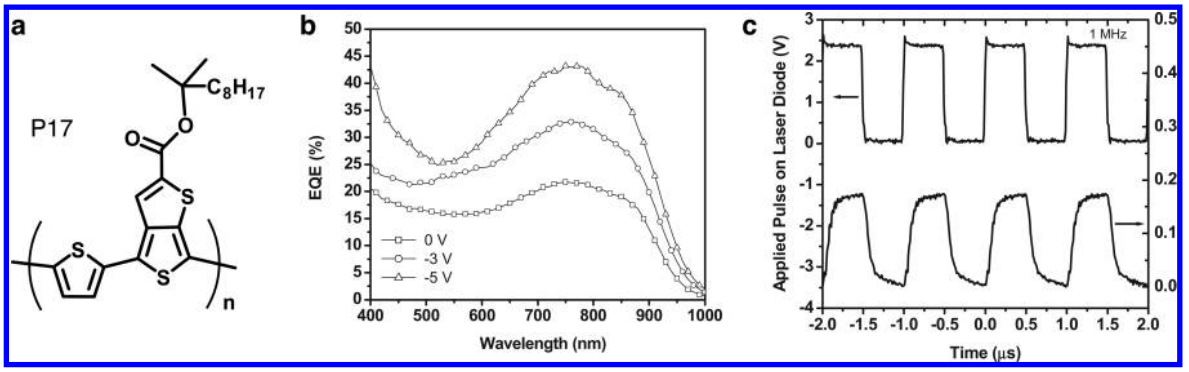

Figure 24. (a) Chemical structure of **P17**. (b) External quantum efficiency of the photodetector using **P17** at different bias voltage. (c) Response speed of **P17**-based photodetectors. Reprinted with permission from ref 157. Copyright 2007 Wiley-VCH.

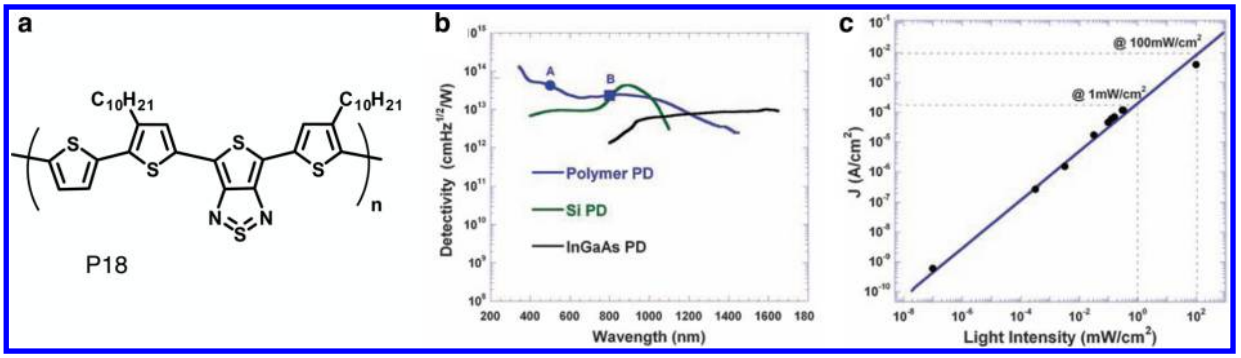

Figure 25. (a) Chemical structure of **P18**. (b) Detectivity of **P18**-based photodetectors at different wavelength (silicon and InGaAs photodetectors are listed for comparison). (c) Linear dynamic range of **P18**-based photodetectors. Reprinted with permission from ref 6. Copyright 2009 American Association for the Advancement of Science.

signals to be detected quantitatively in the circuit.[153] Despite various operational mechanisms of inorganic photodetectors, most of the polymer-based photodetectors use the mechanism of converting absorbed photons into free charge carriers. The decoupling of electrons and holes in strongly bound excitons can be done via various device configurations, traditional diodes, and less popular phototransistors, etc. For imaging purposes, the photodetector array should be defined in a limited area with high resolution, and hence the vertical direction of charge transport in polymer films, that is, the photodiode mode, is favored (Figure 23).[6,152,153] In the transistor structure, however, the charge collection is based on a lateral electrode layout, and requires a gate voltage to have photoresponse. Also considering the charge generation efficiency, the diode type structure is based on a BHJ. As previously described in the OPV section, such a structure has high quantum yield, and is widely adopted in polymer photodetectors.

4.2. Polymer-Based Near-IR Photodetectors

The polymer photodetectors with diode configuration share many common features with solar cells, including the donor/acceptor system, electrodes with different work functions, etc. Basically all organic solar cells can be considered as photodetectors. Yet, to obtain optimal photodetecting performance, photodetectors are not required to deliver any photovoltage as do solar cells. In fact, they must simply deliver photogenerated charge carriers with or without the aid of a bias voltage. There are some photodetectors based on polymer/inorganic nanoparticles that give extremely high photoresponse and detectivity.[154,155] The nonlinear operational mechanisms are not fully understood so far, although it is strongly related to defects in the inorganic semiconductors and interface properties of the hybrid composites. We will exclude this type of photodetector because it is beyond the scope of this Review.

There has been a strong interest in making near-IR photodetectors using low-bandgap organic materials. Early efforts were dominated by the phthalocyanines,[156] until the development of low-bandgap polymers caught up after 2007,[157] when more new polymers became available to pursue high performance polymer photodetectors. For example, Yao et al. explored the near-IR photodetector based on **P17** (chemical structure of **P17** is shown in Figure 24a) and PCBM bulk heterojunction.[157] The polymer has a bandgap of 1.2 eV, with a photoresponse edge at 1000 nm. As shown in Figure 24b, the detector has an average EQE of ~10% for a spectral range of 700−900 nm under 0 V bias, and an average EQE of ~40% under −5 V bias. More importantly, systematic device characterization demonstrated fast response speed (up to 1 MHz as shown in Figure 24c), high noise equivalent power, very low noise current level, etc. Another report in 2007 by Inganäs et al. emphasized a new polymer based on thiadiazoloquinoxaline unit with a bandgap as low as 1 eV, pushing the response tail to 1200 nm.[158] These two pioneering works demonstrated the promising application of low-bandgap polymers for near-IR photodetectors.

Rapid advancement in polymer bandgap engineering has generated a large material library, including some in the polymer solar cell field. It is worth mentioning that high performance solar cells can be used as self-powered photodetectors, because the devices are able to deliver high photocurrent under a zero bias condition. Some polymers with a bandgap of 1.4−1.6 eV have shown a good efficiency of

DOI: 10.1021/acs.chemrev.5b00165
Chem. Rev. XXXX, XXX, XXX−XXX

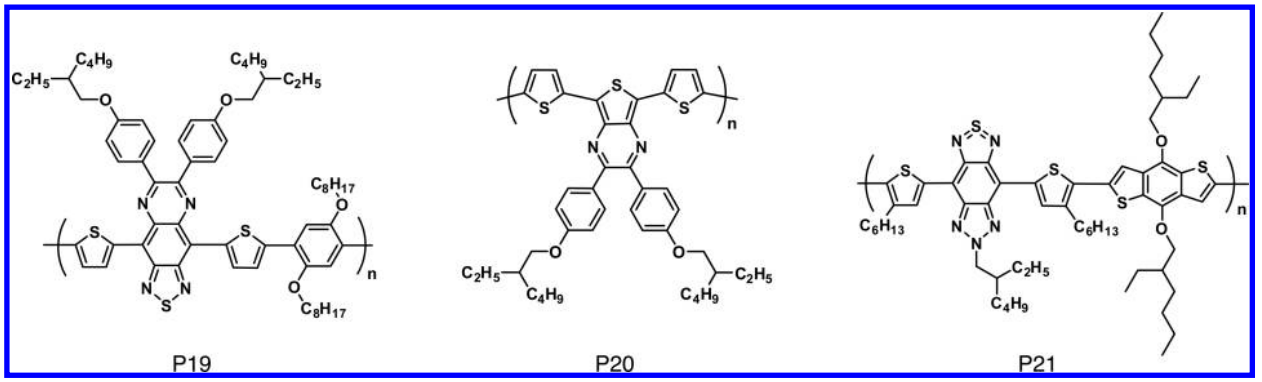

Figure 26. Chemical structures of **P19**−**P21**.

over 7%, such as **P1** and **P8**. In these devices, the photocurrents are relatively independent of voltage in the reverse bias range, and the photodetectors do not require any external power supply. However, with the band-to-band absorption edge extending into the near-IR range, the photovoltage of the polymer−fullerene blend is severely limited by both the bandgap and the HOMO−LUMO offset between the donor and acceptor. In that case, the photodetector devices normally exhibit strong field-dependent recombination loss, and a large reverse bias (e.g., −5 V) is necessary to efficiently extract the photogenerated charge carriers. To operate under strong bias conditions with low noise current, the dark current is minimized by increasing the photoactive layer thickness and by preventing reverse bias injection.[159]

A good example that features high detectivity and a wide spectral range was based on **P18**, as shown in Figure 25a.[6] The strongly electron-withdrawing TP unit in **P18** can also provide a large driving force to stabilize the quinoid resonance structure, and therefore reduce the bandgap very efficiently. **P18** shows a bandgap as small as 0.7 eV with absorption deep into 1450 nm. The device based on the **P18**:PCBM bulk heterojunction hardly gives any photovoltage under light, but gives a broad photoresponse deep into the IR range. The superior photodetector performance is shown in Figure 25b, including high detectivity approaching 10^{12} jones at room temperature. It was demonstrated that with proper interface modification, dark current can be depressed by several orders of magnitude. Figure 25c shows another figure-of-merit for photodetectors, the linear dynamic range (LDR), or photosensitivity linearity. Under illumination at wavelength of 800 nm, the LDR for the best performing device is more than 100 dB, which is close to that of Si (120 dB) and significantly higher than that of InGaAs (66 dB) photodetectors.[6]

Other low-bandgap moieties such as 2-thia-1,3,5,8-tetraazacyclopenta[*b*]naphthalene (**P19**), [1,2,5]-thiadiazolo[3,4-*f*]-benzotriazole (**P20**), and thieno[3,4-*b*]pyrazine (**P21**) units have also been applied into near-IR photodetectors (Figure 26). **P19** has a small bandgap of ∼1.0 eV, and light absorption and photoresponse up to 1200 nm was demonstrated.[158] Investigation of the suitability of **P19**:PCBM photodetectors shows a peak sensitivity at 950 nm and a noise equivalent power (NEP) of 2×10^{-9} W. Chen et al. reported **P20** with intense absorption in the near-IR region, and the estimated optical band-gap of PDTTP was around 1.15 eV.[160] The photodetector based on bulk heterojunction **P20** and PCBM has the incident photon-to-electron conversion efficiency 28.9% at 1000 nm (−5 V) and 6.2% at 1100 nm (−5 V). This photodetector operates at a high speed of 1 MHz. Hu and coauthors reported **P21** with a bandgap of 1.1 eV.[161] Operating at room temperature, the photodetectors have a spectral response from 400 to 1100 nm. By incorporating an alcohol/water-soluble polymer as a cathode interlayer in bulk heterojunction polymer PDs, the polymer photodetectors exhibit a high detectivity of 1.75×10^{13} cm $Hz^{0.5}$ W^{-1} at 800 nm.

There are pros and cons of polymer photodetectors in comparison with their traditional inorganic counterparts. One of the major advantages is that the intrinsic carrier density and thermal emission rate in polymer films are relatively low. Ideally the polymer-based photodetectors give rise to low saturation current (J_o), allowing high detectivity under low light intensity,[6] because J_o is the main component of the noise current at thermal equilibrium. In addition, the carrier density and detectivity are not sensitive to temperature variation, and neither is the detectivity. In reality, the polymer photoactive layer is very thin, and it might cause high leakage current under reverse bias. Meanwhile, undesirable charge recombination may also happen at the interface between the electrodes and the polymer film, where the contact does not have high selectivity of charge carriers. Therefore, to utilize the full strength of the polymers in photodetector devices, device engineering to reduce leakage current and charge recombination is necessary.

Currently the bandgap of polymers can reach 1 eV, while still having reasonable semiconducting properties, such as strong photoluminescence and high carrier mobility etc. However, the challenge remains to (1) further enhance the response time and detectivity to the level comparable to or even superior over the inorganic PDs, and (2) further reach a smaller bandgap range that covers the mid- or even far-infrared light, where thermoelectric polymers might fit in.[162]

4.3. Small Molecule-Based Near-IR Photodetectors

Because of the advantages of high purity, well-defined chemical structures, and easily tunable energy levels, near-IR small molecules-based photodectors have also attracted considerable attention.[163−165]

In 2011, Binda et al. demonstrated a low bandgap squaraine-based photodetector showing high detectivity of 3.4×10^{12} jones at a wavelength of 700 nm.[163] This result was achieved by suppressing the device dark currents while simultaneously preserving its EQE of 15% at 700 nm. The level of reached dark current is in the nA/cm^2 range, analogous to the well mature standard silicon technology.[166] Solution-processed near-IR photodetectors based on a porphyrin small molecule as a donor material and PCBM as an acceptor material were reported by Peng and co-workers in 2014.[164] Operating at

DOI: 10.1021/acs.chemrev.5b00165
Chem. Rev. XXXX, XXX, XXX−XXX

room temperature and at a bias of 0 V, the optimized photodectors show a low dark current density of 3.44 nA/cm^2, a broad spectral response from 380 to 960 nm with a high EQE around 20% in the near-IR region, and detectivities over 10^{12} jones from 380 to 930 nm. In the same year, Wang and co-workers reported two low-bandgap small molecules, which absorb broadly in the spectral region of 300−1000 nm, but weakly in the visible region.[165] The photodetectors based on these two near-IR small molecules exhibited high specific detectivity of 5.0×10^{11} jones at 800 nm at a bias of −0.1 V. By reducing the thickness of the silver electrode, the photodetectors become visibly transparent and still perform well with the detectivities being fairly constant between 10^{11} and 10^{12} jones in the spectral range of 300−900 nm.

5. AMBIPOLAR FIELD-EFFECT TRANSISTORS

5.1. Basic Concepts of Ambipolar Field-Effect Transistors

Organic field-effect transistors show great potential for the fabrication of low cost, flexible, and high-performance electronic devices.[167,168] Ambipolar polymer field-effect transistors (FETs), capable of both hole and electron transport, exhibit more facile processing requirements in circuits and present potential applications in a variety of electronic devices.[21] Most of the conventional conjugated polymers show only p-type transport due to the lack of strongly electron-accepting moieties. Low-bandgap polymers consisting of strong electron-donating and -accepting moieties and possessing shallow HOMO and deep LUMO energy levels are particularly interesting. Such polymers have allowed ambipolar charge transport characteristics in single component FETs.[4,21,28]

A typical organic FET device structure is shown in Figure 27. A thin semiconductor layer is separated from a gate electrode

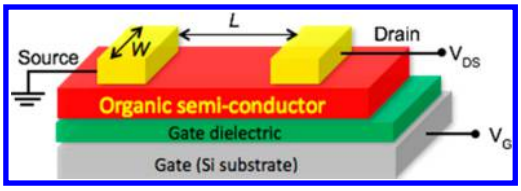

Figure 27. Device structure of bottom-gate top-contact transistor. W is the channel width; L is the channel length; V_{DS} is the voltage between source and drain; and V_G is the gate voltage.

by the insulating gate dielectric (e.g., SiO_2); on top of the semiconductor layer are the source and drain electrodes (e.g., Au) of width W (channel width), separated by a distance L (channel length).[21] Other equivalent device configurations are also used. Voltage is applied to the gate and drain electrode. The source electrode is normally grounded. The potential difference between the source and the gate is the gate voltage (V_G), while the potential difference between the source and the drain is referred to as the source-drain voltage (V_{DS}). In general, high performance for FETs means high charge carrier mobility (μ), large on/off ratio (I_{on}/I_{off}), and low threshold voltage (V_T). The most important and commonly studied parameter is the saturated charge carrier mobility (the channel is pinched off when $V_{DS} \geq V_G - V_T$; the current cannot increase anymore and saturates), which is calculated by

$$\mu_{sat} = \frac{\partial I_{DS}}{\partial V_G} \times \frac{L}{WC} \times \frac{1}{(V_G - V_T)}$$

where I_{DS} is the source-drain channel current and C is the capacitance of the insulating gate dielectric. For an ambipolar field effect transistor, the working mechanism is similar, but can support either hole or electron transport depending on the polarity of the gate voltage.

From a materials point of view, the active semiconductors are required to have HOMO energy levels below −5.0 eV for stable hole transport, and the LUMO level needs to be close to or below −4.0 eV for stable electron transport.[28] Typically, a single metal (i.e., Au) is used as both the source and the drain electrodes. Therefore, the energy gap between the HOMO and LUMO levels should not be too large to avoid charge injection barriers. The development of novel strong electron-withdrawing building blocks plays an essential role for such applications.[4,28]

5.2. Polymer-Based Ambipolar Field-Effect Transistors

5.2.1. Materials Design toward Ambipolar Charge Transport. The chemical structures of some representative low-bandgap polymers for ambipolar FETs are shown in Figure 28. Since Janssen et al. introduced the thiophene-flanked DPP

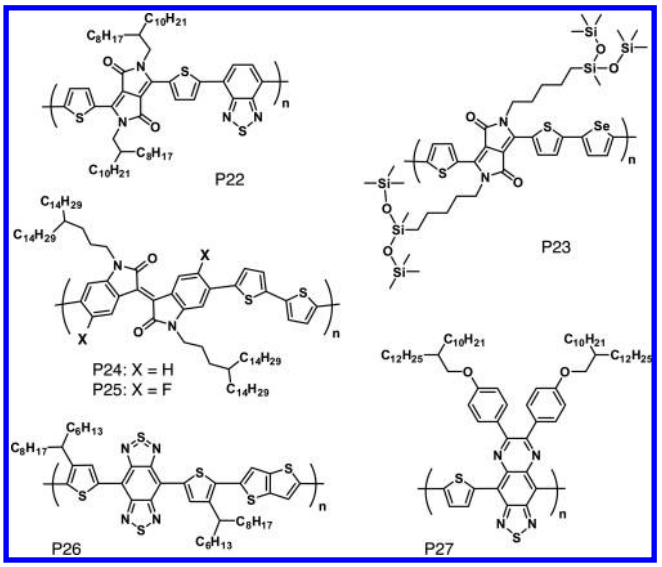

Figure 28. Representative low-bandgap polymers for ambipolar field-effect transistors.

unit into the field of organic solar cells and transistors, many new polymers based on DPP have been designed and synthesized for p-type and ambipolar FET applications.[169] A very high hole mobility of 10 cm^2 V^{-1} s^{-1} in a p-type FET has been achieved recently by Liu et al.[170] One of the very first examples for ambipolar device is **P22**, reported by Sonar and Dodabalapur.[171] Electron-accepting DPP and BT units were used to construct the polymer backbone, and two electron-donating thiophene units were used as spacers, with the aim for balanced hole- and electron-transport properties. Furthermore, fused-ring aromatic DPP and BT structures have a strong tendency to form $\pi-\pi$ stacking with a large overlapping area that favors charge transport. As a result, the polymer has a small optical bandgap of ∼1.1 eV, an electrochemical bandgap of 1.2 eV, and a deep LUMO level of −4.0 eV. The highest hole and electron mobilities of 0.35 and 0.40 cm^2 V^{-1} s^{-1}, respectively, were achieved for P22-based FETs after annealing at 200 °C. Later, by copolymerizing DPP with thieno[3,2-*b*]thiophene, selenophene, naphthalene, azine, emeraldicene, and other units,

DOI: 10.1021/acs.chemrev.5b00165
Chem. Rev. XXXX, XXX, XXX−XXX

high and balanced electron and hole mobility (~1 $cm^2 V^{-1} s^{-1}$) were obtained by several groups.[169] The incorporation of selenium elements into the backbone has been proved to be beneficial, especially for improving electron transport, as indicated by a number of groups.[169,172,173] Side chains on the polymers are also critical. Recently, inspired by Bao's work on siloxane-terminated hexyl chains on an isoindigo-based polymer for p-channel operation,[174] Oh and co-workers synthesized a low-bandgap polymer using diketopyrrolopyrrole-selenophene copolymers featuring hybrid siloxane-solubilizing side groups (**P23**).[7] The polymer exhibited an optical bandgap of ~1.2 eV, a HOMO of −5.1 eV, and a relatively shallow LUMO of −3.5 eV. The alkyl spacer length of the hybrid side chains was systematically tuned to boost ambipolar performance. The optimized three-dimensional charge transport of **P23** yielded unprecedentedly high hole and electron mobilities of 8.84 and 4.34 $cm^2 V^{-1} s^{-1}$. These results demonstrate that the hybrid side chains are promising candidates to improve the self-assembly of the low-bandgap polymers for FETs and bring new insight into molecular design.

Another very interesting electron-accepting building block for ambipolar FETs is fluorinated isoindigo. Reynolds first applied isoindigo in organic solar cells, and then Pei, Bao, Andersson, and others studied it for OPV and FETs.[82,175] Recently, Lei and Pei et al. conducted a systematic investigation on the FET performance on a series of isoindigo-based polymers. Among them, **P24** and **P25** have drawn considerable attention. By introducing two electron-withdrawing fluorine atoms, for the first time, ambipolar charge transport was observed in the isoindigo polymer system.[176] The fluorinated isoindigo-bithiophene polymer, **P25**, has an optical bandgap of 1.5 eV and deep LUMO level of −3.9 eV. It was found that fluorination on the isoindigo unit effectively lowers the LUMO level and significantly increases the electron mobility from 10^{-2} to 0.43 $cm^2 V^{-1} s^{-1}$ while maintaining high hole mobility up to 1.85 $cm^2 V^{-1} s^{-1}$. Another important thing is that the device was fabricated in ambient condition, which indicates that the fluorinated isoindigo polymer has good stability toward moisture and oxygen.

Ultralow-bandgap polymers for high performance ambipolar FETs were reported recently, using a very strong electron-accepting benzobisthiadiazole unit.[177] The BBT unit has four electron-withdrawing nitrogen atoms in the conjugation plan, making it a much stronger acceptor as compared to the BT unit. A representative polymer is **P26**, which has an optical bandgap as small as ~0.6 eV. It has a deep LUMO of −3.8 eV and a high HOMO of −4.4 eV. Maximum mobilities of PBBTTT based FETs were measured to be 1.0 $cm^2 V^{-1} s^{-1}$ for holes and 0.7 $cm^2 V^{-1} s^{-1}$ for electrons. Recently, Andersson and co-workers synthesized another very low-bandgap polymer **P27** using alternating thiadiazoloquinoxaline and thiophene units.[178] Similar to benzobisthiadiazole, the four electron-withdrawing nitrogen atoms make thiadiazoloquinoxaline very strong electron acceptors. In addition, the 2,3-positions of thiadiazoloquinoxaline are connected to electron-donating alkyloxyphenyl groups. Thus, the donor−acceptor interactions not only come from the backbone, but from the vertical direction. **P27** has a very small bandgap of ~0.7 eV and a LUMO of −4.3 eV. Initial investigation shows moderate ambipolar charge transport properties with a hole mobility of 3.0×10^{-2} $cm^2 V^{-1} s^{-1}$ and an electron mobility of 1.4×10^{-2} $cm^2 V^{-1} s^{-1}$. Interestingly, the neutral long-wavelength absorptions of **P27** bleach upon incremental oxidation, and electrochromic contrasts of 25% in the near-IR region (800−1200 nm) were obtained. Worth noting is that these polymers are also promising candidates for plastic photodetectors with responses of up to 2000 nm.

5.2.2. Processing Control toward High Performance. In addition to the bandgap and energy levels, the performance of the ambipolar transistors is also highly dependent on several other important parameters (e.g., solid-state packing and morphology) that are associated with the structure of the polymers. So far, the highest reported mobilities for holes and electrons in an organic ambipolar transistor (using **P23**) are 8.8 and 4.3 $cm^2 V^{-1} s^{-1}$, respectively.[7] The thin film was processed using the solution-shearing method instead of conventional spin coating, which has been proved to be beneficial for achieving better molecular packing by Bao previously.[179] The output characteristics of the device are shown in Figure 29. The

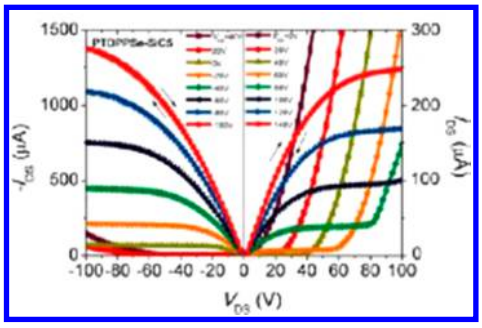

Figure 29. Output characteristics of **P23**-based device. Reprinted with permission from ref 7. Copyright 2013 American Chemical Society.

on−off ratios are lower than unipolar organic transistors (10^5−10^6), especially for the n-channel, which are around 10^2. This is because of the high current engendered by the superior hole-conduction at the "off" state.[7]

Some post-treatments such as thermal annealing are of great importance for achieving better molecular packing and higher mobility. Normally, at elevated temperatures, the polymers will self-organize, and the crystallinity of the film can be enhanced. For example, as shown in Figure 30, **P22** thin film showed an increase in crystallinity when the annealing temperature increased from 25 to 200 °C.[171] High charge carrier mobilities in a **P22** device were obtained from annealing at 200 °C. Thermal annealing also affects the thin film morphology. Figure 31a−c shows the atomic force microscopy (AFM) height images of **P26** films annealed at 80, 240, and 320 °C.[177] For

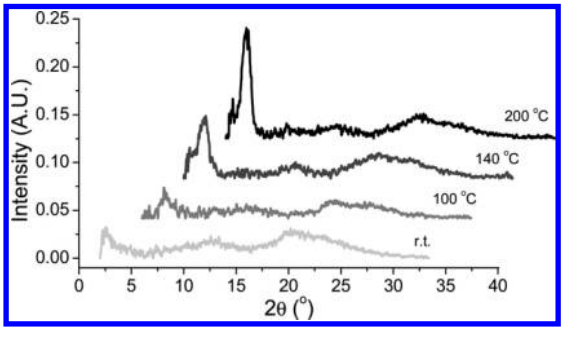

Figure 30. X-ray diffraction data of spin-coated **P22** thin films on decyltrichlorosilane-modified SiO_2/Si substrates annealed at different temperatures. Reprinted with permission from ref 171. Copyright 2010 Wiley-VCH.

DOI: 10.1021/acs.chemrev.5b00165
Chem. Rev. XXXX, XXX, XXX−XXX

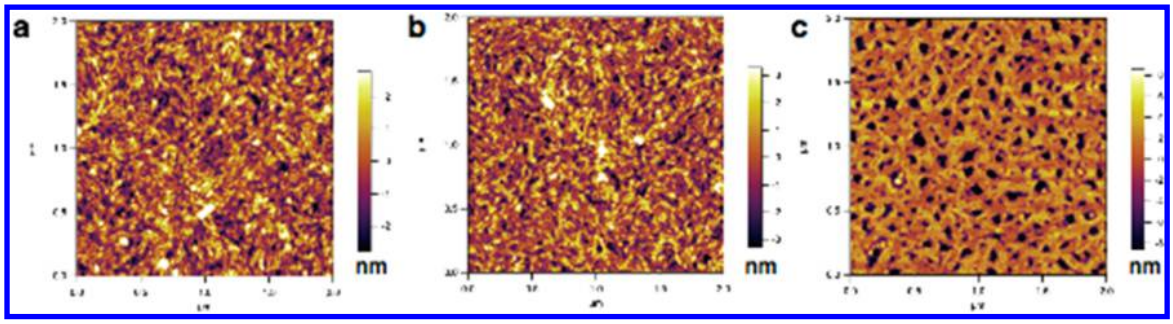

Figure 31. Atomic force microscopy height images of **P26** thin films at 80 °C (a), 240 °C (b), and 320 °C (c) on decyltrichlorosilane-modified SiO_2/Si substrates. Reprinted with permission from ref 177. Copyright 2012 Wiley-VCH.

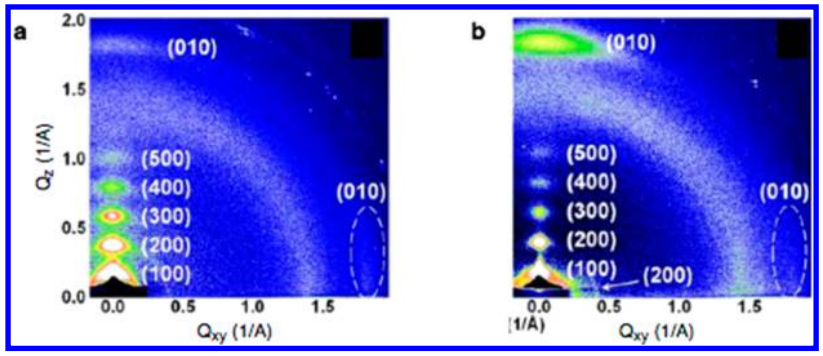

Figure 32. Two-dimensional grazing-incident X-ray diffraction patterns of **P24** (a) and **P25** (b) films. Reprinted with permission from ref 176. Copyright 2012 American Chemical Society.

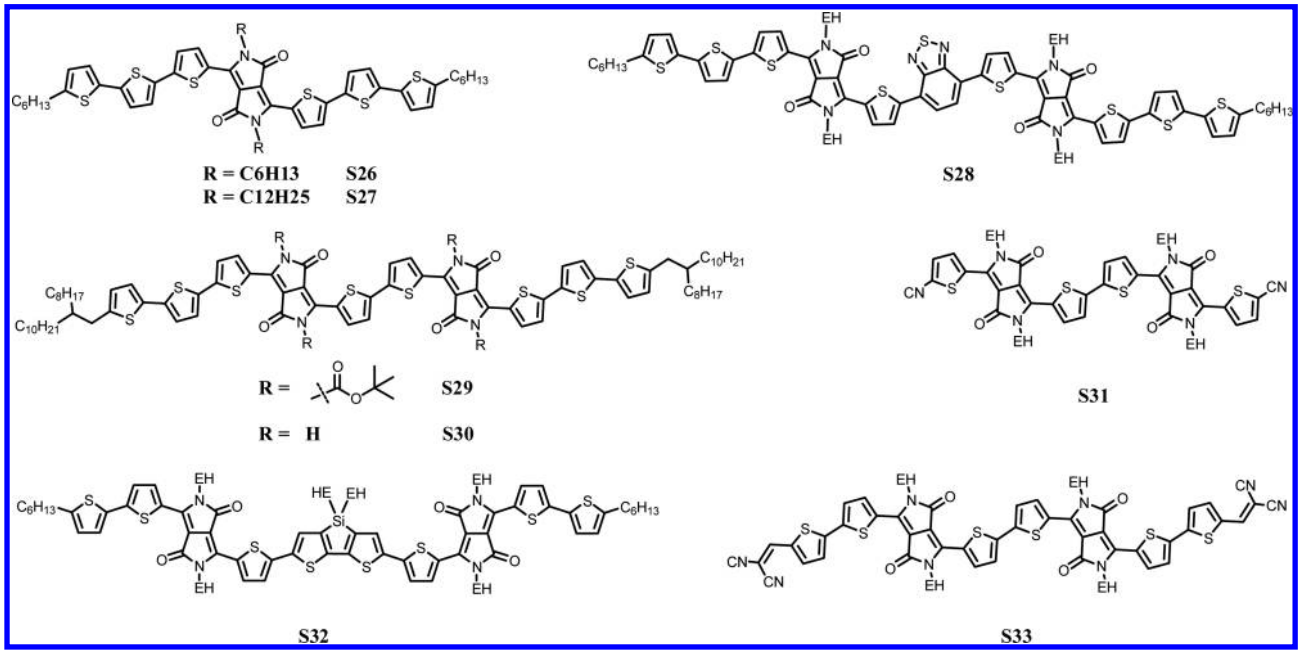

Figure 33. Representative low-bandgap small molecules for ambipolar field-effect transistors.

films annealed at 80 °C, randomly oriented nanorods are shown. Upon annealing at 240 °C, a highly interconnected fiber structure was observed. When annealed at 320 °C, the polymer thin films form uniform nanofibers that establish a more ordered multiple-layer structure. Interestingly, it was found that the p-type mobilities increased with annealing temperature up to 240 °C, indicating that transport improved with the increase in the alignment of the grains within the substrate. However, from 240 to 320 °C, the mobility remains constant despite a significant morphological change.

The molecular orientation of the polymers on the substrates influences the mobility as well. In principle, the "edge-on" orientation (π-conjugation plan perpendicular to the substrate) is more favorable. The type of conjugated backbones and alkyl side chains typically determines the orientation. However, in some cases, the change of a single atom can make a big difference. For instance, introducing two fluorine atoms on the

DOI: 10.1021/acs.chemrev.5b00165
Chem. Rev. XXXX, XXX, XXX−XXX

isoindigo unit can change the polymer orientation preference from "face-on" to "edge-on" on the SiO_2 substrate.[176] As shown in Figure 32a and b, the fluorinated polymer **P25** displays much stronger (h00) diffraction and weaker out-of-plane (010) diffraction, whereas the nonfluorinated polymer **P24** shows very intense (010) diffraction, indicating a strong "face-on" feature. This is probably another reason why **P25** has higher charge carrier mobilities.

5.3. Low-Bandgap Small Molecule-Based Ambipolar Field-Effect Transistors

Conjugated polymers with near-IR absorption have been widely studied in OFETs as discussed above. Near-IR small molecules OFETs also attract great attention. Some representative small molecules with ambipolar properties are shown in Figure 33. In 2008, Nguyen and co-workers first demonstrated two DPP-based low bandgap small molecules for solution-processed FET applications.[180] Thin film morphologies and FET characteristics were investigated as a function of alkyl chain length and thermal annealing. Annealing the films prior to electrode deposition improves the field effect mobility of the devices by increasing the size and regularity of the crystalline domains and reducing the interlayer spacing of both **S26** and **S27**. OTS treatment on Si/SiO_2 substrates also increases the current on/off ratio of the device. The authors found that increasing the alkyl chain length increases the intermolecular spacing and, hence, reduces the field effect mobility. Multiple substitution sites allow for tuning the solubility, leading to ease of processing, and control of thermal properties and intermolecular spacing in the solid state. In 2012, the same group reported a bis-DPP compound, **S28**, with two electron-accepting units (DPP and benzothiadiazole, BT).[181] The BT group strongly increases the electron affinity, leading to n-channel transport characteristics. Solution-processable ambipolar transistors fabricated from DPP-based small molecules show balanced transport behavior with field-effect hole and electron mobilities of up to 1.6×10^{-2} and 1.5×10^{-2} cm^2 V^{-1} s^{-1}, respectively. As shown in Figure 34, the lowest drain current (I_d) from the as-cast **S28** films was observed, and an optimal OFET performance was obtained after annealing at 150 °C. Under different annealing temperatures, all **S28** transistors demonstrate balanced hole and electron carrier mobilities. The sharp increase of μ_{sat} up to 2.1×10^{-3} cm^2 V^{-1} s^{-1} when the annealing temperature increases from 120 to 150 °C may indicate an improved film morphology and/or molecular packing, which were further confirmed by AFM and XRD data.

In 2012, a bis-DPP-based low bandgap molecule (**S29**) with thiophene rings, alkyl chains, and *t*-Boc groups was synthesized by Yamashita and co-workers.[182] The *t*-Boc groups could be subsequently removed by thermal treatment at 200 °C to regenerate NH forms (**S30**). **S40** with bis-DPP cores and four hydrogen-bonding sites showed well-balanced ambipolar behavior with hole and electron mobilities of 6.7×10^{-3} and 5.6×10^{-3} cm^2 V^{-1} s^{-1}, respectively. Hydrogen bonds between the NH groups and adjacent carbonyl groups give highly ordered molecular arrangements in the films, resulting in changes of their electronic properties and FET behaviors.

In 2013, Wang and co-workers demonstrated that the introduction of a cyano group at the terminals of a TDPP dimer not only lowers the HOMO and LUMO energy levels noticeably, but also induces denser intermolecular packing of the oligomer.[183] The bandgap of **S31** calculated from the absorption onsets of the film spectra was 1.48 eV. This

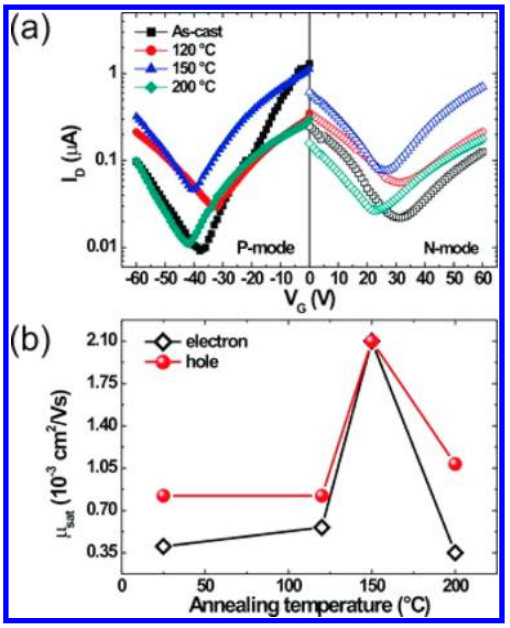

Figure 34. (a) Saturation transfer characteristics of **S28** FETs upon different annealing temperature using Au top contact. (b) **S28** carrier mobility as a function of annealing temperature. Reprinted with permission from ref 181. Copyright 2012 Wiley-VCH.

molecule clearly shows ambipolar semiconducting behavior. For the OTFTs devices based on the pristine **S41** film (~30 nm), a hole mobility of 1.8×10^{-3} cm^2 V^{-1} s^{-1} and an electron mobility of 1.3×10^{-5} cm^2 V^{-1} s^{-1} were obtained. Both hole and electron mobilities were significantly improved upon thermal annealing, which led to hole and electron mobilities of 0.066 and 0.033 cm^2 V^{-1} s^{-1}, respectively, with an on/off ratio of 1.2×10^5 for holes and 4.7×10^3 for electrons at a V_D of ±100 V as measured in air. The ambient ambipolar properties of **S41** were attributed to its relatively low LUMO and dense intermolecular packing, which may be ascribed to its large dipole moment and additional weak intermolecular CN---H hydrogen-bonding interaction.[184,185] The author also claimed that the dense intermolecular packing may help a lot in preventing the diffusion of oxygen and moisture into the dielectric−semiconductor interface.

Cho and co-workers reported a low bandgap silole-based small molecule, **S32**, containing one electron-rich thiophene−dithienosilole−thiophene unit and two electron-deficient DPP units.[186] A solution containing **S32** displayed a strong absorption band over the range 500−780 nm with a maximum absorption at 678 nm. The absorption of the film displayed a large red shift with an absorption onset of 840 nm (1.48 eV), suggesting strong intermolecular interactions of **S32** in the solid state. The as-spun **S42** FET device exhibited ambipolar transport properties with a hole mobility of 7.3×10^{-5} cm^2 V^{-1} s^{-1} and an electron mobility of 1.6×10^{-5} cm^2 V^{-1} s^{-1}. Thermal annealing at 110 °C led to a significant increase in carrier mobility, with hole and electron mobilities of 3.7×10^{-3} and 5.1×10^{-4} cm^2 V^{-1} s^{-1}, respectively. This improvement is strongly correlated with the increased film crystallinity and reduced $\pi-\pi$ intermolecular stacking distance upon thermal annealing. The grazing incidence X-ray diffraction (GIXD) data shown in Figure 35 indicated that thermal annealing induced the **S32** films to undergo a phase transition from an ordered phase I, with $d(h00)$ = 15.6 Å and $d(010)$ = 3.7 Å, to a well-ordered and tightly stacked phase II, with $d(h00)$ = 18.9 Å and

DOI: 10.1021/acs.chemrev.5b00165
Chem. Rev. XXXX, XXX, XXX−XXX

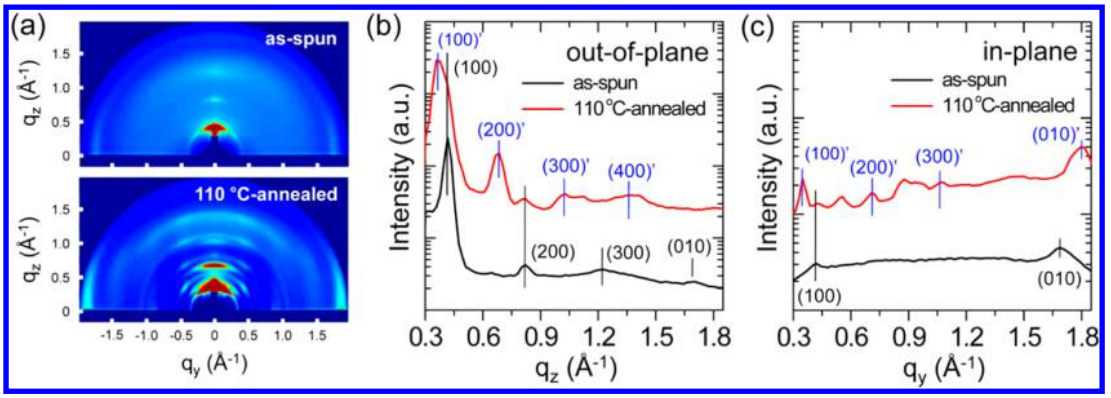

Figure 35. (a) GIXD patterns obtained from the as-spun (top) or 110 °C-annealed (bottom) **S32** films, (b) out-of-plane X-ray diffraction profiles extracted along the q_z direction at q_y = 0.00 Å^{-1}, and (c) in-plane X-ray diffraction profiles along the q_y direction at q_z = 0.03 Å^{-1}. Reprinted with permission from ref 186. Copyright 2014 American Chemical Society.

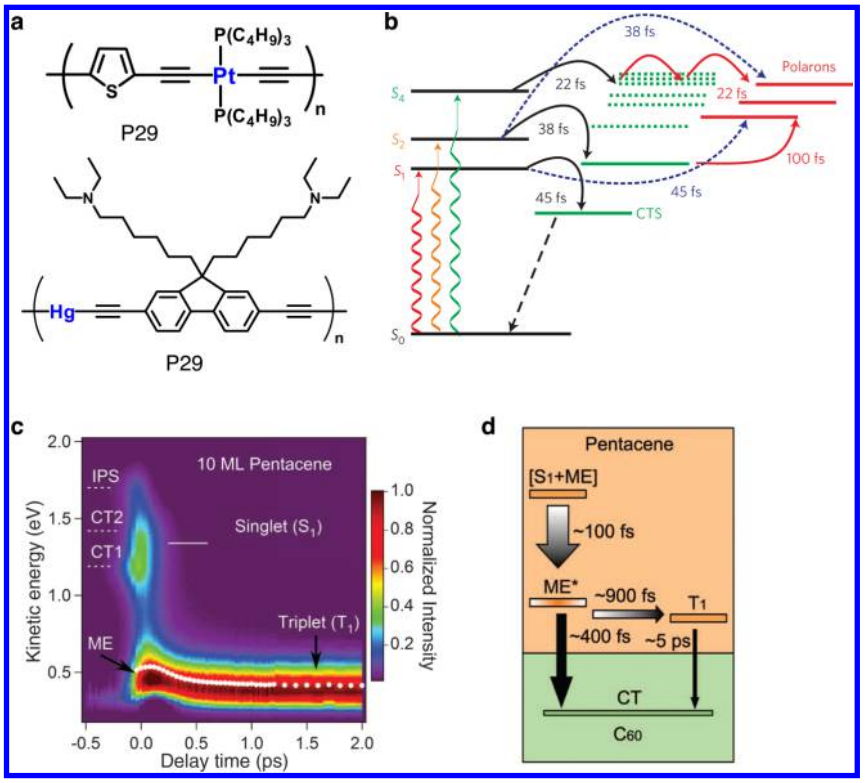

Figure 36. Outlook for potential future directions. (a) Chemical structure of the metal-containing conjugated polymers. (b) Schematic of the proposed mechanism for the hot carrier extraction in the PCPDTBT:PCBM system and excited states involved: singlet exciton states (black lines), interfacial charge transfer states (green-colored levels), and free polarons (red-colored levels). The solid black arrows represent exciton dissociation into the charge transfer state manifold; blue dashed arrows indicate exciton quenching into free polarons, and solid red arrows represent charge transfer state dissociation into free polarons. Reprinted with permission from ref 193. Copyright 2013 Nature Publishing Group. (c) Pseudocolor representation of time-resolved two-photon photoemission spectra for a pentacene sample. The positive delay time with visible-pump and UV-probe shows photoemission from the transiently formed **S1**, the ME, and the T1 states. (d) Summary of exciton decay and charge-transfer dynamics at the pentacene/C60 interface. Reprinted with permission from ref 194. Copyright 2011 American Association for the Advancement of Science.

$d(010)$ = 3.5 Å. At the same time, thermal annealing promoted the development of an edge-on orientation among the crystalline **S32** molecules, in which $\pi-\pi$ stacking interactions among the molecular backbones were oriented parallel to the substrate and the side alkyl chains pointed upward and downward.

A dicyanovinylene-substituted DPP−oligothiophene **S33** with optical bandgap of 1.49 eV was synthesized by Ortiz and co-workers.[187] HOMO and LUMO energies were determined to be −3.68 and −5.27 eV, respectively, from the oxidation and reduction potentials. Field-effect transistors fabricated with **S33** exhibit ambipolar response with balanced hole and electron mobilities of 0.16 and 0.02 cm^2 V^{-1} s^{-1}, respectively, for the as-cast films. No thermal annealing of the semiconductors is necessary to afford high mobility, making it an ideal candidate for low-cost fabrication of devices on inexpensive plastic foils.

DOI: 10.1021/acs.chemrev.5b00165
Chem. Rev. XXXX, XXX, XXX−XXX

6. SUMMARY AND FUTURE PROSPECTS

The above sections present the state-of-the-art low-bandgap near-IR polymers/molecules used in organic photovoltaics, photodetectors, and ambipolar transistors. We believe the rational design of novel donor and acceptor building blocks, fundamental understanding of the basic properties, as well as detailed device engineering are the keys for achieving high performance. Similarities exist among solar cells, light-emitting diodes, detectors, and transistors. People working in different fields can learn and borrow concepts from each other. For instance, Anthopoulos and Patil showed that the triethylene glycol side chain can enhance molecular self-assembly and increase the FET mobility for DPP-based polymers.[188] Borrowing the idea from the FET community, Chang recently demonstrated a **P11** polymer with a certain amount of triethylene glycol side chain instead of using a 100% alkyl chain, and the polymer showed improved charge transport and efficiency (from 6.3% to 7.0%).[189] In another example, Gong applied PS-TPD-PFCB,[190] a commonly used electron-blocking material in light-emitting diodes, in a novel IR photodetector and realized very low dark current and high detection sensitivity.[6]

To achieve more desired properties and even higher performance, new material design concepts as well as a deeper fundamental understanding of the physics and chemistry of the materials are required. For example, as shown in Figure 36a, introducing metallic elements into conjugated polymers may have a strong influence on their optical and electronic properties.[191,192] They can probably reduce the exciton binding energy and enhance the charge transport. Photophysics can be further investigated in the high performance low-bandgap polymer systems, for instance, to utilize the hot carrier extraction for reduction of thermalization loss, and singlet fission for multiple exciton generation. As shown in Figure 36b, Lanzani et al. recently observed hot exciton dissociation in the **P5**:PCBM system.[193] They found that the primary singlet states convert into interfacial charge transfer states and polarons in 20−50 fs, depending on the excess energy. The higher-lying polymer singlet states provide a large amount of excess energy and dissociate before internal conversion, ultimately leading to a higher fraction of polarons. Whether or not this process happens in higher performance polymer systems, and whether hot carriers contribute to higher V_{OC} in photovoltaic devices will be interesting to see. In another work, Zhu et al. directly observed the multiexciton state ensuing from singlet fission (a molecular manifestation of multiexciton generation) in pentacene using femtosecond nonlinear spectroscopies (Figure 36c and d).[194] They found that multiple electron transfer from the multiexciton state to the fullerene occurs on a subpicosecond time scale, which is 1 order of magnitude faster than the triplet exciton state. Again, whether or not these processes happen in low-bandgap materials is fundamentally important. In addition, more advanced characterization techniques should also be introduced to fully understand the photo charge generation. For example, Ginger et al. reported using time-resolved electrostatic force microscopy of studying the local trap states in organic solar cells, which provides a direct link between local morphology, local optoelectronic properties, and device performance.[195] Controlling the thin film morphology of the donor−acceptor blends is critically important for all BHJ organic solar cells.[3,19,38] However, although some effective approaches such as thermal annealing, solvent annealing, and solvent additives have been demonstrated to enhance device efficiency ("better morphology") in specific polymers or small molecules, the practice of device optimization is largely an Edisonian approach. Fully characterizing the complex morphology and establishing a universal molecular structure−property relationship is very challenging. Nevertheless, study of existing polymer morphology still provides quite useful information beneficial to the future materials design. For example, a planar moiety (e.g., BDT) containing polymer often leads to face-on orientation, which is different from the classical P3HT system. These include several families of state-of-the-art polymers for PV application, including BDT-TPD family, BDT-TT family, BDT-DPP family, etc. On the processing technique side, a recent work by Yan et al. shows that by using a hot solution during the spin coating, more ideal morphology can be achieved, and efficiency over 9% has been realized for a series of high performance polymers.[196] Future development of new techniques to fine-tune the phase separation and thin film morphology should lead to higher performance low-bandgap polymer-based solar cells. In fact, the study of polymer solar cell morphology now expanded to multidonor systems.[34] Yang and Li's recent work shows a clear link between the polymers' molecular compatibility (preferred orientations) and the resulting multidonor system morphology, which has a profound impact on the carrier transport and device efficiency. For organic FETs, the charge carrier mobility can be further improved. New chemistry and processing are required to increase the structural order, and preparing single crystalline polymers may be useful. For example, Tseng et al. recently designed a nanogroove on SiO_2 substrate to align the polymers and achieved mobilities as high as 50 $cm^2\ V^{-1}\ s^{-1}$,[197] while Wudl and Dou et al. prepared a highly perfect polymer single crystal using straightforward chemistry.[198] These efforts could inspire new directions for low-bandgap polymers in the near future. We strongly believe novel concepts in materials design and more detailed photophysics study will ultimately drive the organic electronics to a new regime with ultrahigh performance.

In the future, new areas of application could also be explored. So far, the low-bandgap IR polymers/molecules have not been fully investigated in light emitting diodes, lasers, and biosensors, in which they show a promising future. The intrinsic low photoluminescent efficiency and poor stability under a strong field of low-bandgap materials are currently limiting the application in light emitting diodes and lasers. Therefore, new understanding and innovation is required. For biosensor applications, biocompatible and water/alcohol-soluble functional groups should be considered to be attached to the polymers. It is worth mentioning that Bazan and Wang have done pioneering work in this field using wide-bandgap water/alcohol-soluble conjugated polymers, and more efforts are needed to fully uncover the potential of low-bandgap IR polymers for such applications.[199,200] To summarize, important pieces of the low-bandgap IR polymers remain unexplored and unexplained, and there is much room for creativity in the design of new materials for organic electronics, and beyond.

AUTHOR INFORMATION

Corresponding Authors

*E-mail: gangl@ucla.edu.
*E-mail: yangy@ucla.edu.

Author Contributions

[§]L.D. and Y.L. contributed equally.

DOI: 10.1021/acs.chemrev.5b00165
Chem. Rev. XXXX, XXX, XXX−XXX

Notes

The authors declare no competing financial interest.

Biographies

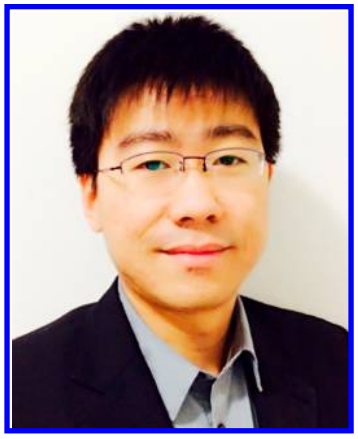

Letian Dou obtained his B.S. in Chemistry from Peking University in 2009. He then joined Prof. Yang Yang's group in the Department of Materials Science and Engineering at UCLA, and obtained his Ph.D. in 2014. His doctoral research focused on the design and synthesis of conjugated polymers for organic/hybrid photovoltaic applications. His research interest also includes the synthesis of small molecules, fullerene derivatives, polymer single crystals, inorganic nanostructures, hybrid materials, and related optoelectronic devices. Currently, he is a Chemist Postdoc Fellow at the Department of Chemistry, University of California-Berkeley and Lawrence Berkeley National Laboratory.

Yongsheng Liu obtained his Ph.D. degree in Organic Chemistry in 2009 from Nankai University under the supervision of Prof. Yongsheng Chen. After two years of postdoctoral training at Nankai University, he joined Prof. Yang Yang's group at UCLA in 2011 as a postdoctoral fellow to work on organic solar cells and perovskite solar cells. His current research interests include organic solar cells, perovskite solar cells, and the investigation of the structure−properties relationship of organic optoelectronic materials and their applications.

Ziruo Hong obtained his B.S. in Chemistry from Sichuan University in 1995. In 1996, he entered Changchun Institute of Optics, Fine Mechanics and Physics of CAS. From 1996 to 2001, he studied condensed matter physics, and received training as a device physicist with expertise in luminescence. His research was focused on excitonic materials-based devices, especially organic light emitting devices (OLEDs) under the supervision of Prof Wenlian Li. From 2005, he started to focus on organic photovoltaics. From 2010 to 2014, he worked on small molecule-based solar cells, as a research/adjunct faculty member of Yamagata University, Japan. He is now doing research on solution-processed organic/inorganic hybrid semiconductors and devices in Prof Yang Yang's group at UCLA. He has published 120 papers.

Gang Li is an associate research professor in the Department of Materials Science and Engineering at UCLA. His current research interest is organic and hybrid semiconductors for energy applications. He has a B.S. in Space Physics from Wuhan University, China, and he got his Ph.D. degree in Condensed Matter Physics from Iowa State University in 2003, studying photophysics of organic light emitting devices (OLEDs). His postdoc work at UCLA was on polymer solar cell/LED with Prof. Yang Yang. Before joining UCLA as research faculty member in 2011, he was the VP of Solarmer Energy Inc. He has over 80 publications and is among Thomson-Reuter's Highly Cited Researchers in Materials Science (2014).

DOI: 10.1021/acs.chemrev.5b00165
Chem. Rev. XXXX, XXX, XXX−XXX

Yang Yang holds a B.S. in Physics from the National Cheng-Kung University in Taiwan in 1982, and he received his M.S. and Ph.D. in Physics and Applied Physics from the University of Massachusetts, Lowell, in 1988 and 1992, respectively. Before he joined UCLA in 1997, he served on the reseasrch staff of UNIAX (now DuPont Display) in Santa Barbara from 1992 to 1996. Yang is now the Carol and Lawrence E. Tannas Jr. Endowed Chair Professor of Materials Science and Engineering at UCLA. He is a materials physicist with expertise in the fields of organic electronics, organic/inorganic interface engineering, and the development and fabrication of related devices, such as photovoltaic cells, LEDs, and memory devices.

ACKNOWLEDGMENTS

This work was supported by the National Science Foundation (CHE 1230598, program manager, Linda S. Sapochak; ECCS 1202231, program manager, Radhakisan S. Baheti; DMR 1335645, program manager, Charles Ying; DMR 1210893, program manager, Andrew J. Lovinger), the Air Force Office of Scientific Research (FA9550-12-1-0074, program manager: Charles Lee), and the Office of Naval Research (N00014-14-1-0648, program manager: Paul Armistead). G.L. would like to thank UCLA Henry Samueli School of Engineering and Applied Science for financial support. We would like to thank Prof. Fred Wudl, Dr. Eric Richard, Mr. Wei-Hsuan Chang, and Ms. Fan Cui for proofreading the manuscript.

REFERENCES

(1) Sun, S.-S.; Dalton, L. R. *Introduction to Organic Electronic and Optoelectronic Materials and Devices*; CRC Press: New York, 2008.
(2) Forrest, S. R. The path to ubiquitous and low-cost organic electronic appliances on plastic. *Nature* **2004**, *428*, 911−918.
(3) (a) Li, G.; Zhu, R.; Yang, Y. Polymer solar cells. *Nat. Photonics* **2012**, *6*, 153−161. (b) Janssen, R. A. J.; Nelson, J. Factors Limiting Device Efficiency in Organic Photovoltaics. *Adv. Mater.* **2013**, *25*, 1847−1858.
(4) Zhao, Y.; Guo, Y.; Liu, Y. 25th anniversary article: recent advances in n-type and ambipolar organic field-effect transistors. *Adv. Mater.* **2013**, *25*, 5372−5391.
(5) You, J.; Dou, L.; Yoshimura, K.; Kato, T.; Ohya, K.; Moriarty, T.; Emery, K.; Chen, C.-C.; Gao, J.; Li, G.; Yang, Y. A polymer tandem solar cell with 10.6% power conversion efficiency. *Nat. Commun.* **2013**, *4*, 1446.
(6) Gong, X.; Tong, M.; Xia, Y.; Cai, W.; Moon, J. S.; Cao, Y.; Yu, G.; Shieh, C.-L.; Nilsson, B.; Heeger, A. J. High-Detectivity Polymer Photodetectors with Spectral Response from 300 to 1450 nm. *Science* **2009**, *325*, 1665−1667.
(7) Lee, J.; Han, A. R.; Yu, H.; Shin, T. J.; Yang, C.; Oh, J. H. Boosting the Ambipolar Performance of Solution-Processable Polymer Semiconductors via Hybrid Side-Chain Engineering. *J. Am. Chem. Soc.* **2013**, *135*, 9540−9547.
(8) Dou, L.; You, J.; Hong, Z.; Xu, Z.; Li, G.; Street, R. A.; Yang, Y. 25th Anniversary Article: A Decade of Organic/Polymeric Photovoltaic Research. *Adv. Mater.* **2013**, *25*, 6642−6671.
(9) Szarko, J. M.; Rolczynski, B. S.; Lou, S. J.; Xu, T.; Strzalka, J.; Marks, T. J.; Yu, L.; Chen, L. X. Photovoltaic Function and Exciton/Charge Transfer Dynamics in a Highly Efficient Semiconducting Copolymer. *Adv. Funct. Mater.* **2014**, *24*, 10−26.
(10) Cheng, Y. J.; Yang, S. H.; Hsu, C. S. Synthesis of Conjugated Polymers for Organic Solar Cell Applications. *Chem. Rev.* **2009**, *109*, 5868−5923.
(11) (a) Carsten, B.; He, F.; Son, H. J.; Xu, T.; Yu, L. Stille Polycondensation for Synthesis of Functional Materials. *Chem. Rev.* **2011**, *111*, 1493−1528. (b) Guo, X.; Facchetti, A.; Marks, T. J. Imide- and Amide-Functionalized Polymer Semiconductors. *Chem. Rev.* **2014**, *114*, 8943−9021. (c) Kroon, R.; Lenes, M.; Hummelen, J. C.; Blom, P. W. M.; de Boer, B. *Polym. Rev.* **2008**, *48*, 531−582. (d) Brédas, J. L. Relationship between band gap and bond length alternation in organic conjugated polymers. *J. Chem. Phys.* **1985**, *82*, 3808−3811.
(12) (a) Li, Y. F. Molecular Design of Photovoltaic Materials for Polymer Solar Cells: Toward Suitable Electronic Energy Levels and Broad Absorption. *Acc. Chem. Res.* **2012**, *45*, 723−733. (b) Li, Y. F.; Cao, Y. *Sci. China: Chem.* **2015**, *58*, 192−209. (c) Li, Y. F.; Zou, Y. P. Conjugated Polymer Photovoltaic Materials with Broad Absorption Band and High Charge Carrier Mobility. *Adv. Mater.* **2008**, *20*, 2952−2958.
(13) (a) Boudreault, P.-L. T.; Najari, A.; Leclerc, M. Processable Low-Bandgap Polymers for Photovoltaic Applications. *Chem. Mater.* **2011**, *23*, 456−469. (b) Roncali, J. Synthetic Principles for Bandgap Control in Linear π-Conjugated Systems. *Chem. Rev.* **1997**, *97*, 173−205. (c) Bundgaard, E.; Krebs, F. C. Low band gap polymers for organic photovoltaics. *Sol. Energy Mater. Sol. Cells* **2007**, *91*, 954−985. (d) Karikomi, M.; Kitamura, C.; Tanaka, S.; Yamashita, Y. New Narrow-Bandgap Polymer Composed of Benzobis(1,2,5-thiadiazole) and Thiophenes. *J. Am. Chem. Soc.* **1995**, *117*, 6791−6792. (e) van Mullekom, H. A. M.; Vekemans, J. A. M.; Meijer, E. W. Band-Gap Engineering of Donor−Acceptor-Substituted π-Conjugated Polymers. *Chem. - Eur. J.* **1998**, *4*, 1235−1243.
(14) Mei, J.; Diao, Y.; Appleton, A. L.; Fang, L.; Bao, Z. Integrated Materials Design of Organic Semiconductors for Field-Effect Transistors. *J. Am. Chem. Soc.* **2013**, *135*, 6724−6746.
(15) Chen, J.; Cao, Y. Development of Novel Conjugated Donor Polymers for High-Efficiency Bulk-Heterojunction Photovoltaic Devices. *Acc. Chem. Res.* **2009**, *42*, 1709−1718.
(16) Mishra, A.; Bäuerle, P. Small Molecule Organic Semiconductors on the Move: Promises for Future Solar Energy Technology. *Angew. Chem., Int. Ed.* **2012**, *51*, 2020−2067.
(17) Pope, M.; Swenberg, C. E. *Electronic Processes in Organic Crystals and Polymers*; Oxford Univ.: UK, 1999.
(18) Wannier, G. H. The Structure of Electronic Excitation Levels in Insulating Crystals. *Phys. Rev.* **1937**, *52*, 191−197.
(19) (a) Brabec, J.; Sariciftci, N. S.; Hummelen, J. C. Plastic Solar Cells. *Adv. Funct. Mater.* **2001**, *11*, 15−26. (b) Günes, S.; Neugebauer, H.; Sariciftci, N. S. Conjugated Polymer-Based Organic Solar Cells. *Chem. Rev.* **2007**, *107*, 1324−1338. (c) Yang, X.; Loos, J.; Veenstra, S. C.; Verhees, W. J. H.; Wienk, M. M.; Kroon, J. M.; Michels, M. A. J.; Janssen, R. A. J. Nanoscale Morphology of High-Performance Polymer Solar Cells. *Nano Lett.* **2005**, *5*, 579−583. (d) Campoy-Quiles, M.; Ferenczi, T.; Agostinelli, T.; Etchegoin, P. G.; Kim, Y.; Anthopoulos, T. D.; Stavrinou, P. N.; Bradley, D. D. C.; Nelson, J. Morphology evolution via self-organization and lateral and vertical diffusion in polymer:fullerene solar cell blends. *Nat. Mater.* **2008**, *7*, 158−164. (e) Hoppe, H.; Niggemann, M.; Winder, C.; Kraut, J.; Hiesgen, R.; Hinsch, A.; Meissner, D.; Sariciftci, N. S. Nanoscale Morphology of Conjugated Polymer/Fullerene-Based Bulk- Heterojunction Solar Cells. *Adv. Funct. Mater.* **2004**, *14*, 1005−1011. (f) Moulé, A. J.; Meerholz, K. Morphology Control in Solution-Processed Bulk-Heterojunction Solar Cell Mixtures. *Adv. Funct. Mater.* **2009**, *19*, 3028−3036. (g) Groves, C.; Reid, O. G.; Ginger, D. S. Heterogeneity in Polymer Solar Cells: Local Morphology and Performance in

DOI: 10.1021/acs.chemrev.5b00165
Chem. Rev. XXXX, XXX, XXX−XXX

Organic Photovoltaics Studied with Scanning Probe Microscopy. *Acc. Chem. Res.* **2010**, *43*, 612−620. (h) Gao, J.; Chen, W.; Dou, L.; Chen, C.-C.; Chang, W.-H.; Liu, Y.; Li, G.; Yang, Y. Elucidating Double Aggregation Mechanisms in the Morphology Optimization of Diketopyrrolopyrrole-Based Narrow Bandgap Polymer Solar Cells. *Adv. Mater.* **2014**, *26*, 3142−3147.

(20) Grimsdale, A. C.; Chan, K. L.; Martin, R. E.; Jokisz, P. G.; Holmes, A. B. Synthesis of light-emitting conjugated polymers for applications in electroluminescent devices. *Chem. Rev.* **2009**, *109*, 897−1091.

(21) Zaumseil, J.; Sirringhaus, H. Electron and Ambipolar Transport in Organic Field-Effect Transistors. *Chem. Rev.* **2007**, *107*, 1296−1323.

(22) Burroughes, J. H.; Bradley, D. C.; Brown, A. R.; Marks, R. N.; Mackay, K.; Friend, R. H.; Burns, P. L.; Holmes, A. B. Light-emitting diodes based on conjugated polymers. *Nature* **1990**, *347*, 539−541.

(23) Yu, G.; Gao, J.; Hummelen, J. C.; Wudl, F.; Heeger, A. J. Polymer Photovoltaic Cells: Enhanced Efficiencies via a Network of Internal Donor-Acceptor Heterojunctions. *Science* **1995**, *270*, 1789−1791.

(24) Wudl, F.; Kobayashi, M.; Heeger, A. J. Poly(isothianaphthene). *J. Org. Chem.* **1984**, *49*, 3382−3384.

(25) Zhou, Z. H.; Maruyama, T.; Kanbara, T.; Ikeda, T.; Ichimura, K.; Yamamoto, T.; Tokuda, K. Unique optical and electrochemical properties of π-conjugated electrically conducting copolymers consisting of electron-withdrawing pyridine units and electron-donating thiophene units. *J. Chem. Soc., Chem. Commun.* **1991**, 1210−1212.

(26) Havinga, E. E.; Hoeve, W.; Wynberg, H. Alternate donor-acceptor small-band-gap semiconducting polymers; Polysquaraines and polycroconaines. *Synth. Met.* **1993**, *55*, 299−306.

(27) Gibson, G. L.; McCormick, T. M.; Seferos, D. S. Atomistic Band Gap Engineering in Donor−Acceptor Polymers. *J. Am. Chem. Soc.* **2012**, *134*, 539−547.

(28) Yuen, J. D.; Wudl, F. Strong acceptors in donor−acceptor polymers for high performance thin film transistors. *Energy Environ. Sci.* **2013**, *6*, 392−406.

(29) Liang, Y.; Wu, Y.; Feng, D.; Tsai, S.-T.; Son, H.-J.; Li, G.; Yu, L. Development of New Semiconducting Polymers for High Performance Solar Cells. *J. Am. Chem. Soc.* **2009**, *131*, 56−57.

(30) Coughlin, J. E.; Henson, Z. B.; Welch, G. C.; Bazan, G. C. Design and Synthesis of Molecular Donors for Solution-Processed High-Efficiency Organic Solar Cells. *Acc. Chem. Res.* **2014**, *47*, 257−270.

(31) (a) Lin, Y. Z.; Li, Y. F.; Zhan, X. W. Small molecule semiconductors for high-efficiency organic photovoltaics. *Chem. Soc. Rev.* **2012**, *41*, 4245−4272. (b) Roncali, J. Molecular Bulk Heterojunctions: An Emerging Approach to Organic Solar Cells. *Acc. Chem. Res.* **2009**, *42*, 1719−1730.

(32) (a) Walker, B.; Kim, C.; Nguyen, T. Q. Small Molecule Solution-Processed Bulk Heterojunction Solar Cells. *Chem. Mater.* **2011**, *23*, 470−482. (b) Wurthner, F.; Meerholz, K. Systems Chemistry Approach in Organic Photovoltaics. *Chem. - Eur. J.* **2010**, *16*, 9366−9373.

(33) (a) Brabec, C. J.; Cravino, A.; Meissner, D.; Sariciftci, N. S.; Fromherz, T.; Rispens, M. T.; Sanchez, L.; Hummelen, J. C. Origin of the Open Circuit Voltage of Plastic Solar Cells. *Adv. Funct. Mater.* **2001**, *11*, 374−380. (b) Rand, B. P.; Burk, D. P.; Forrest, S. R. Offset energies at organic semiconductor heterojunctions and their influence on the open-circuit voltage of thin-film solar cells. *Phys. Rev. B: Condens. Matter Mater. Phys.* **2007**, *75*, 115327. (c) Vandewal, K.; Tvingstedt, K.; Gadisa, A.; Inganäs, O.; Manca, J. V. On the origin of the open-circuit voltage of polymer−fullerene solar cells. *Nat. Mater.* **2009**, *8*, 904−909.

(34) (a) Ameri, T.; Khoram, P.; Min, J.; Brabec, C. J. Organic ternary solar cells: a review. *Adv. Mater.* **2013**, *25*, 4245−4266. (b) Yang, L.; Zhou, H.; Price, S. C.; You, W. Parallel-like bulk heterojunction polymer solar cells. *J. Am. Chem. Soc.* **2012**, *134*, 5432−5435. (c) Khlyabich, P. P.; Burkhart, B.; Thompson, B. C. Efficient ternary blend bulk heterojunction solar cells with tunable open-circuit voltage. *J. Am. Chem. Soc.* **2011**, *133*, 14534−14537. (d) Lu, L.; Xu, T.; Chen, W.; Landry, E. S.; Yu, L. Ternary blend polymer solar cells with enhanced power conversion efficiency. *Nat. Photonics* **2014**, *8*, 716−722. (e) Yang, Y. M.; Chen, W.; Dou, L.; Chang, W.-H.; Duan, H.-S.; Bob, B.; Li, G.; Yang, Y. *Nat. Photonics* **2015**, *9*, 190−198.

(35) Sariciftci, N. S.; Smilowitz, L.; Heeger, A. J.; Wudl, F. Photoinduced Electron Transfer from a Conducting Polymer to Buckminsterfullerene. *Science* **1992**, *258*, 1474−1476.

(36) Padinger, F.; Rittberger, R. S.; Sariciftci, N. S. Effects of Postproduction Treatment on Plastic Solar Cells. *Adv. Funct. Mater.* **2003**, *13*, 85−88.

(37) Ma, W.; Yang, C.; Gong, X.; Lee, K.; Heeger, A. J. Thermally Stable, Efficient Polymer Solar Cells with Nanoscale Control of the Interpenetrating Network Morphology. *Adv. Funct. Mater.* **2005**, *15*, 1617−1622.

(38) Li, G.; Shrotriya, V.; Huang, J.; Yao, Y.; Moriarty, T.; Emery, K.; Yang, Y. High-efficiency solution processable polymer photovoltaic cells by self-organization of polymer blends. *Nat. Mater.* **2005**, *4*, 864−868.

(39) Laird, D. W.; Stegamat, R.; Daadi, M.; Richter, H.; Vejins, V.; Scott, L.; Lada, T. A. Organic Photovoltaic Devices Comparising Fullerenes and Derivatives Thereof. U.S. patent US20080319207A1, Dec. 25, 2008.

(40) Zhao, G.; He, Y.; Li, Y. 6.5% Efficiency of Polymer Solar Cells Based on poly(3-hexylthiophene) and Indene-C_{60} Bisadduct by Device Optimization. *Adv. Mater.* **2010**, *22*, 4355−4358.

(41) Liang, Y.; Feng, D.; Wu, Y.; Tsai, S.-T.; Li; Gang; Ray, C.; Yu, L. Highly Efficient Solar Cell Polymers Developed via Fine-Tuning of Structural and Electronic Properties. *J. Am. Chem. Soc.* **2009**, *131*, 7792−7799.

(42) Liang, Y.; Xu, Z.; Xia, J.; Tsai, S.-T.; Wu, Y.; Li, G.; Ray, C.; Yu, L. For the Bright Future—Bulk Heterojunction Polymer Solar Cells with Power Conversion Efficiency of 7.4%. *Adv. Mater.* **2010**, *22*, E135−E138.

(43) Chen, H. Y.; Hou, J.; Zhang, S.; Liang, Y.; Yang, G.; Yang, Y.; Yu, L.; Wu, Y.; Li, G. Polymer solar cells with enhanced open-circuit voltage and efficiency. *Nat. Photonics* **2009**, *3*, 649−653.

(44) www.Solarmer.com (accessed 2010).

(45) He, Z.; Zhong, C.; Su, S.; Xu, M.; Wu, H.; Cao, Y. Enhanced power-conversion efficiency in polymer solar cells using an inverted device structure. *Nat. Photonics* **2012**, *6*, 593−597.

(46) Zang, H.; Liang, Y.; Yu, L.; Hu, B. Intra-Molecular Donor−Acceptor Interaction Effects on Charge Dissociation, Charge Transport, and Charge Collection in Bulk-Heterojunction Organic Solar Cells. *Adv. Energy Mater.* **2011**, *1*, 923−929.

(47) Carsten, B.; Szarko, J. M.; Son, H. J.; Wang, W.; Lu, L.; He, F.; Rolczynski, B. S.; Lou, S. J.; Chen, L. X.; Yu, L. Examining the Effect of the Dipole Moment on Charge Separation in Donor-Acceptor Polymers for Organic Photovoltaic Applications. *J. Am. Chem. Soc.* **2011**, *133*, 20468−20475.

(48) Tumbleston, J. R.; Collins, B. A.; Yang, L.; Stuart, A. C.; Gann, E.; Ma, W.; You, W.; Ade, H. The influence of molecular orientation on organic bulk heterojunction solar cells. *Nat. Photonics* **2014**, *8*, 385−391.

(49) (a) Cui, C.; Wong, W.-Y.; Li, Y. Improvement of open-circuit voltage and photovoltaic properties of 2D-conjugated polymers by alkylthio substitution. *Energy Environ. Sci.* **2014**, *7*, 2276−2284. (b) Chang, W.-H.; Meng, L.; Dou, L.; You, J.; Chen, C.-C.; Yang, Y.; Young, E. P.; Li, G.; Yang, Y. A Selenophene Containing Benzodithiophene-alt-thienothiophene Polymer for Additive-Free High Performance Solar Cell. *Macromolecules* **2015**, *48*, 562−568.

(50) Liao, S.-H.; Jhuo, H.-J.; Cheng, Y.-S.; Chen, S.-A. Fullerene Derivative-Doped Zinc Oxide Nanofilm as the Cathode of Inverted Polymer Solar Cells with Low-Bandgap Polymer (PTB7-Th) for High Performance. *Adv. Mater.* **2013**, *25*, 4766−4771.

(51) Huo, L.; Zhang, S.; Guo, X.; Xu, F.; Li, Y.; Hou, J. Replacing Alkoxy Groups with Alkylthienyl Groups: A Feasible Approach To Improve the Properties of Photovoltaic Polymers. *Angew. Chem., Int. Ed.* **2011**, *50*, 9697−9702.

DOI: 10.1021/acs.chemrev.5b00165
Chem. Rev. XXXX, XXX, XXX−XXX

(52) Adhikary, P.; Venkatesan, S.; Adhikari, N.; Maharjan, P. P.; Adebanjo, O.; Chen, J.; Qiao, Q. Enhanced charge transport and photovoltaic performance of PBDTTT-C-T/$PC_{70}BM$ solar cells *via* UV−ozone treatment. *Nanoscale* **2013**, *5*, 10007−10013.
(53) Ye, L.; Zhang, S.; Zhao, W.; Yao, H.; Hou, J. Highly Efficient 2D-Conjugated Benzodithiophene-Based Photovoltaic Polymer with Linear Alkylthio Side Chain. *Chem. Mater.* **2014**, *26*, 3603−3605.
(54) Chen, J. D.; Cui, C.; Li, Y.-Q.; Zhou, L.; Ou, Q.-D.; Li, C.; Li, Y.; Tang, J.-X. Single-Junction Polymer Solar Cells Exceeding 10% Power Conversion Efficiency. *Adv. Mater.* **2015**, *27*, 1035−1041.
(55) Shockley, W.; Queisser, H. J. Detailed Balance Limit of Efficiency of p-n Junction Solar Cells. *J. Appl. Phys.* **1961**, *32*, 510−519.
(56) King, R. R.; Law, D. C.; Edmondson, K. M.; Fetzer, C. M.; Kinsey, G. S.; Yoon, H.; Sherif, R. A.; Karam, N. H. 40% efficient metamorphic GaInP/GaInAs/Ge multijunction solar cells. *Appl. Phys. Lett.* **2007**, *90*, 183516.
(57) Green, M.; Emery, K.; Hishikawa, Y.; Warta, W.; Dunlop, E. D. Solar cell efficiency tables (version 40). *Prog. Photovoltaics* **2012**, *20*, 606−614.
(58) Ameri, T.; Dennler, G.; Lungenschmied, C.; Brabec, C. J. Organic tandem solar cells: A review. *Energy Environ. Sci.* **2009**, *2*, 347−363.
(59) You, J.; Dou, L.; Hong, Z.; Li, G.; Yang, Y. Recent trends in polymer tandem solar cells research. *Prog. Polym. Sci.* **2013**, *38*, 1909−1928.
(60) Zhu, Z.; Waller, D.; Gaudiana, R.; Morana, M.; Mühlbacher, D.; Scharber, M.; Brabec, C. Panchromatic Conjugated Polymers Containing Alternating Donor/Acceptor Units for Photovoltaic Applications. *Macromolecules* **2007**, *40*, 1981−1986.
(61) Peet, J.; Kim, J. Y.; Coates, N. E.; Ma, W. L.; Moses, D.; Heeger, A. J.; Bazan, G. C. Efficiency enhancement in low-bandgap polymer solar cells by processing with alkane dithiols. *Nat. Mater.* **2007**, *6*, 497−500.
(62) Hou, J. H.; Chen, H. Y.; Zhang, S. Q.; Li, G.; Yang, Y. Synthesis, Characterization, and Photovoltaic Properties of a Low Band Gap Polymer Based on Silole-Containing Polythiophenes and 2,1,3-Benzothiadiazole. *J. Am. Chem. Soc.* **2008**, *130*, 16144−16145.
(63) Chen, H. Y.; Hou, J.; Hayden, A. E.; Yang, H.; Houk, K. N.; Yang, Y. Silicon Atom Substitution Enhances Interchain Packing in a Thiophene-Based Polymer System. *Adv. Mater.* **2010**, *22*, 371−375.
(64) Morana, M.; Azimi, H.; Dennler, G.; Egelhaaf, H.-J.; Scharber, M.; Forberich, K.; Hauch, J.; Gaudiana, R.; Waller, D.; Zhu, Z.; et al. Nanomorphology and Charge Generation in Bulk Heterojunctions Based on Low-Bandgap Dithiophene Polymers with Different Bridging Atoms. *Adv. Funct. Mater.* **2010**, *20*, 1180−1188.
(65) Kim, J. S.; Fei, Z.; Wood, S.; James, D. T.; Sim, M.; Cho, K.; Heeney, M. J.; Kim, J.-S. Germanium- and Silicon-Substituted Donor−Acceptor Type Copolymers: Effect of the Bridging Heteroatom on Molecular Packing and Photovoltaic Device Performance. *Adv. Energy Mater.* **2014**, *4*, 1400527.
(66) Dou, L.; Chen, C.-C.; Yoshimura, K.; Ohya, K.; Chang, W.-H.; Gao, J.; Liu, Y.; Richard, E.; Yang, Y. Synthesis of 5*H*-Dithieno[3,2-*b*:2′,3′-*d*]pyran as an Electron-Rich Building Block for Donor−Acceptor Type Low-Bandgap Polymers. *Macromolecules* **2013**, *46*, 3384−3390.
(67) Wienk, M. M.; Turbiez, M.; Gilot, J.; Janssen, R. A. J. Narrow-Bandgap Diketo-Pyrrolo-Pyrrole Polymer Solar Cells: The Effect of Processing on the Performance. *Adv. Mater.* **2008**, *20*, 2556−2560.
(68) Bijleveld, J. C.; Zoombelt, A. P.; Mathijssen, S. G.; Wienk, M. M.; Turbiez, M.; de Leeuw, D. M.; Janssen, R. A. Poly-(diketopyrrolopyrrole−terthiophene) for Ambipolar Logic and Photovoltaics. *J. Am. Chem. Soc.* **2009**, *131*, 16616−16617.
(69) Li, W.; Hendriks, K. H.; Roelofs, W. S.; Kim, Y.; Wienk, M. M.; Janssen, R. A. Efficient Small Bandgap Polymer Solar Cells with High Fill Factors for 300 nm Thick Films. *Adv. Mater.* **2013**, *25*, 3182−3186.
(70) Li, W.; Furlan, A.; Hendriks, K. H.; Wienk, M. M.; Janssen, R. A. Efficient Tandem and Triple-Junction Polymer Solar Cells. *J. Am. Chem. Soc.* **2013**, *135*, 5529−5532.
(71) Dou, L.; You, J.; Yang, J.; Chen, C.-C.; He, Y.; Murase, S.; Moriarty, T.; Emery, K.; Li, G.; Yang, Y. Tandem polymer solar cells featuring a spectrally matched low-bandgap polymer. *Nat. Photonics* **2012**, *6*, 180−185.
(72) Dou, L.; Gao, J.; Richard, E.; You, J.; Chen, C.-C.; Cha, K. C.; He, Y.; Li, G.; Yang, Y. Systematic Investigation of Benzodithiophene- and Diketopyrrolopyrrole-Based Low-Bandgap Polymers Designed for Single Junction and Tandem Polymer Solar Cells. *J. Am. Chem. Soc.* **2012**, *134*, 10071−10079.
(73) Dou, L.; Chang, W. H.; Gao, J.; Chen, C. C.; You, J.; Yang, Y. A Selenium-Substituted Low-Bandgap Polymer with Versatile Photovoltaic Applications. *Adv. Mater.* **2013**, *25*, 825−831.
(74) Jung, J. W.; Liu, F.; Russell, T. P.; Jo, W. H. A high mobility conjugated polymer based on dithienothiophene and diketopyrrolopyrrole for organic photovoltaics. *Energy Environ. Sci.* **2012**, *5*, 6857−6861.
(75) Shahid, M.; Ashraf, R. S.; Huang, Z. G.; Kronemeijer, A. J.; Mccarthy-Ward, T.; McCulloch, I.; Durrant, J. R.; Sirringhaus, H.; Heeney, M. Photovoltaic and field effect transistor performance of selenophene andthiophene diketopyrrolopyrrole co-polymers with dithienothiophene. *J. Mater. Chem.* **2012**, *22*, 12817−12823.
(76) Peng, Q.; Huang, Q.; Hou, X.; Chang, P.; Xu, J.; Deng, S. Enhanced solar cell performance by replacing benzodithiophene with naphthodithiophene in diketopyrrolopyrrole-based copolymers. *Chem. Commun.* **2012**, *48*, 11452−11454.
(77) Li, K.; Li, Z.; Feng, K.; Xu, X.; Wang, L.; Peng, Q. Development of Large Band-Gap Conjugated Copolymers for Efficient Regular Single and Tandem Organic Solar Cells. *J. Am. Chem. Soc.* **2013**, *135*, 13549−13557.
(78) Hendriks, K. H.; Heintges, G. H. L.; Gevaerts, V. S.; Wienk, M. M.; Janssen, R. A. J. High-Molecular-Weight Regular Alternating Diketopyrrolopyrrole-based Terpolymers for Efficient Organic Solar Cells. *Angew. Chem., Int. Ed.* **2013**, *52*, 8341−8344.
(79) Park, Y. S.; Wu, Q.; Nam, C.-Y.; Grubbs, R. B. Polymerization of Tellurophene Derivatives by Microwave-Assisted Palladium-Catalyzed *ipso*-Arylative Polymerization. *Angew. Chem., Int. Ed.* **2014**, *53*, 10691−10695.
(80) Ashraf, R. S.; Meager, I.; Nikolka, M.; Kirkus, M.; Planells, M.; Schroeder, B.; Holliday, S.; Hurhangee, M.; Nielsen, C.; Sirringhaus, H.; et al. Chalcogenophene Comonomer Comparison in Small Band Gap Diketopyrrolopyrrole-Based Conjugated Polymers for High-Performing Field-Effect Transistors and Organic Solar Cells. *J. Am. Chem. Soc.* **2015**, *137*, 1314−1321.
(81) Wang, E.; Mammo, W.; Andersson, M. R. 25th Anniversary Article: Isoindigo-Based Polymers and Small Molecules for Bulk Heterojunction Solar Cells and Field Effect Transistors. *Adv. Mater.* **2014**, *26*, 1801−1826.
(82) Stalder, R.; Mei, J.; Graham, K.; Estrada, L. A.; Reynolds, J. R. Isoindigo, a Versatile Electron-Deficient Unit For High-Performance Organic Electronics. *Chem. Mater.* **2014**, *26*, 664−678.
(83) Wang, E.; Ma, Z.; Zhang, Z.; Vandewal, K.; Henriksson, P.; Inganäs, O.; Zhang, F.; Andersson, M. R. An Easily Accessible Isoindigo-Based Polymer for High-Performance Polymer Solar Cells. *J. Am. Chem. Soc.* **2011**, *133*, 14244−14247.
(84) Fang, L.; Zhou, Y.; Yao, Y.-X.; Diao, Y.; Lee, W.-Y.; Appleton, A. L.; Allen, R.; Reinspach, J.; Mannsfeld, S.; Bao, Z. Side-Chain Engineering of Isoindigo-Containing Conjugated Polymers Using Polystyrene for High-Performance Bulk Heterojunction Solar Cells. *Chem. Mater.* **2013**, *25*, 4874−4880.
(85) Van Pruissen, G. W. P.; Gholamrezaie, F.; Wienk, M. M.; Janssen, R. A. J. Synthesis and properties of small band gap thienoisoindigo basedconjugated polymers. *J. Mater. Chem.* **2012**, *22*, 20387−20393.
(86) Ashraf, R. S.; Kronemeijer, A. J.; James, D. I.; Sirringhaus, H.; McCulloch, I. A new thiophene substituted isoindigo based copolymer

DOI: 10.1021/acs.chemrev.5b00165
Chem. Rev. XXXX, XXX, XXX−XXX

for high performance ambipolar transistors. *Chem. Commun.* **2012**, *48*, 3939−3941.
(87) Koizumi, Y.; Ide, M.; Saeki, A.; Vijayakumar, C.; Balan, B.; Kawamoto, M.; Seki, S. Thienoisoindigo-based low-band gap polymers for organic electronic devices. *Polym. Chem.* **2013**, *4*, 484−494.
(88) Dutta, G. K.; Han, A. R.; Lee, J.; Kim, Y.; Oh, J. H.; Yang, C. Visible-Near Infrared Absorbing Polymers Containing Thienoisoindigo and Electron-Rich Units for Organic Transistors with Tunable Polarity. *Adv. Funct. Mater.* **2013**, *23*, 5317−5325.
(89) Kim, J. Y.; Lee, K.; Coates, N. E.; Moses, D.; Nguyen, T. Q.; Dante, M.; Heeger, A. J. Efficient Tandem Polymer Solar Cells Fabricated by All-Solution Processing. *Science* **2007**, *317*, 222−225.
(90) Sista, S.; Park, M. H.; Hong, Z.; Wu, Y.; Hou, J.; Kwan, W. L.; Li, G.; Yang, Y. Highly Efficient Tandem Polymer Photovoltaic Cells. *Adv. Mater.* **2010**, *22*, 380−383.
(91) Li, W.; Roelofs, W. S. C.; Wienk, M. M.; Janssen, R. A. J. Enhancing the Photocurrent in Diketopyrrolopyrrole-Based Polymer Solar Cells via Energy Level Control. *J. Am. Chem. Soc.* **2012**, *134*, 13787−13795.
(92) (a) Veldman, D.; Meskers, S. C. J.; Janssen, R. A. J. The Energy of Charge-Transfer States in Electron Donor−Acceptor Blends: Insight into the Energy Losses in Organic Solar Cells. *Adv. Funct. Mater.* **2009**, *19*, 1939−1948. (b) Tvingstedt, K.; Vandewal, K.; Gadisa, A.; Zhang, F.; Manca, J.; Inganäs, O. Electroluminescence from Charge Transfer States in Polymer Solar Cells. *J. Am. Chem. Soc.* **2009**, *131*, 11819−11824.
(93) Faist, M. A.; Kirchartz, T.; Gong, W.; Ashraf, R. S.; McCulloch, I.; de Mello, J. C.; Ekins-Daukes, N. J.; Bradley, D. D. C.; Nelson, J. Competition between the Charge Transfer State and the Singlet States of Donor or Acceptor Limiting the Efficiency in Polymer:Fullerene Solar Cells. *J. Am. Chem. Soc.* **2012**, *134*, 685−692.
(94) Adebanjo, O.; Maharjan, P. P.; Adhikary, P.; Wang, M.; Yang, S.; Qiao, Q. Triple junction polymer solar cells. *Energy Environ. Sci.* **2013**, *6*, 3150−3170.
(95) Yusoff, A. R. M.; Kim, D.; Kim, H. P.; Shneider, F. K.; da Silva, W. J.; Jang, J. A high efficiency solution processed polymer inverted triple-junction solar cell exhibiting a power conversion efficiency of 11.83%. *Energy Environ. Sci.* **2015**, *8*, 303−316.
(96) Chen, C.-C.; Chang, W.-H.; Yoshimura, K.; Ohya, K.; You, J.; Gao, J.; Hong, Z.; Yang, Y. An Efficient Triple-Junction Polymer Solar Cell Having a Power Conversion Efficiency Exceeding 11%. *Adv. Mater.* **2014**, *26*, 5670−5677.
(97) Che, X.; Xiao, X.; Zimmerman, J. D.; Fan, D.; Forrest, S. R. High-Efficiency, Vacuum-Deposited, Small-Molecule Organic Tandem and Triple-Junction Photovoltaic Cells. *Adv. Energy Mater.* **2014**, *4*, 1400568.
(98) Hecht, D. S.; Hu, L.; Irvin, G. Emerging Transparent Electrodes Based on Thin Films of Carbon Nanotubes, Graphene, and Metallic Nanostructures. *Adv. Mater.* **2011**, *23*, 1482−1513.
(99) Bae, S.; Kim, H.; Lee, Y.; Xu, X.; Park, J.-S.; Zheng, Y.; Balakrishnan, J.; Lei, T.; Kim, H. R.; Song, Y.; et al. Roll-to-roll production of 30-in. graphene films for transparent electrodes. *Nat. Nanotechnol.* **2010**, *5*, 574−578.
(100) Ye, S.; Rathmell, A. R.; Chen, Z.; Stewart, I. E.; Wiley, B. J. Metal Nanowire Networks: The Next Generation of Transparent Conductors. *Adv. Mater.* **2014**, *26*, 6670−6687.
(101) Li, G.; Chu, C.-W.; Shrotriya, V.; Huang, J.; Yang, Y. Efficient inverted polymer solar cells. *Appl. Phys. Lett.* **2006**, *88*, 253503.
(102) Shrotriya, V.; Wu, E. H.-E.; Li, G.; Yao, Y.; Yang, Y. Efficient light harvesting in multiple-device stacked structure for polymer solar cells. *Appl. Phys. Lett.* **2006**, *88*, 064104.
(103) Chueh, C.-C.; Chien, S.-C.; Yip, H.-L.; Salinas, J. F.; Li, C.-Z.; Chen, K.-S.; Chen, F.-C.; Chen, W.-C.; Jen, A. K.-Y. Toward High-Performance Semi-Transparent Polymer Solar Cells: Optimization of Ultra-Thin Light Absorbing Layer and Transparent Cathode Architecture. *Adv. Energy Mater.* **2013**, *3*, 417−423.
(104) Lunt, R. R.; Bulovic, V. Transparent, near-infrared organic photovoltaic solar cells for window and energy-scavenging applications. *Appl. Phys. Lett.* **2011**, *98*, 113305.
(105) Chen, C. C.; Dou, L. T.; Zhu, R.; Chung, C. H.; Song, T. Z.; Zheng, Y. B.; Hawks, S.; Li, G.; Weiss, P. S.; Yang, Y. Visibly Transparent Polymer Solar Cells Produced by Solution Processing. *ACS Nano* **2012**, *6*, 7185−7190.
(106) Zhu, R.; Chung, C. H.; Cha, K. C.; Yang, W. B.; Zheng, Y. B.; Zhou, H. P.; Song, T. B.; Chen, C. C.; Weiss, P. S.; Li, G.; et al. Fused Silver Nanowires with Metal Oxide Nanoparticles and Organic Polymers for Highly Transparent Conductors. *ACS Nano* **2011**, *5*, 9877−9882.
(107) Chen, C.-C.; Dou, L. T.; Gao, J.; Chang, W.-H.; Li, G.; Yang, Y. High-performance semi-transparent polymer solar cells possessing tandem structures. *Energy Environ. Sci.* **2013**, *6*, 2714−2720.
(108) Betancur, R.; Romero-Gomez, P.; Martinez-Otero, A.; Elias, X.; Maymó, M.; Martorell, J. Transparent polymer solar cells employing a layered light-trapping architecture. *Nat. Photonics* **2013**, *7*, 995−1000.
(109) Chen, Y. S.; Wan, X. J.; Long, G. K. High Performance Photovoltaic Applications Using Solution-Processed Small Molecules. *Acc. Chem. Res.* **2013**, *46*, 2645−2655.
(110) Roncali, J.; Leriche, P.; Blanchard, P. Molecular Materials for Organic Photovoltaics: Small is Beautiful. *Adv. Mater.* **2014**, *26*, 3821−3838.
(111) Li, Y. W.; Guo, Q.; Li, Z. F.; Pei, J. N.; Tian, W. J. Solution processable D−A small molecules for bulk-heterojunction solar cells. *Energy Environ. Sci.* **2010**, *3*, 1427−1436.
(112) Ni, W.; Wan, X. J.; Li, M. M.; Wang, Y. C.; Chen, Y. S. A−D−A small molecules for solution-processed organic photovoltaic cells. *Chem. Commun.* **2015**, *51*, 4936−4950.
(113) Zhang, F.; Wu, D. Q.; Xu, Y. Y.; Feng, X. L. Thiophene-based conjugated oligomers for organic solar cells. *J. Mater. Chem.* **2011**, *21*, 17590−17600.
(114) Qin, H. M.; Li, L. S.; Guo, F. Q.; Su, S. J.; Peng, J. B.; Cao, Y.; Peng, X. B. Solution-processed bulk heterojunction solar cells based on a porphyrin small molecule with 7% power conversion efficiency. *Energy Environ. Sci.* **2014**, *7*, 1397−1401.
(115) Roncali, J. Synthetic principles for bandgap control in linear pi-conjugated systems. *Chem. Rev.* **1997**, *97*, 173−205.
(116) Li, Y. N.; Sonar, P.; Murphy, L.; Hong, W. High mobility diketopyrrolopyrrole (DPP)-based organic semiconductor materials for organic thin film transistors and photovoltaics. *Energy Environ. Sci.* **2013**, *6*, 1684−1710.
(117) Tieke, B.; Rabindranath, A. R.; Zhang, K.; Zhu, Y. Conjugated polymers containing diketopyrrolopyrrole units in the main chain. *Beilstein J. Org. Chem.* **2010**, *6*, 830−845.
(118) Tamayo, A. B.; Walker, B.; Nguyen, T. Q. A Low Band Gap, Solution Processable Oligothiophene with a Diketopyrrolopyrrole Core for Use in Organic Solar Cells. *J. Phys. Chem. C* **2008**, *112*, 11545−11551.
(119) Tamayo, A. B.; Dang, X. D.; Walker, B.; Seo, J.; Kent, T.; Nguyen, T. Q. A low band gap, solution processable oligothiophene with a dialkylated diketopyrrolopyrrole chromophore for use in bulk heterojunction solar cells. *Appl. Phys. Lett.* **2009**, *94*, 103301.
(120) Wang, H. Y.; Liu, F.; Bu, L. J.; Gao, J.; Wang, C.; Wei, W.; Russell, T. P. The Role of Additive in Diketopyrrolopyrrole-based Small Molecular Bulk Heterojunction Solar Cells. *Adv. Mater.* **2013**, *25*, 6519−6525.
(121) (a) Lee, J. W.; Choi, Y. S.; Jo, W. H. Diketopyrrolopyrrole-based small molecules with simple structure for high V_{OC} organic photovoltaics. *Org. Electron.* **2012**, *13*, 3060−3066. (b) Shin, W.; Yasuda, T.; Hidaka, Y.; Watanabe, G.; Arai, R.; Nasu, K.; Yamaguchi, T.; Murakami, W.; Makita, K.; Adachi, C. π-Extended Narrow-Bandgap Diketopyrrolopyrrole-Based Oligomers for Solution-Processed Inverted Organic Solar Cells. *Adv. Energy Mater.* **2014**, *4*, 1400879. (c) Jung, M.; Yoon, Y.; Park, J. H.; Cha, W.; Kim, A.; Kang, J.; Gautam, S.; Seo, D.; Cho, J. H.; Kim, H.; et al. Nanoscopic Management of Molecular Packing and Orientation of Small Molecules by a Combination of Linear and Branched Alkyl Side Chains. *ACS Nano* **2014**, *8*, 5988−6003. (d) Yu, Q. C.; Fu, W. F.; Wan, J. H.; Wu, X. F.; Shi, M. M.; Chen, H. Z. Evaluation of Heterocycle-Modified Pentathiophene-Based Molecular Donor Mate-

DOI: 10.1021/acs.chemrev.5b00165
Chem. Rev. XXXX, XXX, XXX−XXX

rials for Solar Cells. 2014. *ACS Appl. Mater. Interfaces* **2014**, *6*, 5798−5809. (e) Liu, J. H.; Sun, Y. M.; Moonsin, P.; Kuik, M.; Proctor, C. M.; Lin, J.; Hsu, B. B.; Promarak, V.; Heeger, A. J.; Nguyen, T. Q. Tri-Diketopyrrolopyrrole Molecular Donor Materials for High-Performance Solution-Processed Bulk Heterojunction Solar Cells. *Adv. Mater.* **2013**, *25*, 5898−5903.

(122) Li, W. W.; Kelchtermans, M.; Wienk, M. M.; Janssen, R. A. J. Effect of structure on the solubility and photovoltaic properties of bis-diketopyrrolopyrrole molecules. *J. Mater. Chem. A* **2013**, *1*, 15150−15157.

(123) Umeyama, T.; Takamatsu, T.; Tezuka, N.; Matano, Y.; Araki, Y.; Wada, T.; Yoshikawa, O.; Sagawa, T.; Yoshikawa, S.; Imahori, H. Synthesis and Photophysical and Photovoltaic Properties of Porphyrin−Furan and − Thiophene Alternating Copolymers. *J. Phys. Chem. C* **2009**, *113*, 10798−10806.

(124) Huang, Y. Y.; Li, L. S.; Peng, X. B.; Peng, J. B.; Cao, Y. Solution processed small molecule bulk heterojunction organic photovoltaics based on a conjugated donor−acceptor porphyrin. *J. Mater. Chem.* **2012**, *22*, 21841−21844.

(125) Li, L. S.; Huang, Y. Y.; Peng, J. B.; Cao, Y.; Peng, X. B. Enhanced performance of solution-processed solar cells based on porphyrin small molecules with a diketopyrrolopyrrole acceptor unit and a pyridine additive. *J. Mater. Chem. A* **2013**, *1*, 2144−2150.

(126) Deng, P.; Zhang, Q. Recent developments on isoindigo-based conjugated polymers. *Polym. Chem.* **2014**, *5*, 3298−3305.

(127) Yassin, A.; Leriche, P.; Allain, M.; Roncali, J. Donor−acceptor−donor (D−A−D) molecules based on isoindigo as active material for organic solar cells. *New J. Chem.* **2013**, *37*, 502−507.

(128) Wang, T.; Chen, Y. H.; Bao, X. C.; Du, Z. K.; Guo, J.; Wang, N.; Sun, M. L.; Yang, R. Q. A new isoindigo-based molecule with ideal energy levels for solution-processable organic solar cells. *Dyes Pigm.* **2013**, *98*, 11−16.

(129) Chen, Y. H.; Du, Z. K.; Chen, W. C.; Han, L. L.; Liu, Q.; Sun, M. L.; Yang, R. Q. Near-infrared response thienoisoindigo-based small molecule for solution-processed bulk-heterojunction solar cells. *Synth. Met.* **2014**, *187*, 24−29.

(130) Odajima, T.; Ashizawa, M.; Konosu, Y.; Matsumoto, H.; Mori, T. The impact of molecular planarity on electronic devices in thienoisoindigo-based organic semiconductors. *J. Mater. Chem. C* **2014**, *2*, 10455−10467.

(131) Vybornyi, O.; Jiang, Y.; Baert, F.; Demeter, D.; Roncali, J.; Blanchard, P.; Cabanetos, C. Solution-processable thienoisoindigo-based molecular donors for organic solar cells with high open-circuit voltage. *Dyes Pigm.* **2015**, *115*, 17−22.

(132) Karakawa, M.; Aso, Y. Narrow-optical-gap pi-conjugated small molecules based on terminal isoindigo and thienoisoindigo acceptor units for photovoltaic application. *RSC Adv.* **2013**, *3*, 16259−16263.

(133) Jiang, J. Q.; Sun, C. L.; Shi, Z. F.; Zhang, H. L. Squaraines as light-capturing materials in photovoltaic cells. *RSC Adv.* **2014**, *4*, 32987−32996.

(134) Beverina, L.; Salice, P. Squaraine Compounds: Tailored Design and Synthesis towards a Variety of Material Science Applications. *Eur. J. Org. Chem.* **2010**, *2010*, 1207−1225.

(135) Silvestri, F.; Irwin, M. D.; Beverina, L.; Facchetti, A.; Pagani, G. A.; Marks, T. J. Efficient Squaraine-Based Solution Processable Bulk-Heterojunction Solar Cells. *J. Am. Chem. Soc.* **2008**, *130*, 17640−17641.

(136) Rao, B. A.; Yesudas, K.; Kumar, G. S.; Bhanuprakash, K.; Rao, V. J.; Sharma, G. D.; Singh, S. P. Application of solution processable squaraine dyes as electron donors for organic bulk-heterojunction solar cells. *Photoch. Photobio. Sci.* **2013**, *12*, 1688−1699.

(137) Yang, D. B.; Yang, Q. Q.; Yang, L.; Luo, Q.; Chen, Y.; Zhu, Y. Q.; Huang, Y.; Lu, Z. Y.; Zhao, S. L. A low bandgap asymmetrical squaraine for high-performance solution-processed small molecule organic solar cells. *Chem. Commun.* **2014**, *50*, 9346−9348.

(138) Cakmak, Y.; Akkaya, E. U. Phenylethynyl-BODIPY Oligomers: Bright Dyes and Fluorescent Building Blocks. *Org. Lett.* **2009**, *11*, 85−88.

(139) Loudet, A.; Burgess, K. BODIPY Dyes and Their Derivatives: Syntheses and Spectroscopic Properties. *Chem. Rev.* **2007**, *107*, 4891−4932.

(140) Lu, H.; Mack, J.; Yang, Y. C.; Shen, Z. Structural modification strategies for the rational design of red/NIR region BODIPYs. *Chem. Soc. Rev.* **2014**, *43*, 4778−4823.

(141) Hayashi, Y.; Obata, N.; Tamaru, M.; Yamaguchi, S.; Matsuo, Y.; Saeki, A.; Seki, S.; Kureishi, Y.; Saito, S.; Yamaguchi, S.; Shinokubo, H. Facile Synthesis of Biphenyl-Fused BODIPY and Its Property. *Org. Lett.* **2012**, *14*, 866−869.

(142) Liu, W. X.; Tang, A. L.; Chen, J. W.; Wu, Y. S.; Zhan, C. L.; Yao, J. N. Photocurrent Enhancement of BODIPY-Based Solution-Processed Small-Molecule Solar Cells by Dimerization via the Meso Position. *ACS Appl. Mater. Interfaces* **2014**, *6*, 22496−22505.

(143) Bessette, A.; Hanan, G. S. Design, synthesis and photophysical studies of dipyrromethene-based materials: insights into their applications in organic photovoltaic devices. *Chem. Soc. Rev.* **2014**, *43*, 3342−3405.

(144) Bura, T.; Leclerc, N.; Fall, S.; Leveque, P.; Heiser, T.; Retailleau, P.; Rihn, S.; Mirloup, A.; Ziessel, R. High-Performance Solution-Processed Solar Cells and Ambipolar Behavior in Organic Field-Effect Transistors with Thienyl-BODIPY Scaffoldings. *J. Am. Chem. Soc.* **2012**, *134*, 17404−17407.

(145) Poe, A. M.; Della Pelle, A. M.; Subrahmanyam, A. V.; White, W.; Wantz, G.; Thayumanavan, S. Small molecule BODIPY dyes as non-fullerene acceptors in bulk heterojunction organic photovoltaics. *Chem. Commun.* **2014**, *50*, 2913−2915.

(146) (a) Liu, Y. S.; Zhou, J. Y.; Wan, X. J.; Chen, Y. S. Synthesis and properties of acceptor-donor-acceptor molecules based on oligothiophenes with tunable and low band gap. *Tetrahedron* **2009**, *65*, 5209−5215. (b) Steinberger, S.; Mishra, A.; Reinold, E.; Mena-Osteritz, E.; Muller, H.; Uhrich, C.; Pfeiffer, M.; Bauerle, P. Synthesis and characterizations of red/near-IR absorbing A−D−A−D−A-type oligothiophenes containing thienothiadiazole and thienopyrazine central units. *J. Mater. Chem.* **2012**, *22*, 2701−2712. (c) Kan, B.; Li, M. M.; Zhang, Q.; Liu, F.; Wan, X. J.; Wang, Y. C.; Ni, W.; Long, G. K.; Yang, X.; Feng, H. R. A Series of Simple Oligomer-like Small Molecules Based on Oligothiophenes for Solution-Processed Solar Cells with High Efficiency. *J. Am. Chem. Soc.* **2015**, *137*, 3886−3893. (d) He, G. R.; Li, Z.; Wan, X. J.; Zhou, J. Y.; Long, G. K.; Zhang, S. Z.; Zhang, M. T.; Chen, Y. S. Efficient small molecule bulk heterojunction solar cells with high fill factors via introduction of π-stacking moieties as end group. *J. Mater. Chem. A* **2013**, *1*, 1801−1809.

(147) Welch, G. C.; Perez, L. A.; Hoven, C. V.; Zhang, Y.; Dang, X. D.; Sharenko, A.; Toney, M. F.; Kramer, E. J.; Nguyen, T. Q.; Bazan, G. C. A modular molecular framework for utility in small-molecule solution-processed organic photovoltaic devices. *J. Mater. Chem.* **2011**, *21*, 12700−12709.

(148) Sun, Y. M.; Welch, G. C.; Leong, W. L.; Takacs, C. J.; Bazan, G. C.; Heeger, A. J. Solution-processed small-molecule solar cells with 6.7% efficiency. *Nat. Mater.* **2011**, *11*, 44−48.

(149) Qian, G.; Wang, Z. Y. Near-Infrared Organic Compounds and Emerging Applications. *Chem. - Asian J.* **2010**, *5*, 1006−1029.

(150) Søndergaard, R.; Hösel, M.; Angmo, D.; Larsen-Olsen, T. T.; Krebs, F. C. Roll-to-roll fabrication of polymer solar cells. *Mater. Today* **2012**, *15*, 36−49.

(151) Azzellino, G.; Grimoldi, A.; Binda, M.; Caironi, M.; Natali, D.; Sampietro, M. Fully Inkjet-Printed Organic Photodetectors with High Quantum Yield. *Adv. Mater.* **2013**, *25*, 6829−6833.

(152) Barone, P. W.; Baik, S.; Heller, D. A.; Strano, M. S. Near-infrared optical sensors based on single-walled carbon nanotubes. *Nat. Mater.* **2004**, *4*, 86−92.

(153) Rogalski, A.; Antoszewski, J.; Faraone, L. Third-generation infrared photodetector arrays. *J. Appl. Phys.* **2009**, *105*, 091101.

(154) Chen, H. Y.; Lo, M. K.; Yang, G.; Monbouquette, H. G.; Yang, Y. Nanoparticle-assisted high photoconductive gain in composites of polymer and fullerene. *Nat. Nanotechnol.* **2008**, *3*, 543−547.

DOI: 10.1021/acs.chemrev.5b00165
Chem. Rev. XXXX, XXX, XXX−XXX

(155) Guo, F.; Yang, B.; Yuan, Y.; Xiao, Z.; Dong, Q.; Bi, Y.; Huang, J. A nanocomposite ultraviolet photodetector based on interfacial trap-controlled charge injection. *Nat. Nanotechnol.* **2012**, *7*, 798−802.
(156) Peumans, P.; Yakimov, A.; Forrest, S. R. Small molecular weight organic thin-film photodetectors and solar cells. *J. Appl. Phys.* **2003**, *93*, 3693−3723.
(157) Yao, Y.; Liang, Y.; Shrotriya, V.; Xiao, S.; Yu, L.; Yang, Y. Plastic Near-Infrared Photodetectors Utilizing Low Band Gap Polymer. *Adv. Mater.* **2007**, *19*, 3979−3983.
(158) Perzon, E.; Zhang, F.; Andersson, M.; Mammo, W.; Inganäs, O.; Andersson, M. R. A Conjugated Polymer for Near Infrared Optoelectronic Applications. *Adv. Mater.* **2007**, *19*, 3308−3311.
(159) Saracco, E.; Bouthinon, B.; Verilhac, J. M.; Celle, C.; Chevalier, N.; Mariolle, D.; Dhez, O.; Simonato, J. P. Work Function Tuning for High-Performance Solution-Processed Organic Photodetectors with Inverted Structure. *Adv. Mater.* **2013**, *25*, 6534−6538.
(160) Chen, E.; Tseng, S.; Chao, Y.; Meng, H.; Wang, C.; Chen, W.; Hsu, C.; Horn, S. Polymer infrared photo-detector with high sensitivity up to 1100 nm. *Synth. Met.* **2011**, *161*, 1618−1622.
(161) Hu, X.; Dong, Y.; Huang, F.; Gong, X.; Cao, Y. Solution-Processed High-Detectivity Near-Infrared Polymer Photodetectors Fabricated by a Novel Low-Bandgap Semiconducting Polymer. *J. Phys. Chem. C* **2013**, *117*, 6537−6543.
(162) Bubnova, O.; Khan, Z. U.; Malti, A.; Braun, S.; Fahlman, M.; Berggren, M.; Crispin, X. Optimization of the thermoelectric figure of merit in the conducting polymer poly(3,4-ethylenedioxythiophene). *Nat. Mater.* **2011**, *10*, 429−433.
(163) Binda, M.; Iacchetti, A.; Natali, D.; Beverina, L.; Sassi, M.; Sampietro, M. High detectivity squaraine-based near infrared photodetector with nA/cm^2 dark current. *Appl. Phys. Lett.* **2011**, *98*, 173303.
(164) Li, L. S.; Huang, Y. Y.; Peng, J. B.; Cao, Y.; Peng, X. B. Highly responsive organic near-infrared photodetectors based on a porphyrin small molecule. *J. Mater. Chem. C* **2014**, *2*, 1372−1375.
(165) Qi, J.; Ni, L.; Yang, D. Z.; Zhou, X. K.; Qiao, W. Q.; Li, M.; Ma, D. G.; Wang, Z. Y. Panchromatic small molecules for UV-Vis-NIR photodetectors with high detectivity. *J. Mater. Chem. C* **2014**, *2*, 2431−2438.
(166) Yotter, R. A.; Wilson, D. M. A review of photodetectors for sensing light-emitting reporters in biological systems. *IEEE Sens. J.* **2003**, *3*, 288−303.
(167) Sirringhaus, H.; Kawase, T.; Friend, R. H.; Shimoda, T.; Inbasekaran, M.; Wu, W.; Woo, E. P. High-Resolution Inkjet Printing of All-Polymer Transistor Circuits. *Science* **2000**, *290*, 2123−2126.
(168) Muccini, M. A bright future for organic field-effect transistors. *Nat. Mater.* **2006**, *5*, 605−613.
(169) Nielsen, C. B.; Turbiez, M.; McCulloch, I. Recent Advances in the Development of Semiconducting DPP-Containing Polymers for Transistor Applications. *Adv. Mater.* **2013**, *25*, 1859−1880.
(170) Li, J.; Zhao, Y.; Tan, H. S.; Guo, Y.; Di, C. A.; Yu, G.; Ong, B. S. A stable solution-processed polymer semiconductor with record high-mobility for printed transistors. *Sci. Rep.* **2012**, *2*, 754.
(171) Sonar, P.; Singh, S. P.; Li, Y.; Soh, M. S.; Dodabalapur, A. A Low-Bandgap Diketopyrrolopyrrole-Benzothiadiazole Based Copolymer for High-Mobility Ambipolar Organic Thin-Film Transistors. *Adv. Mater.* **2010**, *22*, 5409−5413.
(172) Kronemeijer, A. J.; Gili, E.; Shahid, M.; Rivnay, J.; Salleo, A.; Heeney, M.; Sirringhaus, H. A Selenophene-Based Low-Bandgap Donor−Acceptor Polymer Leading to Fast Ambipolar Logic. *Adv. Mater.* **2012**, *24*, 1558−1565.
(173) Shahid, M.; McCarthy-Ward, T.; Labram, J.; Rossbauer, S.; Domingo, E. B.; Watkins, S. E.; Stingelin, N.; Anthopoulos, T. D.; Heeney, M. Low band gap selenophene−diketopyrrolopyrrole polymers exhibiting high and balanced ambipolar performance in bottom-gate transistors. *Chem. Sci.* **2012**, *3*, 181−185.
(174) Mei, J.; Kim, D. H.; Ayzner, A. L.; Toney, M. F.; Bao, Z. Siloxane-Terminated Solubilizing Side Chains: Bringing Conjugated Polymer Backbones Closer and Boosting Hole Mobilities in Thin-Film Transistors. *J. Am. Chem. Soc.* **2011**, *133*, 20130−20133.
(175) Mei, J.; Graham, K. R.; Stalder, R.; Reynolds, J. R. Synthesis of Isoindigo-Based Oligothiophenes for Molecular Bulk Heterojunction Solar Cells. *Org. Lett.* **2010**, *12*, 660−663.
(176) Lei, T.; Dou, J. H.; Ma, Z. J.; Yao, C. H.; Liu, C. J.; Wang, J. Y.; Pei, J. Ambipolar Polymer Field-Effect Transistors Based on Fluorinated Isoindigo: High Performance and Improved Ambient Stability. *J. Am. Chem. Soc.* **2012**, *134*, 20025−20028.
(177) Fan, J.; Yuen, J. D.; Wang, M.; Seifter, J.; Seo, J. H.; Mohebbi, A. R.; Zakhidov, D.; Heeger, A.; Wudl, F. High-Performance Ambipolar Transistors and Inverters from an Ultralow Bandgap Polymer. *Adv. Mater.* **2012**, *24*, 2186−2190.
(178) Steckler, T. T.; Henriksson, P.; Mollinger, S.; Lundin, A.; Salleo, A.; Andersson, M. R. Very Low Band Gap Thiadiazoloquinoxaline Donor−Acceptor Polymers as Multi-tool Conjugated Polymers. *J. Am. Chem. Soc.* **2014**, *136*, 1190−1193.
(179) Diao, Y.; Tee, B. C.; Giri, G.; Xu, J.; Kim, D. H.; Becerril, H. A.; Stoltenberg, R. M.; Lee, T. H.; Xue, G.; Mannsfeld, S. C. B.; et al. Solution coating of large-area organic semiconductor thin films with aligned single-crystalline domains. *Nat. Mater.* **2013**, *12*, 665−671.
(180) Tantiwiwat, M.; Tamayo, A.; Luu, N.; Dang, X. D.; Nguyen, T. Q. Oligothiophene Derivatives Functionalized with a Diketopyrrolopyrrolo Core for Solution-Processed Field Effect Transistors: Effect of Alkyl Substituents and Thermal Annealing. *J. Phys. Chem. C* **2008**, *112*, 17402−17407.
(181) Zhang, Y.; Kim, C.; Lin, J.; Nguyen, T. Q. Solution-Processed Ambipolar Field-Effect Transistor Based on Diketopyrrolopyrrole Functionalized with Benzothiadiazole. *Adv. Funct. Mater.* **2012**, *22*, 97−105.
(182) Suna, Y.; Nishida, J.; Fujisaki, Y.; Yamashita, Y. Ambipolar Behavior of Hydrogen-Bonded Diketopyrrolopyrrole−Thiophene Co-oligomers Formed from Their Soluble Precursors. *Org. Lett.* **2012**, *14*, 3356−3359.
(183) Wang, L.; Zhang, X. J.; Tian, H. K.; Lu, Y. F.; Geng, Y. H.; Wang, F. S. A cyano-terminated dithienyldiketopyrrolopyrrole dimer as a solution processable ambipolar semiconductor under ambient conditions. *Chem. Commun.* **2013**, *49*, 11272−11274.
(184) Barclay, T. M.; Cordes, A. W.; MacKinnon, C. D.; Oakley, R. T.; Reed, R. W. Oligothiophenes End-Capped by Nitriles. Preparation and Crystal Structures of α,ω-Dicyanooligothiophenes NC(C4H2S)-nCN (n = 3−6). *Chem. Mater.* **1997**, *9*, 981−990.
(185) Fitzner, R.; Reinold, E.; Mishra, A.; Mena-Osteritz, E.; Ziehlke, H.; Korner, C.; Leo, K.; Riede, M.; Weil, M.; Tsaryova, O.; et al. Dicyanovinyl-Substituted Oligothiophenes: Structure−Property Relationships and Application in Vacuum Processed Small-Molecule Organic Solar Cells. *Adv. Funct. Mater.* **2011**, *21*, 897−910.
(186) Kang, W.; Jung, M.; Cha, W.; Jang, S.; Yoon, Y.; Kim, H.; Son, H. J.; Lee, D. K.; Kim, B.; Cho, J. H. High Crystalline Dithienosilole-Cored Small Molecule Semiconductor for Ambipolar Transistor and Nonvolatile Memory. *ACS Appl. Mater. Interfaces* **2014**, *6*, 6589−6597.
(187) Riano, A.; Burrezo, P. M.; Mancheno, M. J.; Timalsina, A.; Smith, J.; Facchetti, A.; Marks, T. J.; Navarrete, J. T. L.; Segura, J. L.; Casado, J.; et al. The unusual electronic structure of ambipolar dicyanovinyl-substituted diketopyrrolopyrrole derivatives. *J. Mater. Chem. C* **2014**, *2*, 6376−6386.
(188) Kanimozhi, C.; Yaacobi-Gross, N.; Chou, K. W.; Amassian, A.; Anthopoulos, T. D.; Patil, S. iketopyrrolopyrrole−Diketopyrrolopyrrole-Based Conjugated Copolymer for High-Mobility Organic Field-Effect Transistors. *J. Am. Chem. Soc.* **2012**, *134*, 16532−16535.
(189) Chang, W. H.; Gao, J.; Dou, L.; Chen, C. C.; Liu, Y.; Yang, Y. Side-Chain Tunability via Triple Component Random Copolymerization for Better Photovoltaic Polymers. *Adv. Energy Mater.* **2014**, *4*, 1300864.
(190) Niu, Y. H.; Liu, M. S.; Ka, J. W.; Jen, A. K. Y. Thermally crosslinked hole-transporting layers for cascade hole-injection and effective electron-blocking/exciton-confinement in phosphorescent polymer light-emitting diodes. *Appl. Phys. Lett.* **2006**, *88*, 093505.
(191) Wong, W. Y.; Wang, X. Z.; He, Z.; Djurišić, A. B.; Yip, C. T.; Cheung, K. Y.; Wang, H.; Mak, C. S.; Chan, W. K. Metallated

DOI: 10.1021/acs.chemrev.5b00165
Chem. Rev. XXXX, XXX, XXX−XXX

conjugated polymers as a new avenue towards high-efficiency polymer solar cells. *Nat. Mater.* **2007**, *6*, 521−527.
(192) Liu, S.; Zhang, K.; Lu, J.; Zhang, J.; Yip, H. L.; Huang, F.; Cao, Y. High-Efficiency Polymer Solar Cells via the Incorporation of an Amino-Functionalized Conjugated Metallopolymer as a Cathode Interlayer. *J. Am. Chem. Soc.* **2013**, *135*, 15326−15329.
(193) Grancini, G.; Maiuri, M.; Fazzi, D.; Petrozza, A.; Egelhaaf, H. J.; Brida, D.; Cerullo, G.; Lanzani, G. Hot exciton dissociation in polymer solar cells. *Nat. Mater.* **2012**, *12*, 29−33.
(194) Chan, W. L.; Ligges, M.; Jailaubekov, A.; Kaake, L.; Miaja-Avila, L.; Zhu, X. Y. Observing the Multiexciton State in Singlet Fission and Ensuing Ultrafast Multielectron Transfer. *Science* **2011**, *334*, 1541−1545.
(195) Coffey, D. C.; Ginger, D. S. Time-resolved electrostatic force microscopy of polymer solar cells. *Nat. Mater.* **2006**, *5*, 735−740.
(196) Liu, Y.; Zhao, J.; Li, Z.; Mu, C.; Ma, W.; Hu, H.; Jiang, K.; Lin, H.; Ade, H.; Yan, H. *Nat. Commun.* **2014**, *5*, 5293.
(197) Tseng, H. R.; Phan, H.; Luo, C.; Wang, M.; Perez, L. A.; Patel, S. N.; Ying, L.; Kramer, E. J.; Nguyen, T.-Q.; Bazan, G. C.; et al. High-Mobility Field-Effect Transistors Fabricated with Macroscopic Aligned Semiconducting Polymers. *Adv. Mater.* **2014**, *26*, 2993−2998.
(198) Dou, L.; Zheng, Y.; Shen, X.; Wu, G.; Fields, K.; Hsu, W. C.; Zhou, H.; Yang, Y.; Wudl, F. Single-Crystal Linear Polymers Through Visible Light−Triggered Topochemical Quantitative Polymerization. *Science* **2014**, *343*, 272−277.
(199) Traina, C. A.; Bakus, R. C., II; Bazan, G. C. Design and Synthesis of Monofunctionalized, Water-Soluble Conjugated Polymers for Biosensing and Imaging Applications. *J. Am. Chem. Soc.* **2011**, *133*, 12600−12607.
(200) Feng, F.; Liu, L.; Wang, S. Fluorescent conjugated polymer-based FRET technique for detection of DNA methylation of cancer cells. *Nat. Protoc.* **2010**, *5*, 1255−1264.

DOI: 10.1021/acs.chemrev.5b00165
Chem. Rev. XXXX, XXX, XXX−XXX